Final Report

Title: Synthesis Study Quantifying the Effect of UHPC Fiber Dispersion and Orientation in Structural Members

FDOT Contract Number: BDV30-977-34

Submitted to

The Florida Department of Transportation Research Center
605 Suwannee Street, MS 30 Tallahassee, FL 32399

C/O Christina Freeman
FDOT M.H. Ansley Structures Research Center

Submitted by:

Dr. Qian Zhang (qzhang@eng.famu.fsu.edu) (Principal Investigator)
Md. Mashfiqul Islam (Graduate Assistant)

Civil & Environmental Engineering
FAMU-FSU College of Engineering
Florida State University
2525 Pottsdamer Street, Suite B316
Tallahassee FL 32310

November 2021
Department of Civil & Environmental Engineering
FAMU-FSU College of Engineering
Florida State University

SI (MODERN METRIC) CONVERSION FACTORS (FROM FHWA)

Symbol	When You Know	Multiply By	To Find	Symbol
Length				
in	inches	25.4	millimeters	mm
ft	feet	0.305	meters	m
yd	yards	0.914	meters	m
mi	miles	1.61	kilometers	km
Area				
in^2	square inches	645.2	square millimeters	mm^2
ft^2	square feet	0.093	square meters	m^2
yd^2	square yard	0.836	square meters	m^2
mi^2	square miles	2.59	square kilometers	km^2
Volume				
fl oz	fluid ounces	29.57	milliliters	mL
gal	gallons	3.785	liters	L
ft^3	cubic feet	0.028	cubic meters	m^3
yd^3	cubic yards	0.765	cubic meters	m^3
NOTE: volumes greater than 1000 L shall be shown in m^3				
Mass				
oz	ounces	28.35	grams	g
lb	pounds	0.454	kilograms	kg
Temperature (exact degrees)				
°F	Fahrenheit	5 (F-32)/9 or (F-32)/1.8	Celsius	°C
Illumination				
fc	foot-candles	10.76	lux	lx
fl	foot-Lamberts	3.426	candela/m^2	cd/m^2
Force and Pressure or Stress				
lbf	pound-force	4.45	newtons	N
lbf/in^2	pound-force per square inch	6.89	kilopascals	kPa

TECHNICAL REPORT DOCUMENTATION PAGE

1. Report No.	2. Government Accession No.	3. Recipient's Catalog No.
4. Title and Subtitle Synthesis Study Quantifying the Effect of UHPC Fiber Dispersion and Orientation in Structural Members		5. Report Date November 2021 6. Performing Organization Code
7. Author(s) Qian Zhang, Md. Mashfiqul Islam		8. Performing Organization Report No.
9. Performing Organization Name and Address Florida State University 874 Traditions Way, Tallahassee, FL 32306		10. Work Unit No. 11. Contract or Grant No. BDV30-977-34
12. Sponsoring Agency Name and Address FDOT M.H. Ansley Structures Research Center 2007 E. Paul Dirac Dr., Tallahassee, FL 32310		13. Type of Report and Period Covered Draft Final report Oct.-Nov. 2021 14. Sponsoring Agency Code
15. Supplementary Notes – N/A		

16. Abstract

Ultra high performance concrete (UHPC) has been researched and implemented in the State of Florida for its superior structural and durability performance. Despite several successful structural level demonstrations, fiber dispersion and orientation remain a concern in the UHPC and general fiber-reinforced concrete communities. Quantifying the actual fiber dispersion and orientation status in real structural members and understanding their effect on structural performance are important to understand the reliability of UHPC members and quality control requirements.

UHPC design codes from other countries include reduction factors based on UHPC placement and fiber orientation for full-scale specimens. This research is a synthesis study to understand those factors and what research studies or rationale they are based upon to assist the design and research on UHPC at FDOT.

This technical report summarizes the findings in the synthesis study. All relevant design codes, guidelines, recommendations, and reports in France, Germany, Japan, South Korea, Canada, U.S., Switzerland, and Australia are identified and reviewed with a focus on methods and design factors to address the fiber dispersion and orientation. The background work behind the fiber orientation factors of these documents are also reviewed in detail. In addition, existing literature that correlates casting sequence and flow properties of UHPC with fiber orientation and mechanical properties of UHPC at the material level and the structural scale are also reviewed. All the findings are documented in the report. Recommendations for consideration of fiber orientation in the design and future research work are also provided.

17. Key Word	18. Distribution Statement
UHPC, fiber orientation, fiber dispersion, structural design	No restrictions.

19. Security Classif. (of this report)	20. Security Classif. (of this page)	21. No. of Pages	22. Price
Unclassified.	Unclassified.	140	

ACKNOWLEDGEMENT

The authors acknowledge and thank the Florida Department of Transportation (FDOT) for funding the research presented in this report. The authors thank the project manager Christina Freeman for her technical input and support and for facilitating resources throughout the project. The authors also thank Steve Nolan from FDOT Structures Design Office and Will Potter from FDOT Marcus H. Ansley Structures Research Center for their technical input and assistance in the project.

EXECUTIVE SUMMARY

In the last few decades, ultra high performance concrete (UHPC) has been extensively researched and implemented in transportation infrastructures for its superior mechanical properties, specifically its unique tensile response. The exceptional tensile and flexural performance is not only determined by the material composition but also heavily influenced by the casting method, size and geometry of element, rebar arrangement, rheology of UHPC mix, etc. These factors greatly influence the fiber orientation and dispersion of UHPC and as a result, affect the tensile and flexural performance of UHPC and ultimately the structural performance of UHPC members. As a result, it is critical to quantify the fiber orientation in real UHPC structures and understand how casting procedures and other factors affect the fiber orientation. To synthesize the knowledge that already exists in this arena, this current study reviews the relevant design guidelines, recommendations, and codes on UHPC with a focus on methods and design factors to address the fiber dispersion and orientation, the background work behind the fiber orientation factors of these documents, and other existing literature that correlates casting sequence and flow properties of UHPC with fiber orientation and mechanical properties of UHPC at the material level and the structural scale.

The review work is divided into two parts. Part 1 documents the review of the relevant design codes on UHPC design, focusing on fiber orientation considerations and the background work behind them. In this part, a total of 15 recommendations and guidelines of UHPC structural design from 10 standard organizations from different countries are reviewed. Part 2 documents the review of all other existing literature regarding the effect for UHPC casting procedures and rheology on fiber orientation and dispersion and mechanical performance (tensile, flexural, and rebar pullout behavior).

Based on our study, among all the recommendations and standard documents, the AFGC recommendations (2002, 2013) provide the most reliable method to directly measure the effect of fiber orientation and were followed in many successful large-scale UHPC projects. Moreover, the fib Model Code (fib MC2010 and in progress fib MC2020) and the Canadian Highway Bridge Design Code (2019) (CSA S6:19) closely followed the AFGC recommendations in deriving their respective fiber orientation factors. Guidelines from Germany (DAfStb guidelines 2012; 2019), Australia (AS 3600:2018), and Switzerland (SIA 2052:2016) also used various factors to modify the design tensile properties considering fiber orientation. However, many of these factors still require further investigation. Japanese (JSCE recommendations 2006, 2008) and Korean (KICT Design Guideline for K-UHPC, 2014 and KCl-M-19-006) codes did not consider fiber orientation explicitly, rather they used a lumped material factor to match the overall safety factors to AFGC recommendations (2002, 2013). The AASHTO specification (2021, proposed version) and CSA A23:19 do not consider fiber orientation factors for the structural design of UHPC structural members, rather they specify or require proper construction methods to be taken to ensure adequate fiber dispersion and avoid the adverse effect of fiber orientation.

In the review of other existing literatures, the influence of casting flow direction, formwork geometry, and rheology of UHPC on the fiber orientation, and the influence of fiber orientation on the mechanical performance and rebar pullout behavior of UHPC have been documented. Special casting procedures and casting devices proposed in the literature to promote better fiber alignment are also reviewed. According to the literature, for longitudinal members and flat members poured from the edge, fibers tend to align along the flow direction, while for flat specimens poured from the center, radial flow causes fibers to align perpendicularly to the flow direction. Fibers are generally more aligned at a longer flow distance. Therefore, fiber orientation could be controlled by controlling the flow direction of UHPC to align the fibers in the principal stress direction for enhanced mechanical performance. Additionally, due to the wall effect, the geometry of the specimens also affects the orientation of fibers in UHPC, especially for relatively small specimens and longer fibers. Regarding the rheology, generally low yield stress and high viscosity are desirable for fiber alignment in UHPC; however, excessive low yield stress and high viscosity may cause other workability issues. The bond behavior of rebar in UHPC is also impacted by the fiber orientation, and fiber alignment in the transverse direction to the rebars is considered more desirable to achieve high pullout strength. Regarding special casting procedures and devices, a 30-degree chute and L-shape devices are considered the most efficient in fiber alignment along the flow direction.

Based on the review, several knowledge gaps and future work directions are identified. There is an urgent need for the quantification of fiber orientation in large-scale structures to ensure reliable design. It is recommended that mock-up sections following AFGC recommendations (2002, 2013) be performed to understand the typical fiber orientation for typical FDOT structural elements, especially at critical locations or where the geometry is complex, for typical FDOT structural elements. Furthermore, investigations on the realistic casting procedures and their effect on fiber orientation at large scales are needed, and optimization of the casting procedure is desired to achieve more efficient and economical designs. It is also recommended to evaluate the special casting devices and procedures for their applicability in large-scale casting. In addition, the optimal range of rheology for fiber alignment in UHPC structural elements needs to be further investigated.

This research provides synthesized knowledge on the design considerations of fiber orientation in UHPC members, especially the use of fiber orientation factors to account for the adverse effect of fiber orientation in real structures, which could be implemented by FDOT to improve the reliability of UHPC structural design. The project also provides knowledge on the influence of casting procedures of UHPC members on their structural performance, which could assist FDOT in selecting appropriate casting procedures for UHPC members to achieve adequate structural performance.

TABLE OF CONTENTS

LIST OF FIGURES

Figure 11.1 Design plastic stress-strain models for TSFRC (CSA S6:19). 63
Figure 11.2 Design stress-strain model for THFRC at ULS (CSA S6:19). 63
Figure 11.3 TSFRC post-cracking properties (CSA S6:19). 63
Figure 11.4 Stress-strain and stress-crack width diagrams: (a) THUHPC; (b) TSUHPC (CSA A23:19 Annex U). 65
Figure 11.1 Design plastic stress-strain models for TSFRC (CSA S6:19). 63
Figure 11.2 Design stress-strain model for THFRC at ULS (CSA S6:19). 63
Figure 11.3 TSFRC post-cracking properties (CSA S6:19). 63
Figure 11.4 Stress-strain and stress-crack width diagrams: (a) THUHPC; (b) TSUHPC (CSA A23:19 Annex U). 65

LIST OF TABLES

PART 1: Literature Review of Existing UHPC Codes and Standards and their Background on Design Factors for UHPC Placement and Fiber Orientation

1. Introduction

Ultra-high performance concrete (UHPC) has been researched and implemented in the State of Florida for its superior structural and durability performance. Despite several successful structure-level demonstrations, fiber dispersion and orientation remain a concern in the UHPC and general fiber-reinforced concrete communities. Quantifying the actual fiber dispersion and orientation status in real structural members and understanding their effect on structural performance is important to understand the reliability of UHPC members and quality control requirements.

UHPC design codes from other countries include reduction factors based on UHPC placement and fiber orientation for full-scale specimens. This research is a synthesis study to understand those factors and what research studies or rationale they are based upon to assist the design and research on UHPC at FDOT.

This technical report summarizes the findings in the first research task of the project. In this task, the specifications and design codes relevant to UHPC structural design were identified and reviewed with a focus on methods and design factors to address the fiber dispersion and orientation.

Since 2000, global standards organizations, code bodies, and professional user groups have developed guidelines, standards, and codes for the materials, methods of construction, and the structural design of UHPC. In Europe, the French Association of Civil Engineers (Association Française de Génie Civil [AFGC]) published "the Recommendations on Ultra-High Performance Fiber-Reinforced Concrete (UHPFRC)" in 2002, which was later revised and re-issued in 2013. Subsequently, in 2016 and 2018, the French Standards Institute (Association Française de Normalisation [AFNOR]) published three French standards on UHPFRC, i.e., NF P 18-710 (2016), NF P 18-470 (2016), and NF P 18-451 (2018). In 2014, the Swiss Society of Engineers and Architects (SIA) published SIA 2052: "Ultra-high performance fiber reinforced concrete (UHPFRC) – Materials, design and execution (Béton fibré ultra-performant (BFUP); Matériaux, dimensionnement et exécution or SIA 2052)" and the second edition of SIA 2052 was made available in 2016. In Asia, the Korean Institute of Construction Technology (KICT) and Korea Concrete Institute (KCI) published their guidelines on UHPC entitled "Design Guidelines for Ultra High Performance Concrete (K-UHPC) Structure" in 2014 and "Structural Design Guidelines of Fiber Reinforced SUPER Concrete" in 2019, respectively. In North America, the American Concrete Institute (ACI) subcommittee 239C published an Emerging Technology Report (ETR) on the structural design of UHPC. The subcommittee is also currently working on drafting a guideline for the structural design of UHPC. The Canadian Standards Association, (CSA) also published "Concrete materials and methods of concrete construction/Test methods and standard practices for concrete" in 2019 with UHPC guideline in Annex U "Ultra-high

performance concrete (UHPC)" and the proposed version of the AASHTO (2021) "AASHTO LRFD guide specification for structural design with ultra-high performance concrete, Version 1.0, 2021 (proposed version)".

Additionally, several other guidelines and recommendations were also identified and reviewed. Although they do not focus on UHPC or UHPFRC, they contain relevant information on fiber orientation and dispersion. These include "the fib Model Code for Concrete Structures 2010" (and proposed fib Model Code 2020) published by the International Federation for Structural Concrete (fib), AS 3600 "Concrete Structures" published by the Council of Standards Australia in 2018, "Recommendations for Design and Construction of High-Performance Fiber Reinforced Cement Composites with Multiple Fine Cracks (HPFRCC)" published by the Japanese Society of Civil Engineers (JSCE) in 2008, "Steel Fibre Reinforced Concrete" published by the German Committee for Reinforced Concrete (DAfStb) in 2012 and revised in 2019, and the Annex A8.1 (informative) Fibre-reinforced concrete (FRC) of "Canadian Highway Bridge Design Code" published by the Canadian Standards Association, (CSA) in 2019.

The list of the standards and guidelines reviewed are as follows:

1. AFGC Recommendation on Ultra-High Performance Fiber-Reinforced Concrete (UHPFRC) (2002 and 2013)
2. fib Model Code for Concrete Structures (2010)
3. French National Standards:
   (1) NF P18-710, National addition to Eurocode 2 - Design of concrete structures: specific rules for Ultra-high performance fibre-reinforced concrete (UHPFRC) (2016),
   (2) NF P 18-470, Concrete - Ultra-high performance fibre-reinforced concrete - Specifications, performance, production and conformity (2016),
   (3) NF P 18-451, Concrete - Execution of concrete structures - Specific rules for UHPFRC (2018)
4. ACI 239C Emerging Technology Report (ETR) (The Structural Design of Ultra-High Performance Concrete, 2018; and Overview of the Methods for the Structural Design of Ultra-High Performance Concrete, 2019) (Draft copies)
5. Korean Guidelines:
   (1) KICT Design Guideline for K-UHPC (2014)
   (2) The Structural Design Guidelines of Fiber Reinforced SUPER Concrete (2019) (KCl-M-19-006)
6. Swiss Society of Engineers and Architects (SIA), Béton fibré ultra-performant (BFUP); Matériaux, dimensionnement et exécution (2016) (SIA 2052)
7. Australian Standard, Concrete Structures (2018) (AS 3600)
8. DAfStb Guideline, Steel Fibre Reinforced Concrete (2012 and 2019) (Draft copy)
9. JSCE Recommendations:
   (1) Recommendations for the Design and Construction of Ultra High Strength Fiber-Reinforced Concrete (UFC) (2006) (In English)
   (2) Recommendations for Design and Construction of High Performance Fiber Reinforced Cement

Composites with Multiple Fine Cracks (HPFRCC) (2008)

10. Canadian standards:
    (1) Concrete materials and methods of concrete construction/Test methods and standard practices for concrete (2019) (CSA A23.1:19)
    (2) Canadian Highway Bridge Design Code (2019) (CSA-S6:19)
11. AASHTO LRFD guide specification for structural design with ultra-high performance concrete, Version 1.0, 2021 (proposed version) (AASHTO 2021)

For each document, a brief introduction of the document is provided; the definition of the materials that are covered in the document is briefly described, and detailed information regarding the fiber orientation factors (or alternative methods to consider fiber orientation) and the background are summarized. Several documents focus on UHPC or similar materials. Other documents do not focus on UHPC, rather, they cover the design of fiber reinforced concrete, steel fiber reinforced concrete, or high-performance fiber reinforced concrete, etc. They are also reviewed as they provide relevant information on the fiber orientation factors.

2. AFGC Recommendations on Ultra-High Performance Fiber-Reinforced Concrete (UHPFRC) (2002 and 2013)

2.1 Overview

The Association Française de Génie Civil (French Association for Civil Engineering or AFGC) Recommendation on Ultra-High Performance Fibre-Reinforced Concrete (UHPFRC) was first published in 2002 and later revised in 2013. These Recommendations on UHPFRC were intended to constitute a reference document serving as a basis for the use of UHPFRC as the new material in civil engineering applications. The AFGC recommendation on UHPFRC was published by the AFGC/SETRA working group on UHPFRC chaired first by Benoit Lecinq, then by -Jacques Resplendino (CETE de Lyon) in January 2002. The revised edition of the AFGC recommendation, requested by the AFGC's Scientific and Technical Committee, was drafted by the AFGC/SETRA working group on UHPFRC chaired by Jacques Resplendino (SETEC TPI) in 2013. Since 2002, UHPFRCs have been increasingly used in the construction industry and extensively researched around the world. Therefore, AFGC published its revised edition in June 2013 by rewriting the design regulations in accordance with Eurocode 2.

2.2 Definition of UHPFRC

According to AFGC recommendation (2013), the Ultra High Performance Fiber-Reinforced Concrete (UHPFRC) that are covered in this document are materials with a cement matrix and having a characteristic compressive strength (f_{ck}) between 150 MPa and 250 MPa (21,750 psi and 36,250 psi). The material is characterized by a high post-cracking tensile strength obtained by the systematic use of a high percentage of steel fibers (more than 2% in volume) to achieve ductile behavior under tension. The mix-design and high binder content help to eliminate the capillary porosity, which results in good durability of the fibers in UHPFRC. The self-healing characteristic of the cracks ensures long-term retention of tensile strength provided that certain crack width limits are verified. The direct tensile strength of the matrix is usually greater than 7 MPa (1,015 psi). The UHPFRCs covered by these recommendations require that:

$$150\ MPa\ \leq f_{ck} \leq 250\ MPa \qquad \ldots(2.1)$$

where f_{ck} is the characteristic compressive strength of UHPFRC. The characteristic value of a parameter, which corresponds, in all this document, to a probability of exceedance equal to 95%.

Based on experimental results of stress-crack width behavior ($\sigma_f - w$) from bending test or direct tension tests, the AFGC recommendation has categorized UHPFRC into the following types:

- Type 1 – Strain-softening UHPFRC shows a strain-softening response after the peak stress (Figure 2.1a). This type of material is characterized by crack localization after reaching the matrix strength due to a low fiber content (or poorly dispersed fibers) or containing fibers that

are not very efficient in bridging the cracks.

- Type 2 – Low strain-hardening UHPFRC shows a strain-hardening response, however, with consideration of the fiber alignment and dispersion, it is a strain-softening material (Figure 2.1b). This type of behavior corresponds to most of the UHPFRCs currently on the market. For material characterization and design purposes, these UHPFRCs are treated as strain-softening UHPFRCs.
- Type 3 – High strain- hardening UHPFRC (Figure 2.1c) shows the post-cracking peak remains higher than $f_{ct,el}$ (limit of elasticity under tension which is the mechanical resistance of cement matrix with the presence of fibers). Therefore, type 3 UHPFRC is considered to be strain-hardening in the design. Typically, type 3 UHPFRC has a high fiber content. For type 3 UHPFRC, once the elastic strength $f_{ct,el}$ is reached, micro-crack forms instead of generating localized cracks.

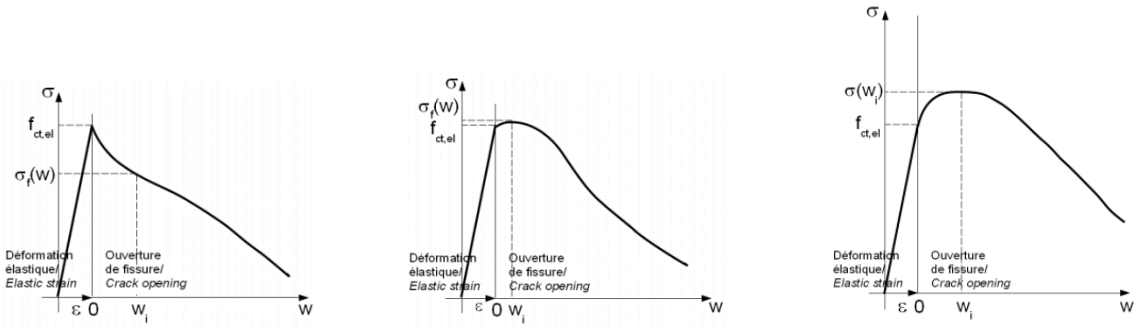

(a) (b) (c)

Figure 2.1 Example of tensile constitutive curves of a UHPFRC: (a) Type 1— strain-softening material; (b) Type 2— low strain-hardening material; (c) Type 3— strain-hardening material (AFGC recommendation, 2013).

2.3 Fiber orientation factor

The AFGC recommendation was the first to introduce the fiber orientation factor to address the effect of fiber dispersion and orientation. The factor is considered in the constitutive model of UHPFRC and the structural design of UHPFRC structures.

As per AFGC recommendation (2002 and 2013), the fiber orientation factor K is a reduction factor to take into account the difference between the fiber orientation of the cast prisms that are used to determine the material property and the actual orientation of the fibers in the structure. Two K factors are defined: a local value and a global value. K_{local} is used when stresses of very localized areas (for example, prestressing stress distribution at anchorage zone) are of concern. K_{global} is used when the overall effects in larger areas (for example, the shear or the bending strength of a slab) are of concern, which will not be affected by a local defect. The K factor is only applied to the post-cracking part of the tensile constitutive law.

To obtain the K-factors, direct tensile tests or four-point bending tests are carried out ($\geq$ 6 numbers of tests) on sawn prisms from the actual structure or a representative model (mock-up) built during the suitability tests prior to the construction and lab cast prisms. Figure 2.2 shows the arrangement of sawn cut specimens to determine the K factor. To determine the K factor relating to disparities in fiber orientation, samples are taken along the directions of principal stresses. Equations 2.2/2.3 and 2.4/2.5 are used to determine K_{global} and K_{local}, respectively. Equations 2.2/2.3 and 2.4/2.5 are calculated using the results of bending tests or direct tensile tests, respectively.

$$K_{global} = \frac{\overline{M_{m,max,\iota}}}{\overline{M_{s,max,\iota}}} \quad \ldots(2.2)$$

$$K_{local} = \frac{\overline{M_{m,max,\iota}}}{(M_{s,max,i})_{min}} \quad \ldots(2.3)$$

$$K_{global} = \frac{\overline{F_{m,max,\iota}}}{\overline{F_{s,max,\iota}}} \quad \ldots(2.4)$$

$$K_{local} = \frac{\overline{F_{m,max,\iota}}}{(F_{s,max,i})_{min}} \quad \ldots(2.5)$$

Where, $\overline{M_{m,max,\iota}}$ = the mean value of maximum moment obtained by bending test (four-point bending test for type 3 UHPFRC, three-point bending test for type 1 and 2 UHPFRC) on all individual cast specimens; $\overline{M_{s,max,\iota}}$ =the mean value of maximum moment obtained by bending test (four-point bending for type 3 UHPFRC, three-point bending test for type 1 and 2 UHPFRC)) on all individual sawn specimens; $(M_{s,max,i})_{min}$= the minimum value out of all measured maximum moment obtained by bending test of individual sawn specimens; $\overline{F_{m,max,\iota}}$ =the mean value of maximum force obtained by direct tension test on all individual cast specimens; and $\overline{F_{s,max,\iota}}$ =the mean value of maximum force obtained by direct tension test on all individual sawn specimens; $(F_{s,max,i})_{min}$ = the minimum value out of all measured maximum force obtained by direct tension test on all individual sawn specimens.

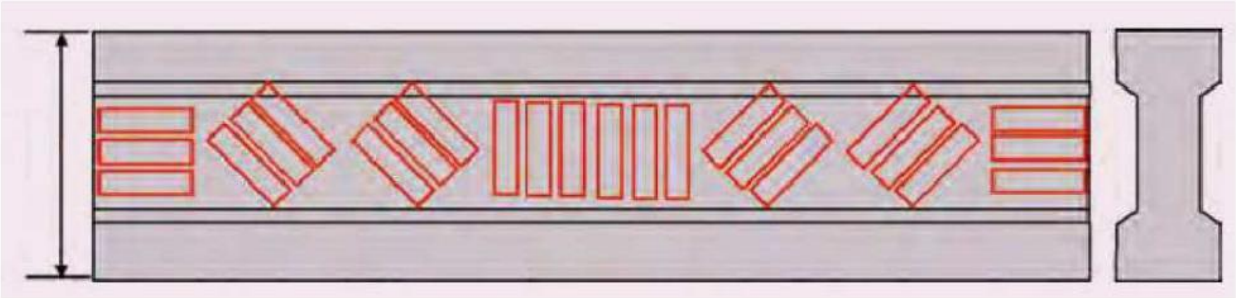

Figure 2.2 Example of sawn specimens to determine the K factor.

AFGC also recommends that the edge effect be considered when calculating the K factors to remove the influence of boundaries in both cast and sawn prisms. The edge effect is taken into account by dividing the measured moments or forces by correction factors λ for both sawn and cast samples.

Edge effects at formed surfaces

Considering a prism sample with formed surfaces, such as cast prism samples, the fibers in the middle of a prism is not disturbed by the formwork, and thereby they are assumed to have a random 3D orientation. If we consider the fiber efficiency to be 1.0 (i.e., α1D=1.0) when all fibers are aligned in the direction under consideration. Because, in the corners, at the intersection of two formed surfaces, a quasi-1D distribution can be considered, i.e., an orientation factor of 1.0. AFGC recommendation (2013) considers an average orientation factor equal to 0.841. The factor 0.841/ α3D is therefore applied

The fiber efficiency is considered to be 0.41 when the fibers are randomly oriented in 3D (i.e., α3D = 0.41). Theoretically, α3D = 0.5 can be derived purely based on the probability density of fiber orientation as per Simon et al. 2013 (also detailed in section 3.4). However, in reality, the fibers may have low efficiency when they are at high angles to the loading direction, and therefore, AFGC Recommendation uses α3D = 0.41 when considering the edge effect to be on the conservative side. The fibers, of which the center of gravity fall inside a $l_f/2$ (l_f=fiber length) the wide band along these formed surfaces are subjected to the wall effect. The fiber orientation is in between a 2D (i.e., α2D = 2/π=0.637) and 3D fiber orientation (i.e., α3D = 0.41) (Figure 2.3a and 2.4a). An average value α2D-3D = 0.597 can be assumed for this region. Then the factor λ can be calculated as a weighted average of these efficiency factors in the width direction of the prism. By dividing the measured moments or forces by this λ, it removes the edge effect due to formed surfaces. It should be noted that a free surface should also be considered as a formed surface since fibers are typically troweled and smoothed for free surfaces.

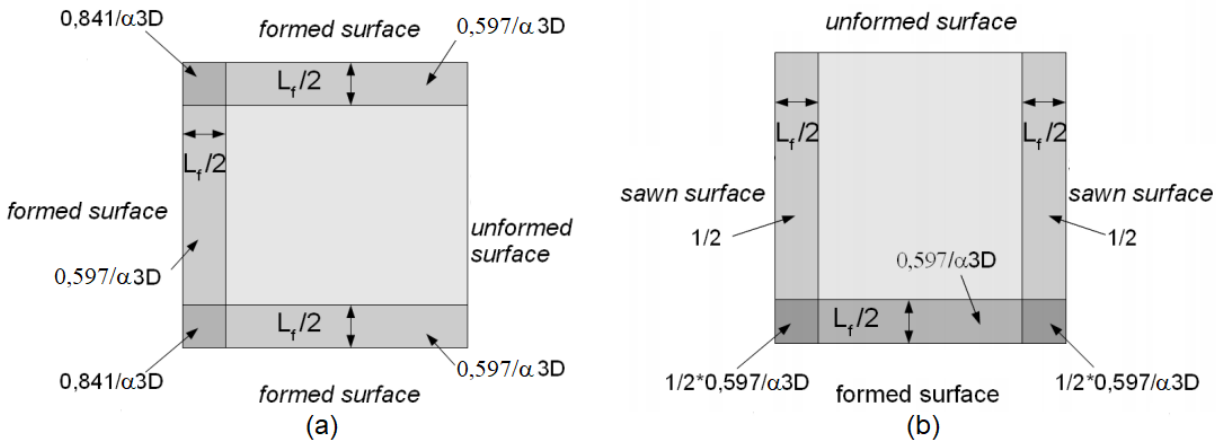

Figure 2.3 Example of surface: (a) formed surface; (b) sawn prism (AFGC recommendation, 2013).

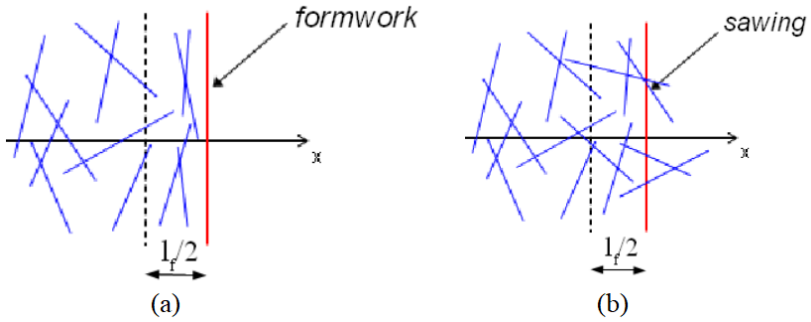

Figure 2.4 Effect of surface: (a) formed surface; (b) sawn surface (AFGC recommendation, 2013).

Edge effects at sawn surfaces

For sawn samples, the fibers in the middle of a prism are not disturbed by the sawing. They are assumed to have a random 3D orientation (i.e., α3D = 0.41). The fibers whose center of gravity is located inside a $l_f/2$ wide band along the sawn surface (Figure 2.3 and 2.4) also have a random 3D orientation, but their lengths have been reduced by sawing. In this region, it is then assumed that the fibers are 50% effective and therefore an additional factor of 0.5 should be considered for this region. For sawn samples, the λ factor can also be calculated based on the weighted average of the efficiency factors in the prism width direction, which is then used to correct the measured moment or force values.

Edge effects at notched surfaces

For tests on notched samples, the notch depth has to be higher or equal to $l_f/2$. The indirect consequence of this notch is to delete any formwork effect on the fiber orientation of this face and thereby no correction is required.

The K factors should have a minimum value of one. A K value of less than one would assume a beneficial preferential orientation effect in a given direction. The resistance of the structure in all the other directions in which the K values are generally greater than one (which is due to the negative fiber orientation effect) would then need to be validated even if the said directions do not correspond to those of the principal loads. Without any direct test results, the designer can begin with the following K values: K_{global} = 1.25 for all loading other than local effects, and K_{local} = 1.75 for local effects.

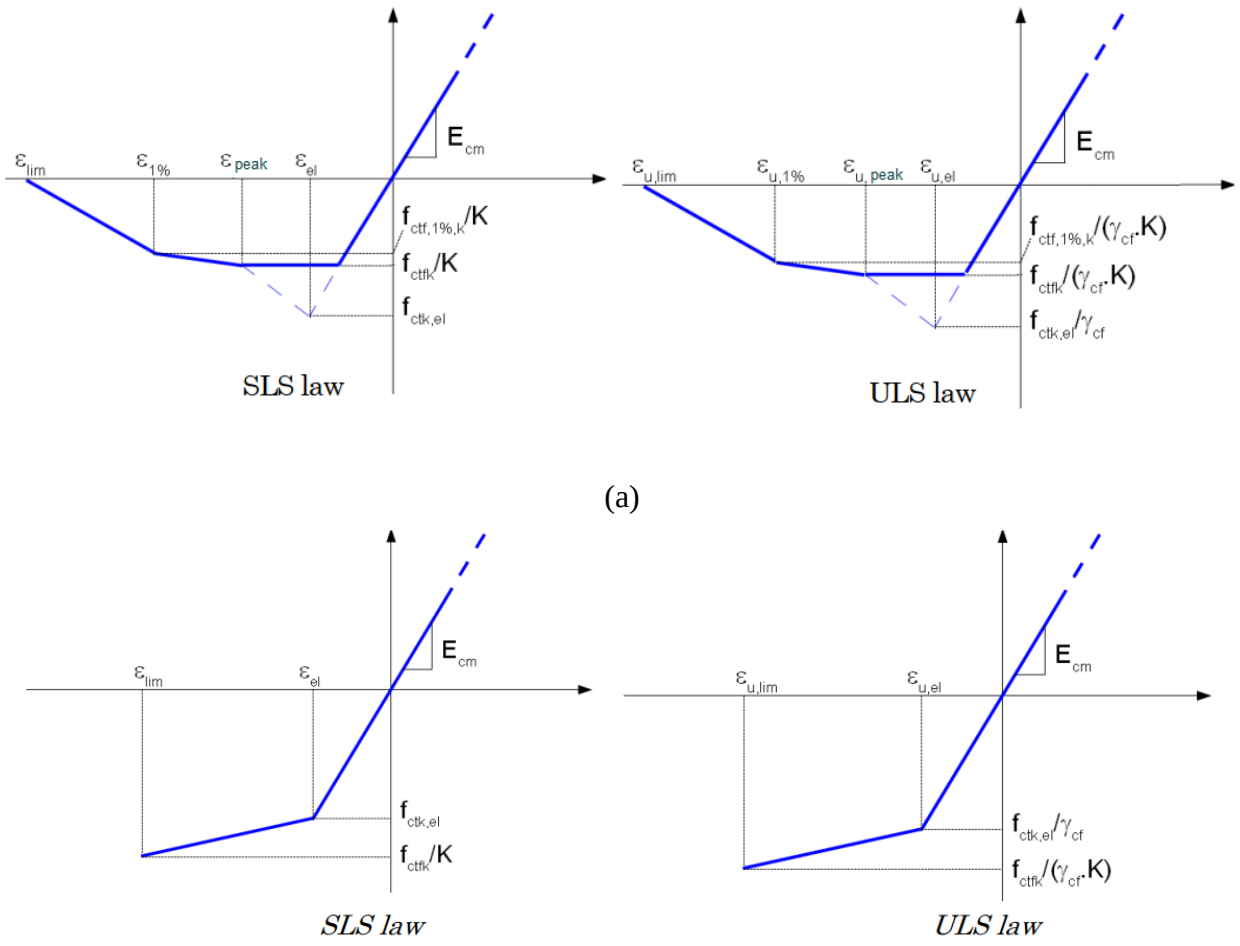

Figure 2.5 Tensile strength constitutive law of UHPFRC for thick cross-sections: (a) strain-softening or low strain hardening law; (b) strain hardening law (AFGC recommendation 2013).

The typical constitutive laws of UHPFRC material in compression and tension are defined in this document and used in the design methodology of UHPFRC structures. Particularly, the tensile constitutive law takes the disparity on fiber orientation due to placement method into account, and K factors are used when determining the post-peak behavior. Several types of tensile constitutive laws are observed experimentally based on their post-peak behavior. The different behaviors are caused by differences in the number of fibers, fiber length and length/diameter aspect ratios, as well as fiber distribution. The tensile constitutive law of UHPFRC is important for designing or checking UHPFRC structures and is characterized by: (1) a linear elastic stage limited by a stress value $f_{ct,el}$, (2) a post-cracking stage generally characterized by a stress-crack width ($\sigma_f - w$) law or a stress-strain ($\sigma_f - \varepsilon$) law.

Based on different types of tensile behaviors (measured characteristic stress-strain or stress-crack width curves), AFGC defines the following typical tensile constitutive laws shown in Figures 2.5 and 2.6 for thick and thin sections, respectively. Figure 2.5(a) exhibits the strain-softening (Type 1) or low

strain hardening law (Type 2) behavior of UHPFRC under tension for serviceability limit state (SLS) and ultimate limit state (ULS) conditions. Similar to ordinary concrete, UHPFRC exhibits a linear elastic tensile behavior up to a limit value f_{ctfk}/K and $f_{ctfk}/(\gamma_{cf}.K)$ with Young's modulus (E_{cm}), where f_{ctfk} is the characteristic maximal post − cracking stress, γ_{cf} is the partial safety factor on fibers in order to take manufacturing defects (those causing the inability to achieve the required mechanical properties of UHPFRC) into account. The curve shows a plateau up to ε_{peak} and $\varepsilon_{u,peak}$ for SLS and ULS, respectively. Here, ε_{peak} and $\varepsilon_{u,peak}$ are the strains corresponding to the local peak in the post-cracking phase or to a crack width equal to 0.3 mm if there is no peak for SLS and ULS conditions, respectively. Then the curve linearly decreases to $f_{ctf,1\%,k}/K$ and $f_{ctf,1\%,k}/(\gamma_{cf}.K)$ for SLS and ULS respectively and finally decreases to the ε_{lim} and $\varepsilon_{u,lim}$ for SLS and ULS conditions respectively and the tensile stress vanishes. Here, $f_{ctf,1\%,k}$ is the characteristic post- cracking stress corresponding to a crack width of 0.01H, where H is the depth of the tested prism; and ε_{lim} and $\varepsilon_{u,lim}$ are the strains beyond which fibers participation is no longer taken into account at SLS and ULS, respectively. In the case of high strain hardening UHPFRC (type 3), the curve linearly reaches to limit value of $f_{ctk,el}$ and $f_{ctk,el}/\gamma_{cf}$ for SLS and ULS conditions respectively with Young's modulus (E_{cm}) being the same in both tension and compression and then further increases to $f_{ctk,el}/K$ and $f_{ctk,el}/(\gamma_{cf}.K)$ for the SLS and ULS conditions (Figure 2.5b).

Similarly, Figure 2.6 shows the tensile constitutive law for the thin section of UHPFRC. The thinness of the slabs and the way the concrete is placed are likely to affect the orientation of fibers. It can therefore be expected the post-cracking performance will vary, depending on the direction tested. Thin sections are defined as elements whose thickness e is such that: $e \leq 3l_f$ where l_f = length of individual fibers. For Type 1 or 2 UHPFRCs, the curve linearly reaches to limit value of f_{ctfk}/K and $f_{ctfk}/(\gamma_{cf}.K)$ for SLS and ULS conditions, respectively (where 1/K acts as a reduction factor due to fiber orientation effect) with Young's modulus (E_{cm}) being the same in both tension and compression. Then the curve remains constant at the plateau value until the strain reaches ε_{lim} and $\varepsilon_{u,lim}$ for SLS and ULS conditions, respectively (Figure 2.6a). The tensile constitutive law of thin section UHPFRC Type 3 is the same as thick section UHPFRC (Type 3) for both SLS and ULS conditions (Figure 2.6b).

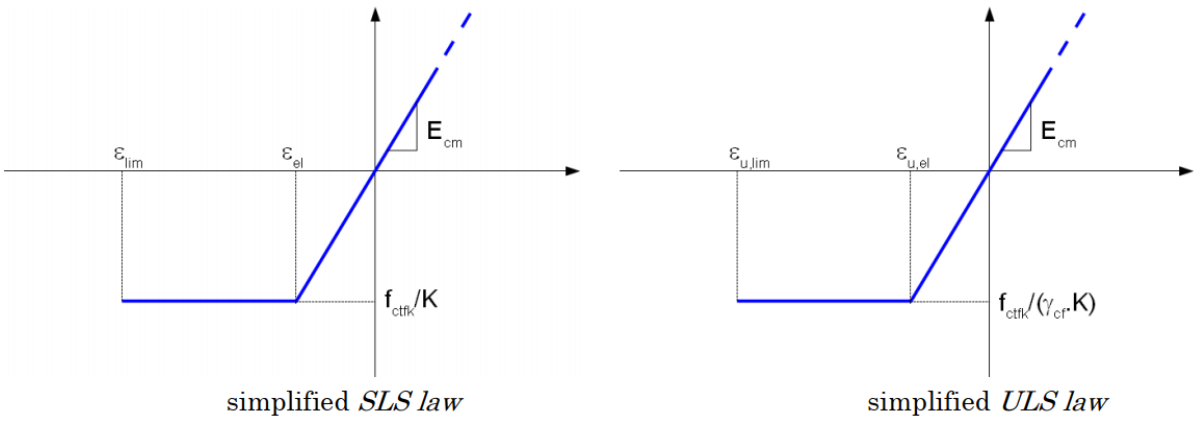

(a)

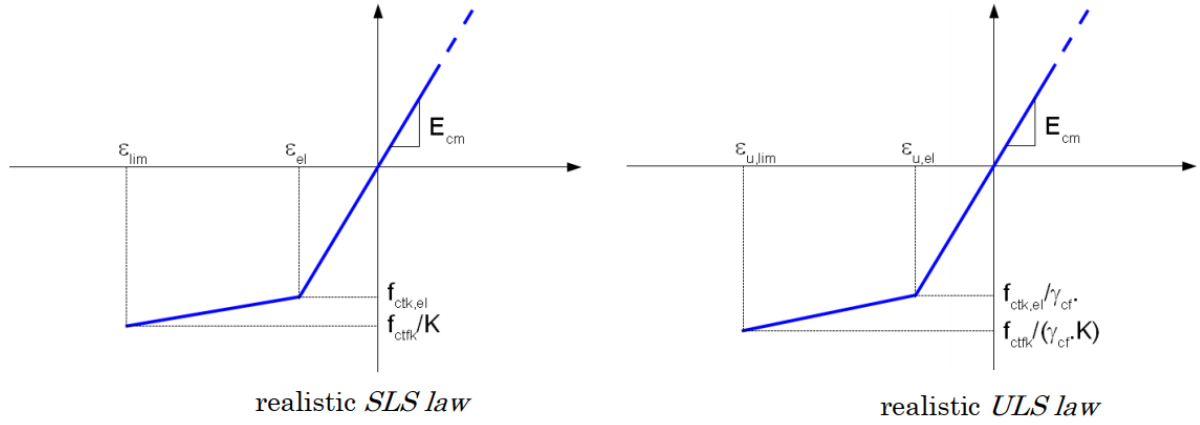

(b)

Figure 2.6 Tensile strength constitutive law of UHPFRC for thin cross-sections: (a) strain-softening or low strain hardening law; (b) strain hardening law (AFGC recommendation 2013).

These constitutive laws (with modification of K factors) are then applied in the analysis and design of UHPFRC structural members, e.g., UHPFRC beams, prestressed girders, columns, etc.

2.4 Background

The default values of K factors in 2002 French AFGC recommendations are based on the measured values in real projects (Simon et al. 2013). The two of Bourg-Lès-Valence bridges, France (Figure 2.7), built-in 2001-2002, were the first road bridge made of UHPFRC. In these bridges, the girders and deck were made of UHPFRC. The girders are made of π-shaped prestressed beams precast in BSI® UHPFRC ("Béton Special Industriel" or special industrial concrete, developed by Eiffage, France) and jointed together longitudinally with in-situ BSI® onsite. A mock-up of one-half of the π-shape beam (see Figures 2.7 and 2.8) was cast in the Hürks Beton plant in the Netherlands for suitability test. Five different sets of prism samples were sawn (Figure 2.7 and 2.8) for the flexure test to calculate the K factors from different zones.

The results obtained for the K factors in the different zones are gathered in Table 2.1. For this project, only one value for global effects (K_{global} = 1.25) and one value for local effects (K_{local} = 1.75) were chosen based on the largest measured values. These values were then considered in 2002 French AFGC recommendations, as default values for new projects without suitability test (Simon et al. 2013).

(a)

(b)

Figure 2.7 (a) General view of one of the Bourg-Les-Valence Bridges, France (Valente 2017); (b) mock-up of one half of a π-shape beam before and after sawing (Simon et al. 2013).

Table 2.1 Obtained K values (Simon et al. 2013)

	Zone A	**Zone B**	**Zone C**	**Zone D**	**Zone E**	**Chosen value**
Global effects	1.025	0.832→1	1.247	1.089	0.882→1	K=1.25
Local effects	1.456	1.225	1.722	1.340	1.135	K=1.75

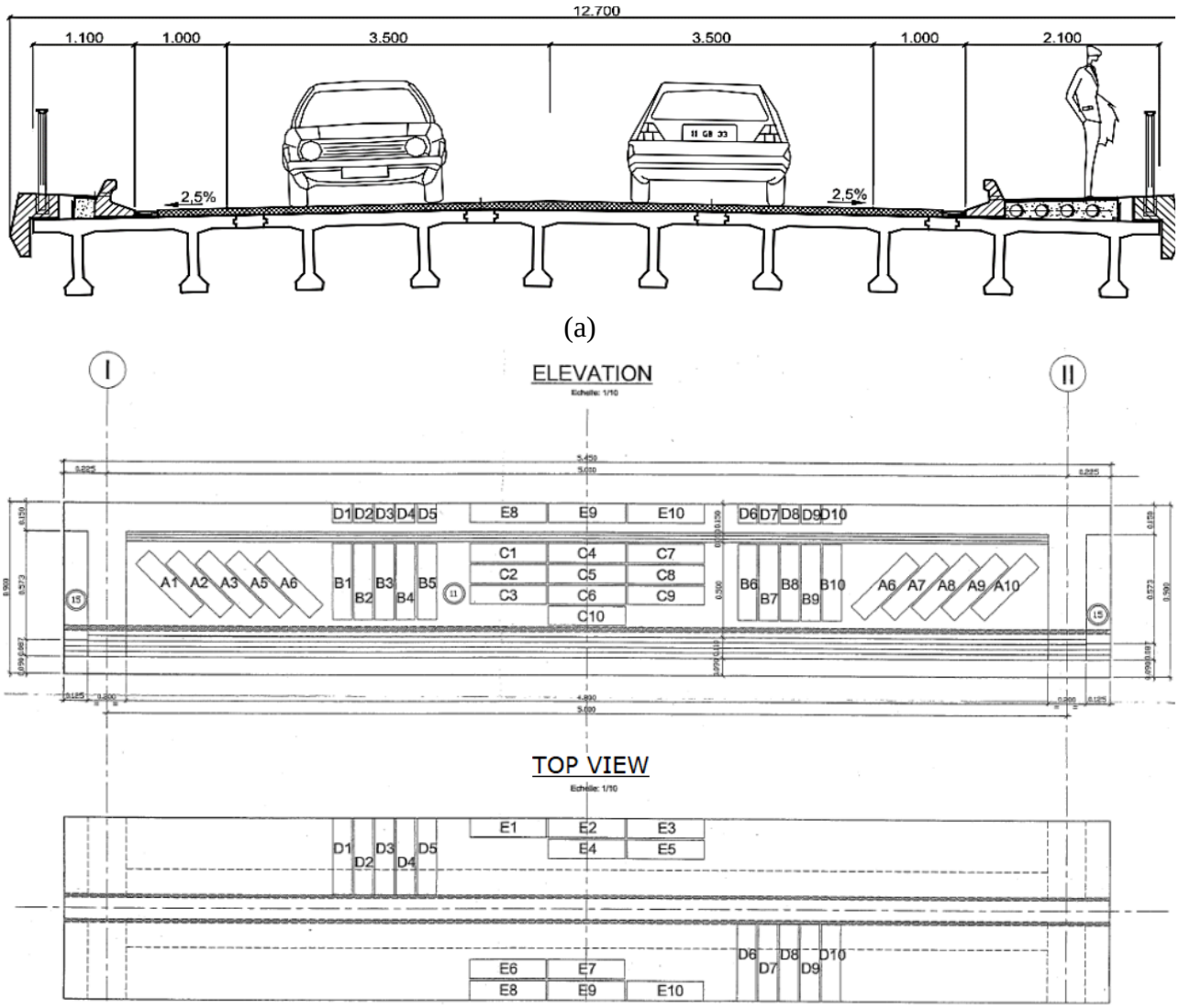

Figure 2.8 (a) Standard cross-section π-shape beams of the Bourg-Les-Valence Bridges, France (Valente 2017); (b) scheme of extracted samples from one half of a π-shape beam (the sample ID initials represent the zones A, B, C, D, and E) (Simon et al. 2013).

Although the frequency of suitability test is not explicitly specified in the AFGC Recommendations, from the reported case studies following AFGC Recommendations (Simon et al., 2013), it can be summarized that at least one mock-up specimen should be prepared for each (different) type of member for each UHPFRC mix design in a project. The AFGC recommendations (2002 and 2013) specified that during the production of a control mock-up representative of the actual structure and its production conditions, certain dimensions of a mock-up specimen may be reduced, but others may not; it shall be full-scale in the directions of least thickness, and in areas where concentrated forces are applied, and it shall enable any difficulties in casting the UHPFRC and restrained deformations to be identified. At least one nominal mix whose volume is representative of the actual production should

be used to cast samples and measure the material properties (compression, bending, direct tension, consistency, etc.) for each mock-up specimen. These tests should be repeated for every batch needed for the casting of each mock-up specimen. In the case of prestressing and/or heat treatment, mechanical measurements including the compressive strength must be carried out for the key steps, i.e., before prestressing and also before and after heat treatment.

Following the Bourg-Lès-Valence bridges, France (described above), several other projects in France also reported using the fiber orientation factor K and suitability tests. A brief review of these projects is provided below.

Saint-Pierre-La-Cour bridge

The Saint-Pierre-La-Cour bridge built-in 2005 was constructed using Ductal® (a UHPC mixture by LaFarge) girders and an ordinary concrete deck. This bridge, with a span of 19.0 m (62.3 ft) and width of 12.6 m (41.3 ft) (Behloul and Batoz, 2008), supports a continuous reinforced concrete road (Figure 2.9a and 2.9 b). The bridge consists of ten 20 m (65.6 ft) long prestressed girders without passive re-bars and 83 precast slabs, which are all made of Ductal®. A 3.0 m (9.84 ft) long girder mock-up was made during the suitability test (Figure 2.9) according to the chosen procedure to manufacture the definitive girders.

The sawn samples were extracted from the mock-up section as shown in Figure 2.9. The K_{global} and K_{local} factors were calculated from four-point flexure test results using the 45° oriented specimens (series B2, B3, B6, and B7 in Table 2.3). In the longitudinal direction, the tensile stress is carried by the prestressing steel, thereby the 45° orientation is the most critical direction.

These measured strength values of the sawn samples are listed in Table 2.2 and 2.3 column 2. These values were further corrected to take into account the edge effects and the K factors were then calculated using the corrected strength values (Table 2.2 and 2.3 column 3). The maximum values of K_{global} and K_{local} obtained in Table 2.2 and 2.3 ($K_{global} = 1, K_{local} = 1.36$) were selected to be used in the design.

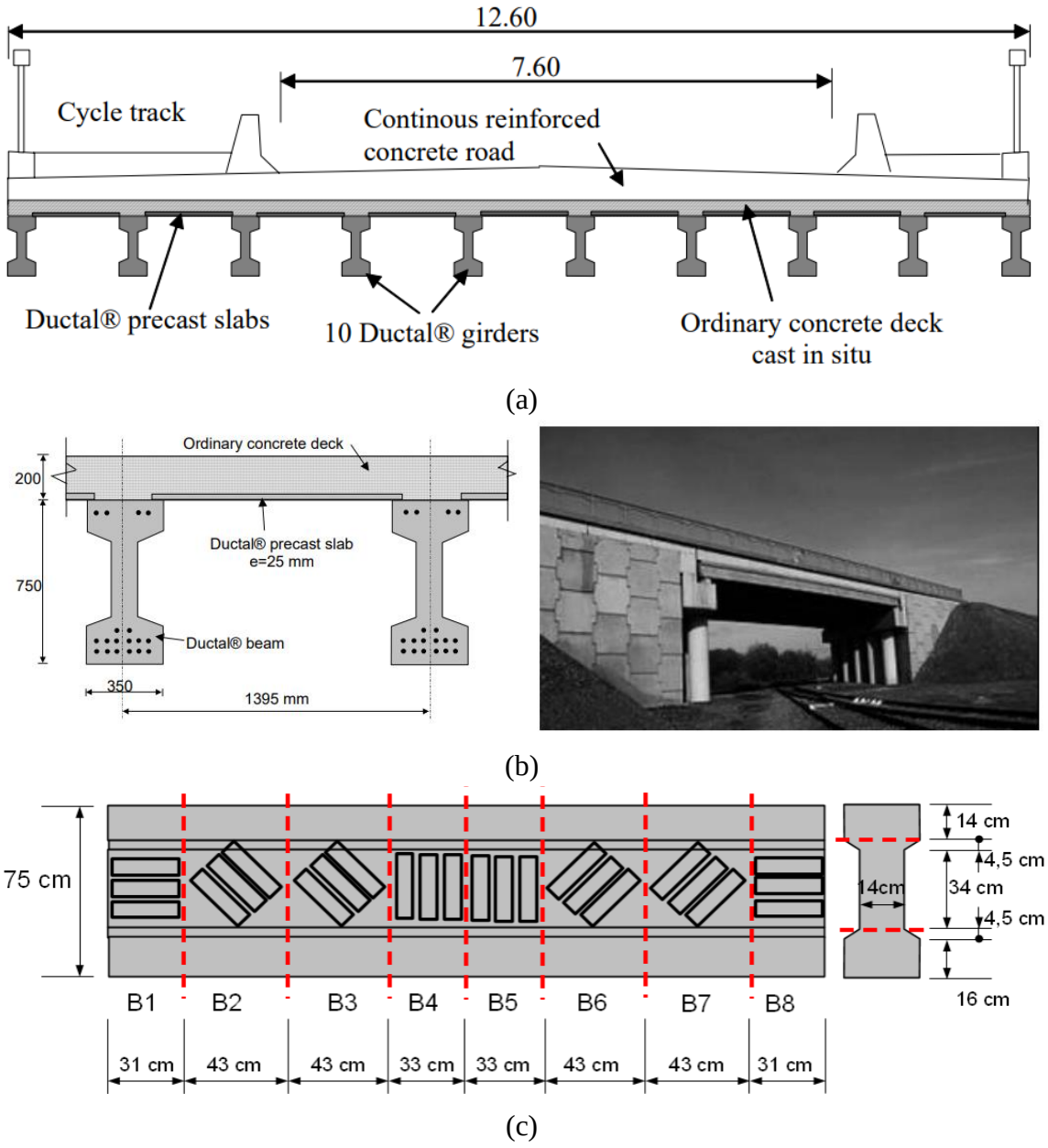

Figure 2.9 (a) Transverse section of the Saint-Pierre-la-Cour bridge (Behloul and Batoz, 2008); (b) detailing and completed bridge; (c) sawing of the mock-up for Saint-Pierre-la-Cour bridge (Simon et al., 2013).

Table 2.2 Tests results obtained for determination of K_{global}

Zone	Mean stress value	Corrected value	K_{global}
45°: B2 and B7	31.2 MPa	34.4 MPa	0.73→1
45°: B3 and B6	33.3 MPa	36.7 MPa	0.68→1

Table 2.3 Tests results obtained for determination of K_{local}

Zone	Minimal stress value	Corrected value	K_{local}
45°: B2 and B7	26.5 MPa	29.2 MPa	0.86→1
45°: B3 and B6	16.7 MPa	18.4 MPa	1.36→1

PS34 Overpass

The PS34 Overpass is a single span road bridge of 47.4 m (155.5 ft) long made of a prestressed box girder over the A51 motorway, France, with no intermediate pier (Figure 2.10a). The overpass was built with BCV®, the UHPFRC developed by the Vicat cement factory, and the Vinci group. It was built in 2005 by Campenon Bernard Regions. The girder was made of 22 UHPFRC prefabricated segments, assembled together by post-tensioning. Two full-scale mock-ups of the precast segments were built in Campenon Bernard plant, France, prior to the construction to validate the structural response and to obtain the fiber orientation factors in the different characteristic zones outlined in Figure 2.10b.

(a)

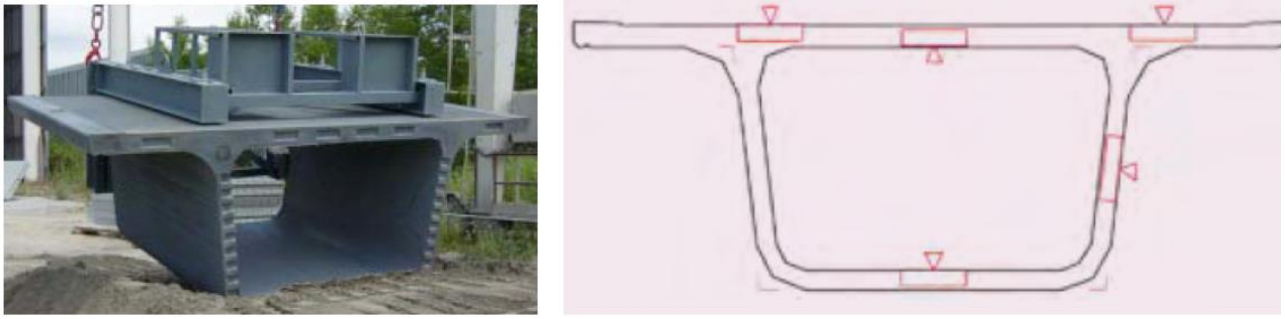

(b)

Figure 2.10 (a) General view of PS34 overpass (Resplendino 2008); (b) full-scale mock-up of a precast segment, with the scheme of extracted samples (AFGC recommendation 2013).

Due to the shape of the box girder and the way to pour the concrete (from one fixed point at the top of the formwork), different values for K factors were obtained in the different characteristic zones. Considering this special placement method, a value of $K = 1.5$ (although the reference only noted it as K factor, the authors believe the mentioned K factor is the global K factor) was used for the preliminary design. The results of the suitability test showed that 1.5 was a safe value except at the flux front in

the middle of the lower flange. Due to difficulties in modifying the casting procedure, locally, traditional reinforcement was added to enhance that region, without changing the K factors (Resplendino 2008).

Pinel Bridge

The Pinel bridge is a 27 m (88.5 ft) long bridge located in Le petit Quevilly, south of Rouen, France (Figure 2.11a), which was built in 2007. The girders of the Pinel bridge are precast pre-tensioned inverted T sections (ITE) made with UHPFRC (BSI®) (Figure 2.11), whereas the deck is made of ordinary concrete. The suitability tests were carried out in the Hürks Beton plant, France, before the precast. The formwork of the mock-up was identical to what had been chosen for the precast process, with a representative length of 5.0 m (16.4 ft). The mock-up also took into account the varying dimensions of the actual girder at different locations. Three different zones were chosen to extract sawn prisms from the web considering the principal stress path and avoiding varying web width zones (Figure 2.11c). Three successive mock-ups were manufactured and tested to modify the casting method. The first mockup was abandoned immediately after formwork removal because the web surfaces had a lot of bug holes, which could negatively affect the result of the flexural tests on the extracted cores. The second test showed non-uniform fiber dispersion. This was attributed to a slightly low batch volume of UHPFRC during mixing (the batch volume was 300 liters, instead of 500 liters as recommended for the specific mixer used) and significant flocculation of the fibers probably due to prolonged storage in a humid atmosphere (de Matteis et al. 2008b). Consistent results were obtained from the third test. The K factors obtained from the three zones were selected: K_{global} = 1.33 and K_{local} = 1.75.

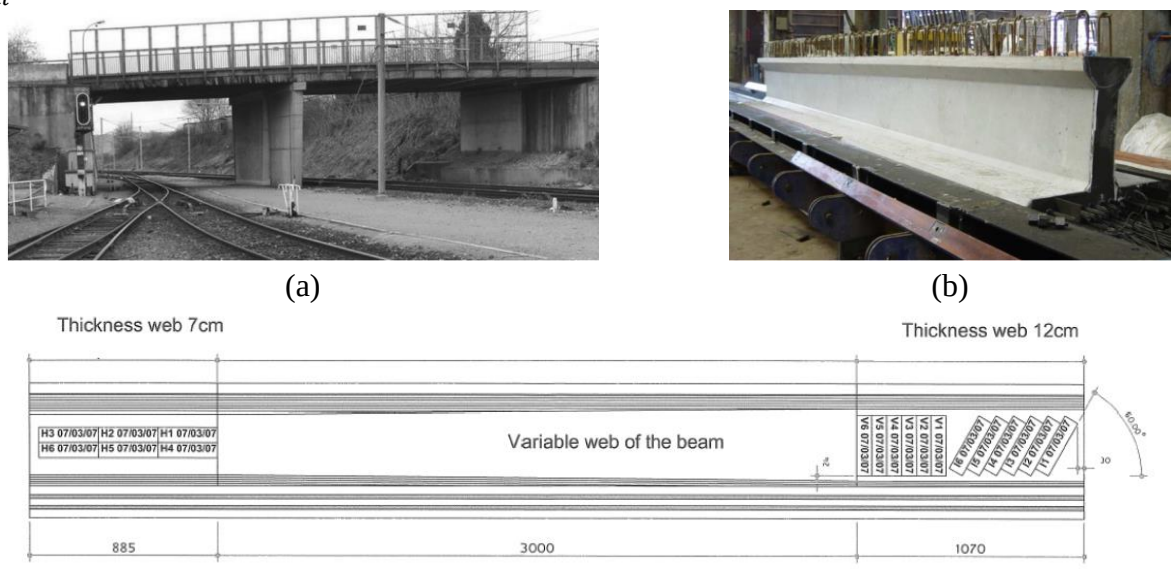

(a) (b)

(c)

Figure 2.11 (a) General view of the Panel bridge (de Matteis et al. 2008a); (b) mock-up of the Pinel bridge in BSI® (Simon et al., 2013); (c) the location of the extracted samples (AFGC recommendation 2013).

Shells of the water treatment plant of Achères

The Seine Aval sewage treatment plant operated by SIAAP is located on the banks of the Seine River downstream of Paris, France, which was built in 2013. The treatment plant tank roofing involves multiple precast shells made of post-tensioned UHPFRC (BSI®) (Figure 2.12). The individual precast shell (tank roofing) is 2.8 m (9.2 ft) in width and 10.6 m (34.8 ft) in length and 50 mm (2 in) in thickness (Delplace et al. 2012). They were post-tensioned without any passive reinforcements. A full-scale mockup of the precast shell was constructed in the Eiffage plant in France before the actual construction to validate the structural response. Prisms were sawn along with the principal stress directions in two characteristic zones of the mockup (Figure 2.12a): at mid-span and in the prestress bearing zone and tested under flexure. In this project, two sets of K factors were considered in design calculations based on the suitability test, e.g., at mid-span section, K_{global}=1.20 and K_{local}=1.65, and in bearing zones, K_{global}=1.35 and K_{local}=1.55 (Table 2.4).

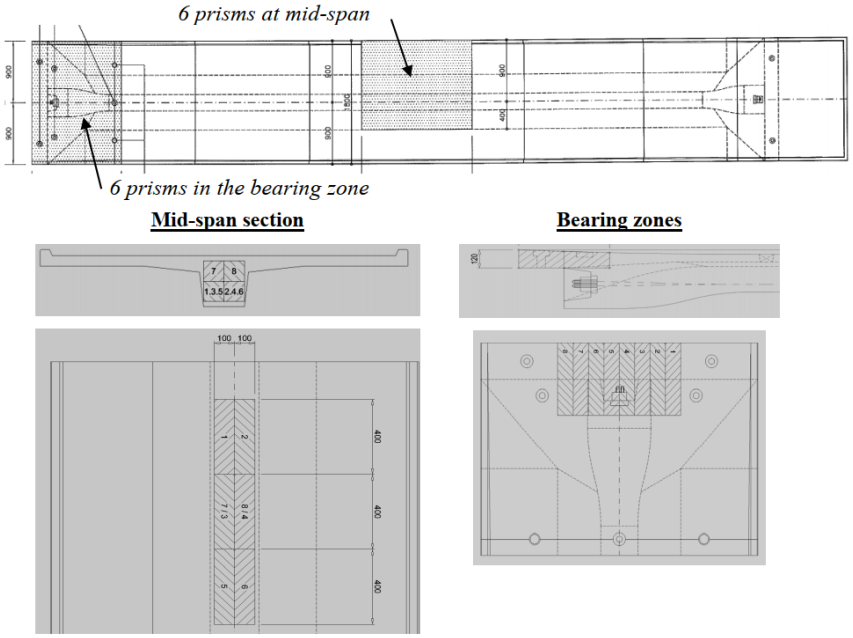

(a)

(b) (c) (d)

Figure 2.12 (a) Mock-up of a shell, with the scheme of extracted samples (Simon et al., 2013); (b) mock-up sample after collecting sawn samples; (c) erection of shell by crane; (d) BSI® shells over Biostyr™ tanks (Delplace et al. 2012).

Table 2.4 K values obtained

	Mid-span section	**Bearing zones**
Global effect	K=1.20	K=1.35
Local effect	K=1.65	K=1.55

Pont du Diable footbridge

The "Pont du Diable" is a footbridge in Gorges de l'Herault, France, built jointly by the companies Freyssinet, France and Bonna Sabla, France (Behloul et al. 2008) in 2009. The bridge was constructed with precast post-tensioned Ductal® (UHPC) segments (Figure 2.13a and 2.13b). This footbridge has a total span length of 68 m (223 ft). The bridge cross-section is composed of two bone-shaped webs, with a height of 1.8 m (5.9 ft), connected by a light ribbed deck. During the construction, fifteen 4.6 m (15 ft) long segments were prefabricated and assembled by prestressing and then erected in one day. A mock-up of the bridge with a full-scale cross-section (Figure 2.13c) and 0.8 m (2.6 ft) length was constructed during the suitability test. Prism samples were extracted from the two webs of the mock-up sections in four zones (two zones in each web) and at different inclination angles: 90° (vertical direction) and 45° (Figure 2.13d). It was considered that the tensile strength of UHPFRC was not used in the longitudinal direction as prestressing steel was provided. Hence, only results obtained in the vertical direction and at 45° angle were important for the shear resistance of the structure. Consequently, the K values are determined based on the maximum values obtained for the 4 zones, i.e., K_{global} = 1.26 and K_{local} = 2.12 (Table 2.5).

Table 2.5 K values obtained

Samples inclination	**Global effect**	**Local effect**
45° - zone 1	0.79→1.00	0.85→1.00
Vertical – zone 1	0.93→1.00	1.04
Vertical – zone 2	1.26	2.12
45° - zone 2	1.24	1.37

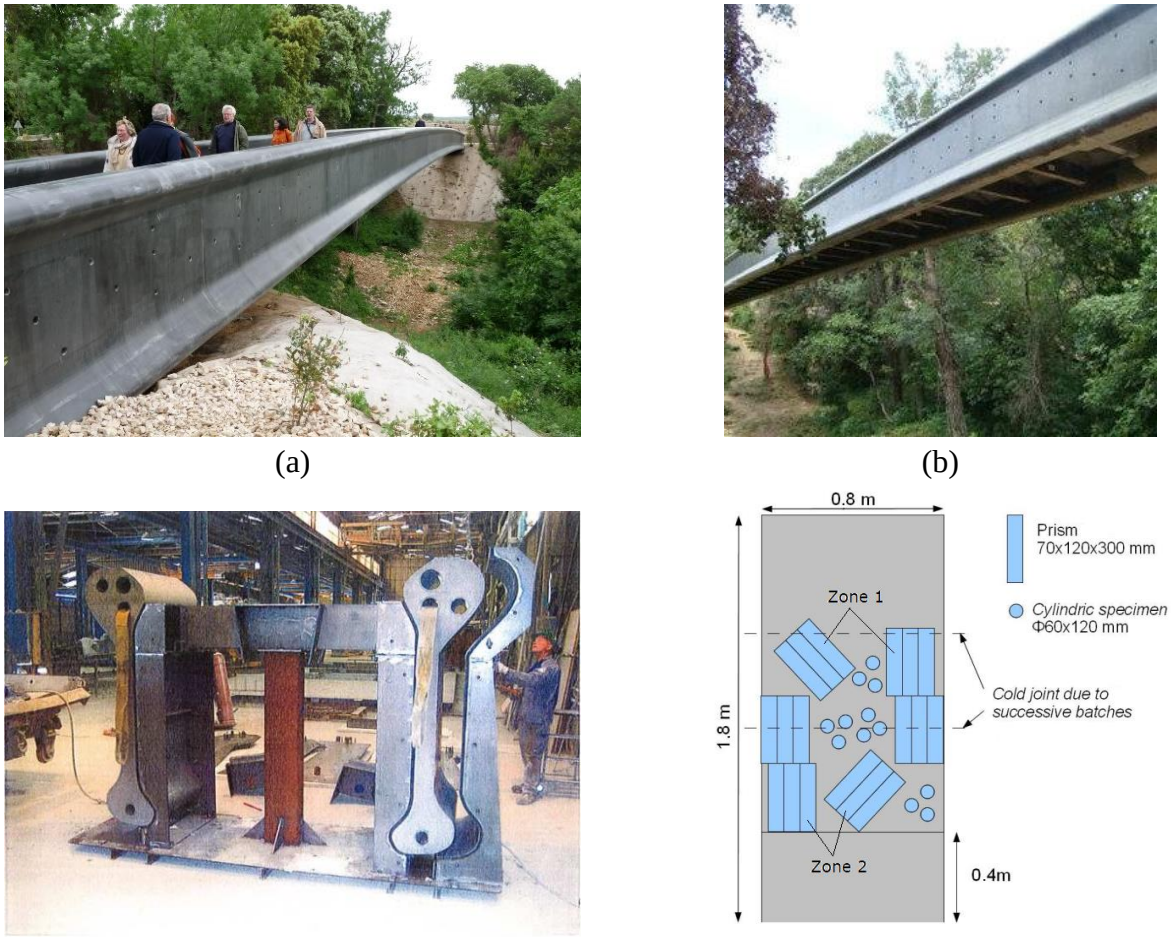

Figure 2.13 The Pont du Diable footbridge: (a, b) general view of the span; (c) mock-up of the footbridge section; (d) locations of sawn and drilled samples (AFGC recommendations 2013).

The practical K factor method, proposed by AFGC recommendations (2002 and 2013) has shown high robustness and reliability in these projects. In many cases, it led to the modification of the way to cast the UHPFRC or the local shape of a formwork, to obtain results consistent with the design hypothesis (Simon et al., 2013). It means that in several cases if the K factor method had not been applied, a safe design would not have been obtained. The method of determination of K for UHPFRC structural design by suitability tests prior to the construction must not be neglected. It is one of the most important steps during the building process of a structure in UHPFRC structures. As per the AFGC recommendation (2013), at the stage of suitability tests, the K factors taken into account in the design of a project must be verified experimentally. In order to do this, several samples have to be taken from a mock-up at full scale, sufficiently representative of the structure under design, and fabricated with the same material in the same conditions (in terms of formwork and casting process).

3. fib Model Code for Concrete Structures (2010)

3.1 Overview

The International Federation for Structural Concrete (fib) is the pioneering organization in the codification of the fib Model Code for Concrete Structures 2010 (fib MC2010). The objectives of the fib MC2010 are to (a) serve as a basis for future codes for concrete structures and (b) present new developments with regard to concrete structures, related structural materials, and new ideas in order to achieve optimum behavior. The fib MC2010 includes the whole life cycle of a concrete structure, from design and construction to conservation (assessment, maintenance, strengthening) and dismantlement, in one code for buildings, bridges, and other civil engineering structures. Design is largely based on performance requirements. The chapter on materials is particularly extended with new types of concrete and reinforcement (such as fibers and non-metallic reinforcements).

Unlike the AFGC recommendations and other codes and standards regarding material and structural design of ultra-high performance concrete (UHPFRC), the fib MC2010 does not cover any information related to UHPFRC or UHPC. Instead, this code deals with FRC in Section 5.6 (fib MC2010) and verification of the safety and serviceability of FRC structures in Section 7.7 (fib MC2010). Design recommendations, especially focusing on high and ultra-high strength fiber concrete, are currently in preparation (fib Task Group 8.6) and are expected to be included in fib Model Code 2020 (fib MC2020).

3.2 Definition of FRC

The definition of the fiber-reinforced concrete (FRC) covered in fib MC2010 is a composite material characterized by a cement matrix and discrete fibers. The matrix is made of either concrete or mortar. Fibers can be made of steel, polymers, carbon, glass, or natural materials. Fiber materials with a Young's modulus which is significantly affected by time and/or thermo-hygrometrical phenomena are not covered by this fib MC2010.

According to the fib MC2010, for structural use, a minimum mechanical performance of FRC must be guaranteed. Fibers can be used to improve the behavior at SLS because they can reduce crack spacing and crack width, thereby improving durability. Fibers can be used to improve the behavior at ULS, where they can partially or totally substitute conventional reinforcement. The structural design of FRC elements is based on the post-cracking residual strength provided by fiber reinforcement.

3.3 Fiber orientation factor

In accordance with the AFGC recommendations (2002), the fib MC2010 also introduced the concept of fiber orientation factor K. It is worth noticing that the fib MC2010 focused on fiber-reinforced concrete (FRC) instead of ultra-high performance concrete (UHPC) or ultra-high performance fiber-reinforced concrete (UHPFRC).

In general, as per fib MC2010, isotropic fiber distribution is assumed, so that the fiber orientation factor K=1.0. For favorable effects, an orientation factor K<1.0 may be applied if experimentally verified. For unfavorable effects, an orientation factor K>1.0 must be experimentally determined and applied. The behavior observed in the standard tests can deviate substantially (beneficial and non-beneficial) from the behavior of the corresponding FRC in the structural element or structure. Thus, the manufacturing method and the concrete consistency should be considered by the designer. The fib MC2010 also suggests that when $K < 1.0$ is applied in one direction, the K in the other direction should be checked. However, the fib MC2010 did not clarify the condition of favorable effects and unfavorable effects as well as the procedure for calculating the factor K.

The post-cracking residual strength provided by fiber reinforcement is considered in the structural design of FRC structures and this strength is modified by the K factors. fib MC2010 provides a stress-crack opening law ($\sigma - w$) under uniaxial tension to represent the post-cracking behavior of FRC. Two simplified $\sigma - w$ constitutive laws may be deduced from the bending test results: a plastic rigid behavior (rigid-plastic model), or a linear (linear model) post-cracking behavior (hardening or softening considering ULS) as schematically shown in Figure 3.1, where f_{Fts} represents the serviceability residual strength, defined as the post-cracking strength for serviceability crack openings, and f_{Ftu} represents the ultimate residual strength. The application of the K factor is only available for calculating the modified values of f_{Ftsd} and f_{Ftud} as follows:

$$f_{Ftsd,mod} = f_{Ftsd}/K \qquad \ldots(3.1)$$
$$f_{Ftud,mod} = f_{Ftud}/K \qquad \ldots(3.2)$$

where f_{Ftsd} is defined as the design value of post-cracking strength for serviceability crack opening for fiber-reinforced concrete, and $f_{Ftsd} = f_{Ftsk}/\gamma_F$; f_{Ftud} is defined as the design value of post-cracking strength for an ultimate crack opening for fiber-reinforced concrete, and $f_{Ftud} = f_{Ftuk}/\gamma_F$; f_{Ftsk} and f_{Ftuk} are the characteristic values of f_{Fts} and f_{Ftu}, respectively, which should be determined by flexure test of FRC; γ_F is the partial safety factor for FRC. The γ_F for residual tensile strength of FRC is 1.5 and 1.0 in the case of ULS and SLS, respectively. $f_{Ftsd,mod}$ and $f_{Ftud,mod}$ are corresponding modified versions considering the effect of fiber orientation (multiplied by $1/K$).

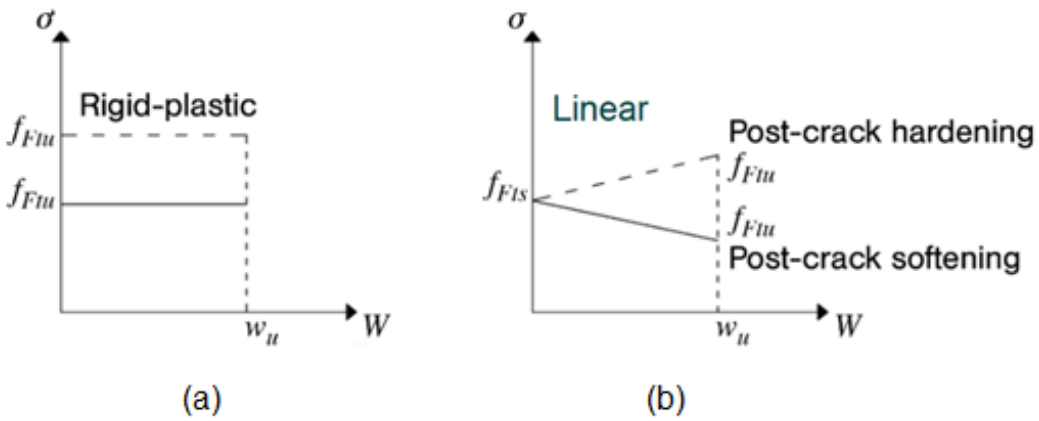

Figure 3.1 Simplified post-cracking constitutive laws: stress-crack opening: (a) rigid-plastic model; (b) linear model (continuous and dashed lines refer to softening and hardening post-cracking behavior, respectively) (fib MC2010).

3.4 Background of fiber orientation factor

The fib MC2010 does not provide a clear concept, calculation procedure, or the value range of the fiber orientation factor. However, the concept and the application of the fiber orientation factors in the design formula were quite similar to that of AFGC recommendations (2002 and 2013). Through some private conversations with one of the fib MC2020 (in progress) committee members, we learned that there is a significant update and clarification of the fiber orientation factor in the upcoming 2020 code, which is described below.

First of all, the definition of K factors has changed in the fib MC2020 from the fib MC2010. In the fib MC2010, the fiber orientation factor K was used as a dividing factor (as shown in Equations 3.1 and 3.2). However, in fib MC2020, it will be used as a multiplying factor (Equation 3.5 and 3.6), and therefore the K factor criteria has been changed to its inverse.

$$f_{Fts,ef} = K f_{Fts} \quad \ldots(3.5)$$
$$f_{Ftu,ef} = K f_{Ftu} \quad \ldots(3.6)$$

Where $f_{Fts,ef}$ and $f_{Ftu,ef}$ represent the effective residual tensile strength values for SLS and ULS, respectively, determined by bending tests according to EN 14651:2005 (Precast concrete products-test method for metallic fiber concrete—Measuring the flexural tensile strength); f_{Fts} and f_{Ftu} represent the residual tensile strength values for design under SLS and ULS, respectively.

The new fib Model Code (fib MC2020) also clarified the values of the K factor. In absence of a suitability test following the AFGC Recommendations, the K factors can also be determined based on the geometry of the structural components. The rationale and values of K factors are explained below.

Considering that the residual tensile strength of steel fiber reinforced concrete is directly proportional

to the number of fibers in the crack plane, the relation between the effective number of fibers in a given cross-section, the geometrical characteristics, and volume concentration of the fibers and the fiber orientation is given by (Dupont and Vandewalle, 2005; Kasper et al., 2014):

$$N_f = \alpha_0 \frac{V_f}{\frac{d_f^2}{\pi \frac{}{4}}} \qquad \ldots(3.3)$$

Where, N_f= average number of fibers per unit cross-sectional area in a given cross-section, V_f= fiber concentration by volume, d_f= fiber diameter, α_0= factor representing the fiber orientation, with the following values considered for "standard" fiber orientations:

α_0 = 0.5 in the case of 3D random fiber orientation;

α_0 = 0.64 in the case of 2D random fiber orientation (for any sectional plane perpendicular to the fiber plane) (Dupont and Vandewalle, 2005).

α_0 = 0 in the case of 2D random fiber orientation (for a sectional plane parallel to the fiber plane) (Kasper et al., 2014)

α_0 = 1 in the case of 1D aligned fibers (for a sectional plane perpendicular to the fiber direction) (Kasper et al., 2014)

α_0 = 1 in the case of 1D aligned fibers (for a sectional plane perpendicular to the fiber direction) (Kasper et al., 2014)

The K factor is then defined as the ratio between the fiber orientation α_0 in the actual structure and that in the EN 14651:2005 standard specimen (specimen width and depth of 150 mm or 6 in, length L such that 550 mm ≤ L ≤ 700 mm or 21.6 in ≤ L ≤ 27.5 in, and the span length is 500 mm or 19.7 in, $\alpha_0 = 0.58$) (Kasper et al. 2014):

$$K = \frac{\alpha_0}{0.58} \qquad \ldots(3.4)$$

Typically, the computation of N_f and K can be required if a check on the cracked plane has to be performed. If no experimental measurement is available, the following values for slabs and walls are suggested (Table 3.1 and 3.2) based on previous studies:

Table 3.1 K values suggested for solid slabs (Kasper et al. 2014)

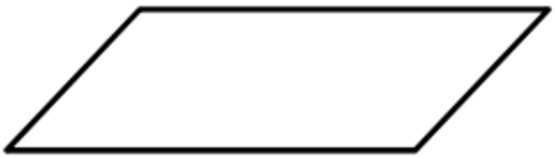

Longitudinal	Vertical	Transverse
1.00	0.30	1.00

Table 3.2 K values suggested for walls (Kasper et al. 2014)

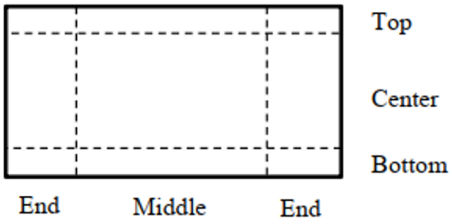

	Middle			End		
	Longitudinal	Vertical	Transverse	Longitudinal	Vertical	Transverse
Bottom	1.25	0.42	0.42	0.92	0.42	0.42
Center	1.00	0.50	0.42	0.83	0.56	0.50
Top	0.83	0.50	0.27	0.67	0.67	0.50

The fib MC2020 also clarifies that for favorable effects, an orientation factor $K > 1.0$ may be applied if experimentally verified (similar process to suitability test as per AFGC recommendations). A maximum value of 1.5 can be assumed. When $K > 1.0$ is applied in one direction, the K in the orthogonal direction $K_{\perp}$ has to be considered lower than 1.0. For unfavorable effects, an orientation factor $K < 1.0$ must be experimentally determined and applied. In a local check without any experimental investigation, a value $K = 0.5$ should be considered as an unfavorable effect.

Dupont and Vandewalle (2005) described the procedures used to derive the α_0 (and thereby K) value. Take a square section for example, at first, the orientation factor is calculated for fibers that are not limited by any boundaries. This is the case for a fiber in bulk (zone 1 in Figure 3.2). Secondly, one boundary condition is considered, parallel to the direction in which the orientation factor is determined. This simulates the condition along one mold edge (zone 2 in Figure 3.2). And finally, a second boundary condition is added, also parallel to the direction in which the orientation factor is determined, but now perpendicular to the first boundary condition. This simulates a fiber situated in a corner of the mold (zone 3 in Figure 3.2). b and h (Figure 3.2) are the width and the height of the beam section, for square sections, b=h. l_f stands for the fiber length. Here, A_1, A_2, and A_3 represent the areas of zone 1, 2, and 3 respectively (Figure 3.2), where $A_1 = \left(b - l_f\right)^2$, $A_2 = \left(b - l_f\right) l_f/2$, $A_3 = l_f^2/4$ (considering, $b = h$).

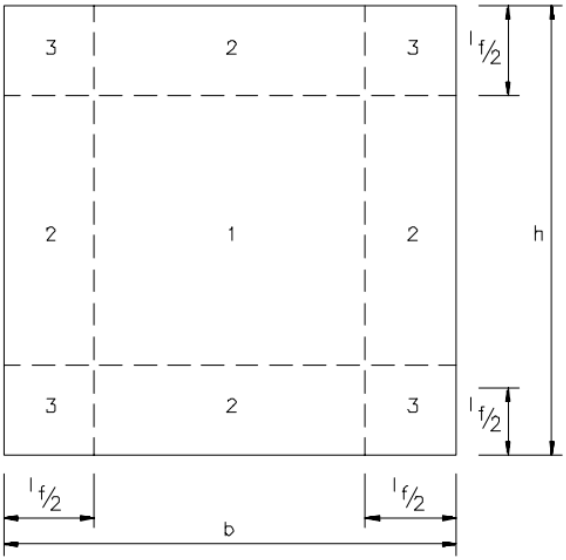

Figure 3.2 Cross-section of a beam divided into three different orientation zones, e.g., 1, 2, and 3 (Dupont and Vandewalle, 2005).

The following seven assumptions are made for calculating the orientation factor in each of these three areas:

1) The fibers are straight. For hooked end fibers, the same orientation factor can be taken since the effect of the hooks is negligible on the orientation factor.
2) If the fresh concrete is vibrated for a long time or when it has high workability (e.g. self-compacting concrete), the fibers tend to orient in a horizontal plane. This orientation effect depends highly on the vibration time and frequency and the workability and composition of the concrete, and it is therefore very difficult to quantify. However, from other research (Barragán et al. 2000), it is concluded that the vibration does not have a significant effect on the orientation, if the specimen is only vibrated for 1 or 2 min and if the workability of the fresh concrete is not too high. The effect of vibration on the orientation of the fibers is not considered here.
3) The location of the fiber in the beam is characterized by its point of gravity. Each point of the cross-section is considered to have an equal probability of being the gravity point of a fiber.
4) The fiber orientation in area 1 (Figure 3.2) is not influenced at all by the boundary conditions.
5) The fiber orientation in area 2 (Figure 3.2) is only influenced by one side of the mold.
6) The fiber orientation in area 3 (Figure 3.2) is influenced by two sides of the mold.
7) The top surface of the section is assumed to have the same boundary condition as the sides of the mold. After casting, this surface is smoothened so that there are no fibers sticking out. There could be a higher number of fibers at the surface due to the topping off and leveling of the specimen.

Considering the orientation factor for the areas 1, 2, and 3 (Figure 3.2) are α_1, α_2 and α_3, respectively, then the overall orientation factor can be calculated as follows by taking the geometrical average over the section:

$$\alpha_0 = \frac{[\alpha_1 \times (b-l_f)(h-l_f) + \alpha_2 \times [(b-l_f)l_f + (h-l_f)l_f] + \alpha_2 l_f^2]}{bh} \quad \ldots(3.5)$$

Where, α_1, α_2 and α_3 = orientation factor in zone 1 (i.e., orientation factor in bulk), zone 2 (orientation factor of a fiber with 1 boundary condition), and zone 3 (orientation factor of a fiber with 2 boundary conditions) respectively (Figure 3.2). The calculation of the α_1, α_2 and α_3 are as follows:

Orientation factor in bulk

A fiber in bulk (zone 1 in Figure 3.2) is not limited by any boundary condition and can rotate freely around its gravity point. If all the possible orientations of the fiber are considered, the end points of the fiber describe the surface of a sphere. Each point on the sphere has an equal probability to be the end of the fiber. This means that the probability that the fiber makes an angle θ with the longitudinal axis of the beam is proportional to the area dA (Figure 3.3) with:

$$dA = \underbrace{\frac{\pi l_f^2}{2} \sin\theta \, d\theta}_{A_1} \quad \ldots(3.6)$$

Where θ is the angle that the fiber makes with the longitudinal axis of the beam. The contribution of the area dA to the orientation factor is then $cos\theta dA$. Integrating this over half the sphere and dividing by the surface of half the sphere gives:

$$\alpha_1 = \frac{\int_0^{\pi/2} \cos\theta \, dA}{2\pi\left(\frac{l_f}{2}\right)^2} = \frac{\int_0^{\pi/2} \mathrm{A1} \times \cos\theta \, d\theta}{2\pi\left(\frac{l_f}{2}\right)^2} = 0.5 \quad \ldots(3.7)$$

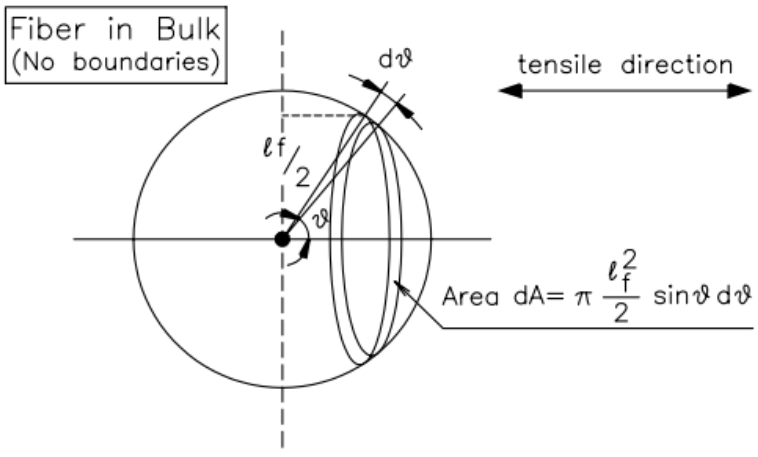

Figure 3.3 A fiber in bulk (Dupont and Vandewalle, 2005).

Orientation factor of a fiber with 1 boundary condition

Suppose that the gravity point of the fiber is within a distance of y from the mold such that y < $l_f/2$. The fiber can no longer rotate freely. The end points describe a sphere that is cut on one side by a sphere cap (Figure 3.4), which also enforces that:

$$\theta < \theta_{crit} = arcsin\left(\frac{2y}{l_f}\right) \qquad \ldots(3.8)$$

Under this condition, the elementary surface dA is still given by Equation 3.6. When the angle θ is bigger than θ_{crit}, the area dA reduces to the bold lines in the cut A–A (Figure 3.4):

$$dA = \underbrace{l_f \sin\theta \cdot arcsin\left(\frac{2y}{l_f \sin\theta}\right)}_{A_2} d\theta \qquad \ldots(3.9)$$

For a fiber with its gravity point at a distance y from the side of the mold, the orientation coefficient becomes:

$$\alpha_y = \frac{\int_0^{arcsin\left(\frac{2y}{l_f}\right)} A_1 \times \cos\theta \, d\theta + \int_{arcsin\left(\frac{2y}{l_f}\right)}^{\pi/2} A_2 \times \cos\theta \, d\theta}{2\pi\left(\frac{l_f}{2}\right)^2 - 2\pi\frac{l_f}{2}\left(\frac{l_f}{2} - y\right)} \qquad \ldots(3.10)$$

The average orientation coefficient for area 2 is calculated as:

$$\alpha_2 = \frac{2}{l_f}\int_0^{l_f/2} \left[\frac{\int_0^{arcsin\left(\frac{2y}{l_f}\right)} A_1 \times \cos\theta \, d\theta + \int_{arcsin\left(\frac{2y}{l_f}\right)}^{\pi/2} A_2 \times \cos\theta \, d\theta}{2\pi\left(\frac{l_f}{2}\right)^2 - 2\pi\frac{l_f}{2}\left(\frac{l_f}{2} - y\right)}\right] dy \qquad \ldots(3.11)$$

Numerical integration of Equation 3.11 returns for α_2 the value 0.60, which is independent of the fiber length (Dupont and Vandewalle, 2005).

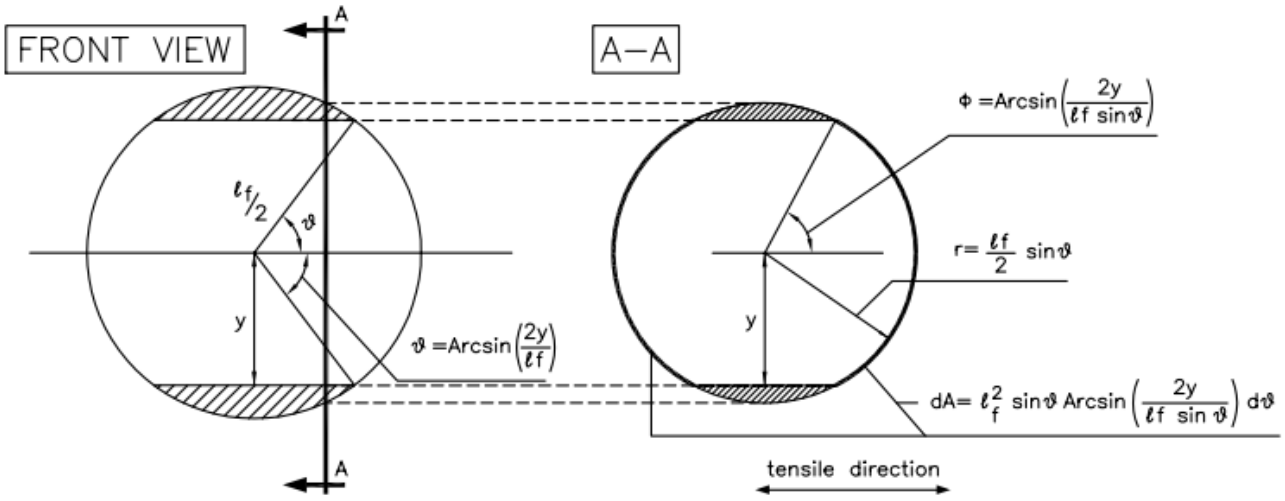

Figure 3.4 A fiber near one side of the mold (Dupont and Vandewalle, 2005).

Orientation factor of a fiber with 2 boundary conditions

This is the case for area 3 in Figure 3.2. Consider a fiber with a gravity center at a distance y from one mold side and at a distance z from another mold that is perpendicular to the first (Figure 3.5). There are two cases:

Firstly, in the case of $y < z < l_f/2$, there is no problem as long as:

$$\theta < \theta_{crit} = arcsin\left(\frac{2y}{l_f}\right) \quad \ldots(3.12)$$

When

$$\theta_{crit} = arcsin\left(\frac{2y}{l_f}\right) \leq \theta \leq \theta_{crit2} = arcsin\left(\frac{2z}{l_f}\right) \quad \ldots(3.13)$$

the area dA can be found with Equation 3.9. If $\theta > \theta_{crit2}$, it can be concluded from Figure 3.5 that the area dA is

$$dA = \underbrace{l_f^2 \sin\theta \left[arcsin\left(\frac{2y}{l_f \sin\theta}\right) - arccos\left(\frac{2z}{l_f \sin\theta}\right)\right]}_{A_3} d\theta \quad \ldots(3.14)$$

Equation 3.14 is only valid, if:

$$z^2 + y^2 > \left(\frac{l_f}{2}\sin\theta\right)^2 \quad \ldots(3.15)$$

If Equation 3.15 is not true, dA should be set equal to 0. The total area of the sphere that is cut on four sides by a sphere cap is calculated as follows:

$$S_1 = \int_0^{arcsin\left(\frac{2y}{l_f}\right)} A_1 d\theta + \int_{arcsin\left(\frac{2y}{l_f}\right)}^{arcsin\left(\frac{2z}{l_f}\right)} A_2 d\theta + \int_{arcsin\left(\frac{2y}{l_f}\right)}^{\pi/2} Max[0; A_3] d\theta \quad \ldots(3.16)$$

Secondly, in the case of $z < y < l_f/2$, for $\theta < \theta_{crit2} = arcsin\,(2z/l_f)$ the surface dA is given by Equation 3.6. For $\theta_{crit2} < \theta < \theta_{crit}$ the surface dA should be calculated as:

$$dA = \underbrace{l_f^2 \sin\theta \times arcsin\left(\frac{2z}{l_f \sin\theta}\right)}_{A_3} d\theta \quad \ldots(3.17)$$

Equation 3.17 is simply found by replacing y for z in Equation 3.9. For $\theta < \theta_{crit}$ the area dA is again calculated by means of Eq. 3.14 taking into consideration the restriction of Equation 3.15. The total area of the sphere that is cut on four sides by a sphere cap is calculated as follows:

$$S_1 = \int_0^{arcsin\left(\frac{2z}{l_f}\right)} A_1 d\theta + \int_{arcsin\left(\frac{2z}{l_f}\right)}^{arcsin\left(\frac{2y}{l_f}\right)} A_2 d\theta + \int_{arcsin\left(\frac{2y}{l_f}\right)}^{\pi/2} Max[0; A_3] d\theta \quad \ldots(3.18)$$

Bringing everything together an expression can be formulated for the orientation coefficient α_3:

$$\alpha_3 = \frac{4}{l_f^2}\int_0^{l_f/2}\left[\int_0^{y} \frac{\int_0^{arcsin\left(\frac{2z}{l_f}\right)} A_1 \cos\theta d\theta + \int_{arcsin\left(\frac{2z}{l_f}\right)}^{arcsin\left(\frac{2y}{l_f}\right)} A_4 \cos\theta d\theta + \int_{arcsin\left(\frac{2y}{l_f}\right)}^{\pi/2} Max[0;A_3]cos\theta d\theta}{S_2} dz + \right.$$

$$\left. \int_y^{\frac{l_f}{2}} \frac{\int_0^{arcsin\left(\frac{2y}{l_f}\right)} A_1 \cos\theta d\theta + \int_{arcsin\left(\frac{2y}{l_f}\right)}^{arcsin\left(\frac{2z}{l_f}\right)} A_2 \cos\theta d\theta + \int_{arcsin\left(\frac{2z}{l_f}\right)}^{\pi/2} Max[0;A_3]cos\theta d\theta}{S_1} dz \right] dy \quad \ldots(3.19)$$

Numerical integration of this integral converges slowly into the value 0.84 and this value is independent of the fiber length (Dupont and Vandewalle, 2005).

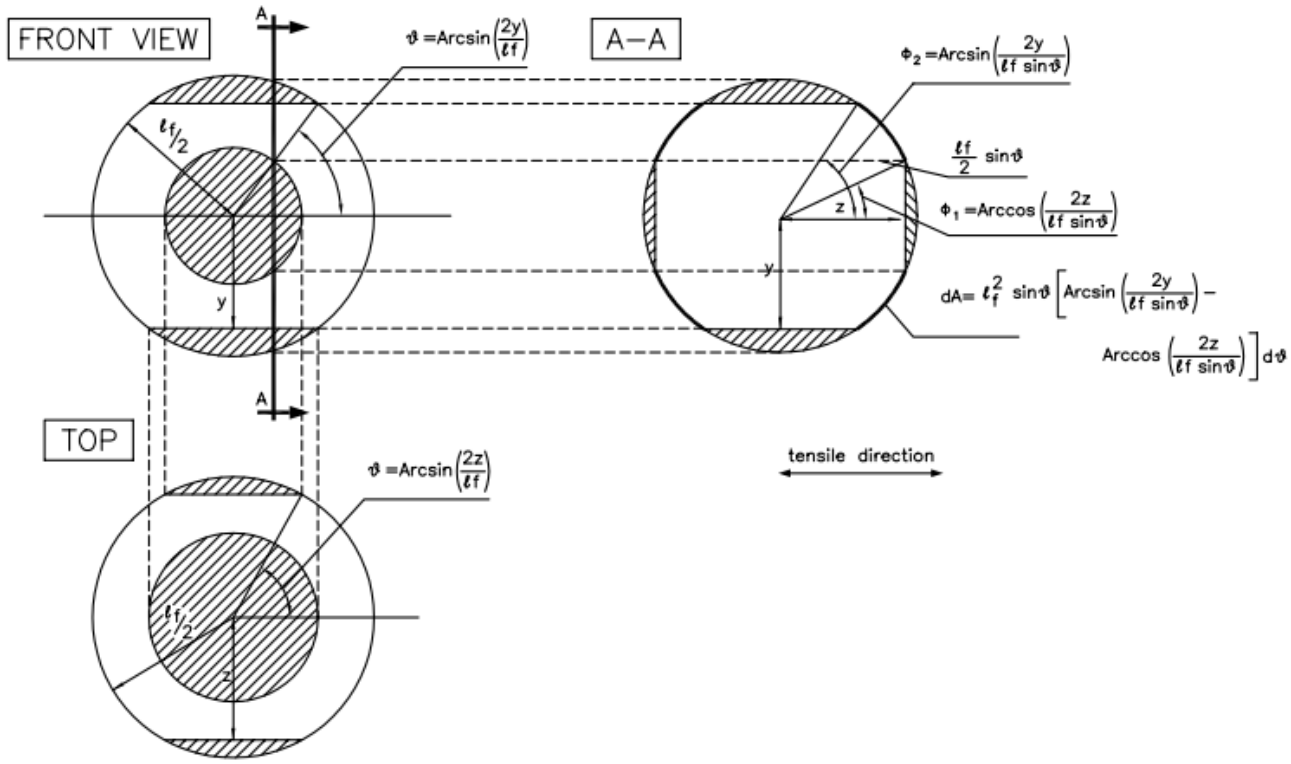

Figure 3.5 A fiber in a corner of the mold (Dupont and Vandewalle, 2005).

In summary, the fib MC2020 (in progress) mentioned that the K factor can be determined experimentally (using Equation 3.4) following the similar procedure of AFGC recommendation (2013) (i.e. suitability test). However, fib MC2020 (in progress) also provides an analytical method to determine α_0 to calculate the K factor based on the geometry of the samples (Equation 3.5 to 3.19). The K factors presented in Tables 3.1 and 3.2 are for different sections and derived based on the procedure described (Equation 3.5 to 3.19). For a different geometry or in cases when there is not enough experimental data, the same procedure can be followed to calculate the α_0 factor.

4. French National Standards

(1) NF P18-710, National addition to Eurocode 2 - Design of concrete structures: specific rules for Ultra-high performance fibre-reinforced concrete (UHPFRC) (2016),
(2) NF P 18-470, Concrete - Ultra-high performance fibre-reinforced concrete - Specifications, performance, production and conformity (2016),
(3) NF P 18-451, Concrete - Execution of concrete structures - Specific rules for UHPFRC (2018)

4.1 Overview

The French Standards Institute (Association Française de Normalisation [AFNOR]) published three French standards on UHPFRC, i.e., NF P 18-710 (2016), NF P 18-470 (2016), and NF P 18-451 (2018). NF P 18-710 (2016) " National addition to Eurocode 2 - Design of concrete structures: specific rules for ultra-high performance fibre reinforced concrete (UHPFRC)" which constitutes a national complement to Eurocode 2, has been prepared within the BNTRA CN EC2 "Design of concrete structures" committee to meet the French requirement to standardize the use of ultra-high performance fiber-reinforced concrete (UHPFRC) in building and civil engineering designs. This standard provides the requirements in terms of resistance, serviceability, durability, and fire resistance for these structures. It applies to the design of buildings and civil engineering structures in unreinforced UHPFRC, reinforced UHPFRC, or prestressed UHPFRC. It complies with the principles and requirements for safety and serviceability of structures and the design and data verification bases in EN 1990: Basis of structural design. This standard is intended to be used in conjunction with the two other standards dealing with the topic of UHPFRCs:

- standard NF P 18-470 (2016) "Concrete - Ultra-high performance fibre-reinforced concrete - Specifications, performance, production and conformity" which deals more specifically with the UHPFRC material itself and which may be considered as an adaptation of the standard NF EN 206 to the case of UHPFRCs, and
- standard NF P 18-451 (2018) "Concrete - Execution of concrete structures - Specific rules for UHPFRC" The present standard is aimed at the design of structures in UHPFRC (buildings and civil engineering structures).

Figure 4.1 shows the architecture of these standards dealing UHPFRCs:

- standard NF P 18-470 (2016), which covers and classifies UHPFRCs without prejudging their application domain
- standard NF P 18-710 (2016), which provides design rules for structures in UHPFRC
- standard NF P 18-451 (2018), which sets out the provisions to be implemented for executing structures in UHPFRC,

The technical concepts of these documents are based on the French AFGC recommendations (revised edition 2013) and the technical feedback of more than 15 years of UHPFRC projects and realizations. NF P 18-710 (2016) has been drafted by adapting Eurocode 2 to the case of UHPFRC structures. The

table of contents for the present standard identically reproduces that of parts 1-1 of Eurocode 2, and where there is no particularity with regards to UHPFRCs, the word "Unchanged" is presented. The sections specific to UHPFRCs are mostly based on the "Structural design methods" section of the recommendations on UHPFRCs by the Association Française de Génie Civil (AFGC) (French Association for Civil Engineering) working group 3.

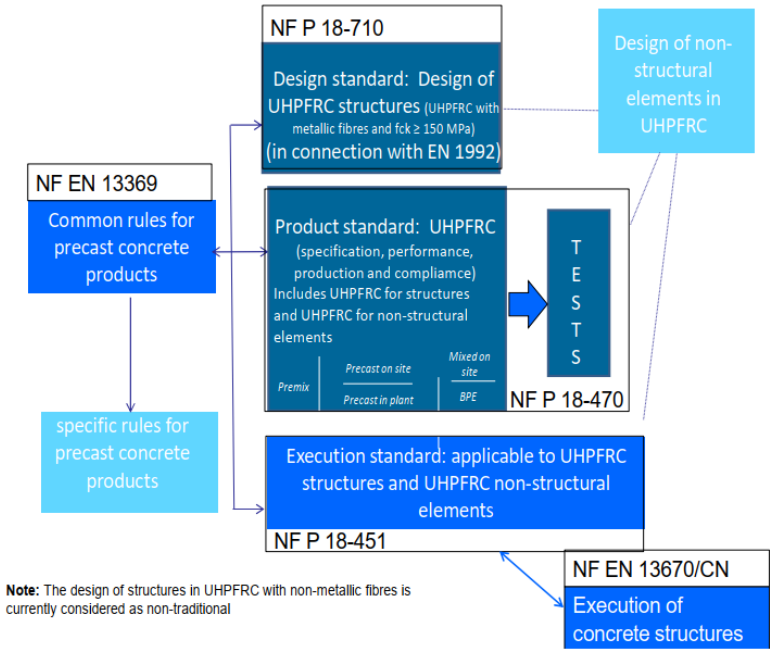

Figure 4.1 French standardization of UHPFRCs — Standards architecture (NF P 18-451, 2018).

4.2 Definition of UHPFRC

The definition of UHPFRC according to NF P 18-470 (2016) is concrete characterized by a high compressive strength (greater than 150 MPa or 21,750 psi), high post-cracking tensile strength giving ductile behavior under tension, and whose lack of brittleness makes it possible to design and produce structures and structure members without using reinforcing steel. This standard, therefore, covers the use of UHPFRCs of classes 150/165 (minimum characteristic cylinder strength 150 MPa or 21,750 psi and minimum characteristic cube strength 165 MPa or 23,925 psi) and above containing steel fibers, which is included in design standard NF P 18-710 (2016). It also covers the use of UHPFRCs containing other types of fibers or UHPFRCs with a lower strength (130 MPa or 18,850 psi), which is not referred to in NF P 18-710 (2016). These UHPFRCs may be used in non-structural or architectonic structures.

According to the nature of the fibers contributing to the strain hardening behavior under flexure, the UHPFRCs are classified as type M when these are metallic fibers and type A when these are other fibers, in particular organic fibers. Again, UHPFRCs of type M whose characteristic compressive strength is at least 150 MPa (21,750 psi) are graded UHPFRC-S and whose characteristic compressive strength is greater than 130 MPa (18,850 psi) and strictly less than 150 MPa (21,750 psi) are graded

UHPFRC-Z. Only the UHPFRC-S concretes are deemed usable for designing structures, precast products, and precast elements of structures in accordance with standard NF P 18-710 (2016). These UHPFRCs, therefore, demonstrate the following attributes:

- Type M UHPFRCs
- characteristic compressive strength f_{ck} is between 150 MPa and 250 MPa (21,750 psi and 36,250 psi)
- characteristic tensile strength $f_{ctk,el}$ is greater than 6.0 MPa (870 psi)
- density should be between 2300 and 2800 kg/m^3 (144 and 175 lb/ft^3)
- sufficiently ductile behavior under tension such that:

$$\frac{1}{w_{0.3}} \int_0^{w_{0.3}} \frac{\sigma(w)}{1.25} dw \geq \max\left(0.4 f_{ctm,el}; 3\ MPa\right) \qquad \ldots(4.1)$$

where, $w_{0.3}$ = 0.3 mm, $f_{ctm,el}$ is the mean value of the tensile limit of elasticity, $\sigma(w)$ is the characteristic post-cracking stress as a function of the crack width, w. As per NF P 18-470 (2016), characteristic strength is the value of strength above which 95 % of the test results are expected to fall. The characteristic strength is estimated from a sample of experimental values assuming a normal distribution.

4.3 Fiber orientation factor

The whole concept of the fiber orientation factor introduced in the AFGC recommendation (2013) is adopted to the French National Standards NF P 18-470 (2016) and NF P 18-710 (2016). These recommendations completely follow the AFGC recommendation (2002 and 2013) and the background of fiber orientation factor is the same as the AFGC recommendation (2002 and 2013) as discussed earlier.

5. ACI 239C Emerging Technology Report (ETR) (2018 and 2019) (Draft copy)

5.1 Overview

The ACI 239C "Structural Design of Ultra-High Performance Concrete" (UHPC) Subcommittee was formed in 2015 with the mid-term goal of developing a new structural design guide for UHPC. Under the guidelines of the American Concrete Institute (ACI), an Emerging Technology Report (ETR) (an overview of the methods for the structural design of ultra-high performance concrete) on the structural design of ultra-high performance concrete was prepared by the subcommittee ACI 239C. The ETR was planned to cover the background and brief outline of the future structural design document and other North American code and standard developments, with an overview of the technology development and challenges facing the deployment.

The ACI 239C ETRs (The Structural Design of Ultra-High Performance Concrete, 2018; and Overview of the Methods for the Structural Design of Ultra-High Performance Concrete, 2019) give an overview of the Structural Design of Ultra-High Performance Concrete (UHPC). It briefly introduces UHPC and its properties and design principles. It is not intended to provide mandatory design rules, but rather to serve as a starting point for the structural engineer to understand design methodologies for this class of materials.

This ETR integrates national and international experiences with UHPC and utilizes recent experimental and computational research to describe a design basis that advances UHPC design and construction. Structural design considerations for cast-in-place concrete and precast construction methods are noted. But the document does not cover or develop new test methods or construction methods.

5.2 Definition of UHPC

The ACI 239C ETR (2018) discussed the use of ultra-high performance concrete (UHPC), which is defined as a cementitious composite material, normally containing fibers, with enhanced strength, durability, and ductility compared to high performance concretes. UHPCs normally contain fibers for post-cracking ductility, should have a specified compressive strength of at least 120 MPa (17,400 psi) by 28 days, and are formulated with a modified multi-scale particle packing of inorganic materials of normally less than 0.6 mm diameter (larger sizes may be used). The UHPC should possess a tensile post-cracking ductility with a minimum specified direct tensile strength of 4.0 MPa (580 psi). As per ACI 239C ETR (2018), the term UHPFRC is sometimes used to denote UHPC containing fibers.

5.3 Fiber orientation factor

The ACI 239C ETR (2018) adopted the concept of fiber orientation factors and suitability test from French national recommendations (AFGC recommendations 2013) and French national standard (NF P 18-470, 2016 and NF P 18-710, 2016). Here the local and global fiber orientation factors are denoted as K_L and K_G, respectively, and defined as follows:

K_L = a factor calculated by comparing the flexural strength to that of a molded specimen with cast specimen to determine the local impact of random fiber orientation (AFGC Recommendation)

K_G = a factor calculated by comparing the flexural strength to that of a molded specimen with cast specimen to determine the global impact of random fiber orientation (AFGC Recommendation)

The ACI 239C ETR (2018) recommends following the procedure in AFGC recommendation (2013) to calculate the K_L and K_G and considered K_L=1.7 and K_G=1.3 in the case of lack of a suitability test. Currently, only the draft copies of the ACI 239C ETR (2018 and 2019) are available, and these do not provide detailed information about the application of the fiber orientation factor in structural design. This document only provides a summary of design methodologies currently reported in the literature and available for the designer; however, it is not a design standard, nor a guide or specification. The document also does not provide test methods for the characterization of UHPC, but it does present options for obtaining the mechanical properties based on available test methods. The characterization of the mechanical properties of UHPC will be covered in a separate American Concrete Institute (ACI) Guide on Materials and Methods of Construction for UHPC. At the time of being, this document is still under development.

6. Korean Guidelines

(1) KICT Design Guideline for K-UHPC (2014)
(2) KCl-M-19-006, The Structural Design Guidelines of Fiber Reinforced SUPER Concrete (2019)

6.1 Overview

The Korea Concrete Institute established the "Design Guidelines for Ultra High Performance Concrete (K-UHPC) Structure" in 2014 based upon the structure and contents of the "Structural Concrete Design Code" (2012) enacted by the Korea Concrete Institute (KCI). This guideline reflects the latest worldwide research results and the achievements of the Super Bridge 2004 Project of the Korean Institute of Construction Technology (KICT) and compiles and analyzes foreign specifications dedicated to the design of UHPC structures under the supervision of experts and designers who participated in the establishment of the "Structural Concrete Design Code". This provisional guideline specifies the minimal requirements necessary to secure the safety, serviceability, and durability of structures using the Ultra High Performance Concrete developed by the KICT (hereinafter referred to as K-UHPC). These guidelines specify the general and basic requirements necessary for the design of K-UHPC structures.

The KCI also published the “Structural Design Guidelines of Fiber Reinforced SUPER Concrete” in 2019. This guideline is also structured with reference to the Structural Concrete Design Code (2012). It compiled the latest research conducted worldwide on UHPC as well as the achievements of the project “Development of SUPER Concrete with Compressive Strength of 80~180 MPa and its Applications (Super Structure 2020)” performed by KICT and were prepared by comparative analysis with the structural design codes on UHPC published worldwide. This guideline is to specify the minimum requirements necessary to secure the safety, serviceability, and durability of structures using high performance fiber reinforced concretes with compressive strength of 120 MPa (17,400 psi), 150 MPa (21,750 psi), and 180 MPa (26,100 psi) (hereinafter referred to as fiber-reinforced SUPER Concrete or FRSC) developed by the SUPER STRUCTURE 2020 Research Group.

6.2 Definition of K-UHPC and FRSC

The KICT Design Guideline focused on the application and design of the material K-UHPC, which is a special type of Ultra High Performance Concrete (UHPC) developed by KICT. The average compressive strength of K-UHPC is 198.68 MPa (28,809 psi) with a standard deviation of 9.49 MPa (1,376 psi). Assuming a normal distribution, the characteristic compressive strength is found to be 188.75 MPa (27,389 psi) if a probability of 5% is considered for the compressive strength of the cylinders to fall below the characteristic strength. Accordingly, a conservative value of 180 MPa (26.100 psi) can be recommended for the characteristic compressive strength, f_{ck}. The characteristic crack strength is 9.5 MPa (1,378 psi), and the characteristic tensile strength is 13.0 MPa (1,885 psi) (determined by direct tension test of dogbone specimens).
KCl-M-19-006 document focused on the Fiber reinforced SUPER Concrete or FRSC, which is high performance fiber reinforced concretes with compressive strength of 120 MPa, 150 MPa and 180 MPa

(17,400 psi, 21,750 psi, and 26,100 psi) developed by the "SUPER STRUCTURE 2020" Research Group. FRSC is categorized into the following types:

(1) SC120f: High performance fiber reinforced concrete with compressive strength of 120 MPa (17,400 psi) developed by the SUPER STRUCTURE 2020 Research Group. The characteristic compressive strength f_{ck} of SC120f shall be 120 MPa (17,400 psi), and the average compressive strength f_{cm} shall be 132 MPa (19,140 psi), the characteristic tensile strength f_{ctk} and the average tensile strength f_{ctm} of SCI20f shall be 7.0 MPa (1,015 psi) and 10.0 MPa (1,450 psi), respectively.

(2) SC150f: High performance fiber reinforced concrete with compressive strength of 150 MPa (21,750 psi) developed by the SUPER STRUCTURE 2020 Research Group. The characteristic compressive strength f_{ck} of SC120f shall be 150 MPa (21,750 psi), and the average compressive strength f_{cm} shall be 161 MPa (23,345 psi), the characteristic tensile strength f_{ctk} and the average tensile strength f_{ctm} of SCI20f shall be 9.0 MPa (1,305 psi) and 11.0 MPa (1,595 psi), respectively.

(3) SC180f: High performance fiber reinforced concrete with compressive strength of 180 MPa (26,100 psi) developed by the SUPER STRUCTURE 2020 Research Group. The characteristic compressive strength f_{ck} of SC120f shall be 180 MPa, and the average compressive strength f_{cm} shall be 189 MPa (27,405 psi), the characteristic tensile strength f_{ctk} and the average tensile strength f_{ctm} of SCI20f shall be 11.0 MPa (1,595 psi) and 13.0 MPa (1,885 psi), respectively.

6.3 Reduction factors addressing the fiber orientation factor

Unlike the concept of fiber orientation factors considered in AFGC recommendation, both the KICT and KCI guidelines follow the concept of material reduction factor (material factor) similar to JSCE Recommendations (Recommendations to the Japanese Provisional Recommendations for the Design and Construction of Ultra High Strength Fiber-Reinforced Concrete (UHSFRC) of JSCE, 2004).

As per JSCE Guidelines 2007 (Standard Specifications for Concrete Structures 2007 "Design", JSCE Guidelines for concrete, No.15), the material factor defines as the safety factor to consider the unfavorable deviations of material strengths from the characteristic values, differences in material properties between test specimens and actual structures, the effect of material properties on the specific limit states, and time-dependent variations of material properties. In addition, a separate member factor is defined as the safety factor to consider the uncertainties in the computation of capacity of the member, differences in the design and actual size of the member, and the importance of the member which reflects the influence on the overall structure when it reaches a certain limit state. The material reduction factor and the constitutive laws considered by these two guidelines (KICT guideline and KCI guidelines) are mostly the same, and the constitutive law is presented later in this section. However, due to the fact that it is still difficult to clearly determine the fiber orientation effect for K-UHPC and FRSC due to insufficient experimental data, these guidelines conservatively calculate the design strength by applying simultaneously the material reduction factor and the member reduction

factor (multiplying them to get the final safety factor).

Table 6.1 presents the material reduction factor and member reduction factor for K-UHPC and FRSC. As mentioned above, due to insufficient experimental data to find out appropriate fiber orientation factors by a similar procedure as AFGC recommendations (2013), the Final report on FRSC (2020) updated the member reduction factor to match the overall reduction factor in UHPFRC designs. The latest changes of the member reduction factors for FRSC are presented in the rightmost column as per the Final report on FRSC (2020).

Table 6.1 Material reduction factor and member reduction factor for K-UHPC and FRSC

Material condition	KICT 2014	KCI 2019	Member condition	KICT 2014	KCI 2019	Final report on FRSC 2020
	Material reduction factor in K-UHPC ϕ_c	Material reduction factor in FRSC ϕ_c		Member reduction factor in K-UHPC ϕ_b	Member reduction factor in FRSC ϕ	Member reduction factor in FRSC ϕ
Comp.	0.91	1.00 (SLS) 0.80 (ULS)	Flexure	0.77	0.90	0.80
Tension	0.80	1.00 (SLS) 0.80 (ULS)	Flexure+ Comp.	0.77	0.90	0.80
			Comp.	0.77	0.75	0.80
			Shear	0.77	0.80	0.80
			Torsion	0.77	0.80	0.80

These guidelines describe the effects of the material reduction factor ϕ_c on compressive and strain-hardening tensile stress-strain curves as shown in Figure 6.1. Both of the stress-strain curves consider the effect of fiber orientation using the material reduction factor. The compressive stress-strain curve shows a linear behavior up to $0.85\phi_c f_{ck}$ followed by a plateau up to $\varepsilon_{cu} = f_{ck}/E_C$ (for FRSC and for K-UHPC up to 0.004 strain), where f_{ck} is the characteristic compressive strength of K-UHPC and FRSC, ε_{cu} is the ultimate strain. The strain-hardening tensile stress-strain curve presents a linear response up to $\phi_c f_{crk}$ and followed by strain hardening response up to $\phi_c f_{tk}$ and then a gradual decrease of tensile strength to zero at ε_{lim}, where f_{crk} = characteristic crack strength of K-UHPC/FRSC, f_{tk} = characteristic tensile strength of K-UHPC/FRSC, E_c is the modulus of elasticity of K-UHPC/FRSC, L_{eq}= equivalent length used to transform the tension softening curve into tensile stress-strain curve considering the height of the beam, w_u = crack opening displacement or crack width at tensile strength caused by strain-softening after cracking, w_{lim} = crack opening displacement or

crack width once tensile stress vanishes, ε_{lim} = strain once tensile stress vanishes. The L_{eq} is calculated using the following equation:

$$\frac{L_{eq}}{h_{beam}} = 0.8\left[1 - \frac{1}{\left(1.05+6\frac{h_{beam}}{l_{ch}}\right)^4}\right] \qquad \ldots(6.1)$$

Where, h_{beam} is the height of beam (mm), l_{ch} is characteristic length $=G_F E_c / f_{tk}^2$=1.01×10^4 mm (397.63 in), G_F is fracture energy of K-UHPC/FRSC = 37.9 MPa (5,496 psi), E_c is elastic modulus of K-UHPC/FRSC (4.5x10^4 MPa (6,525,000 psi) for K-UHPC, 4.1x10^4 MPa (5,945,000 psi) for SC120f, 4.4x10^4 MPa (6,380,000 psi) for SC150f , and 4.7x10^4 MPa (6,815,000 psi) for SC180f), f_{tk} is characteristic tensile strength of K-UHPC/FRSC (13 MPa (1,885 psi) for K-UHPC, 10.7 MPa (1,552 psi) for SC120f, 11.1 MPa (1,610 psi) for SC150f, and 12.7 MPa (1,842 psi) for SC180f).

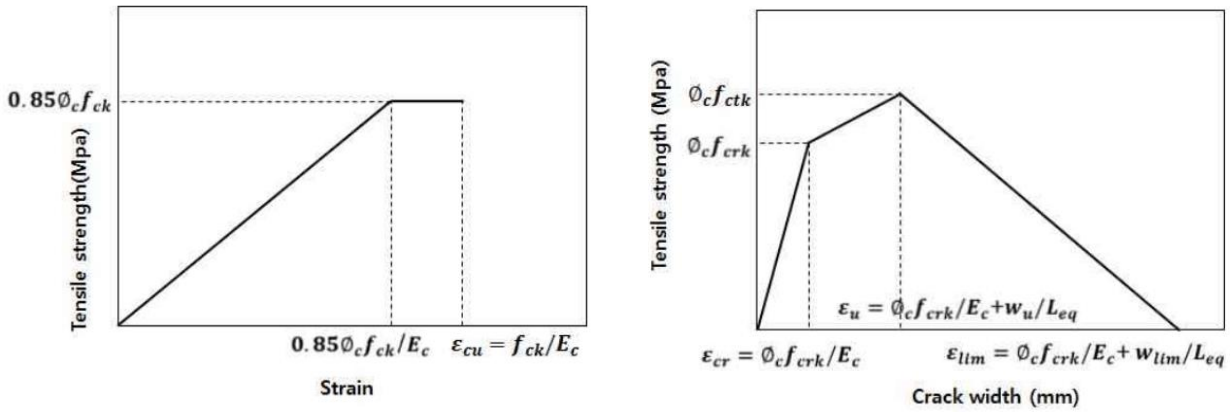

(a) (b)

Figure 6.1 Stress-strain curve of K-UHPC and FRSC: (a) compressive; (b) tensile (KICT Design Guideline for K-UHPC 2014).

The KICT and KCI guidelines also provide a method for calculating crack width of K-UHPC or FRSC analytically for serviceability check. In this procedure, they consider another orientation factor of steel fiber, η. This orientation factor is only used for this specific purpose in these documents. The equation of the factor is as follows:

$$\eta = \frac{\eta_{1D} l_f + \eta_{2D}(b - l_f)}{b} \qquad \ldots(6.2)$$

where b = maximum dimension of the placed member cross-section (mm); and η_{1D} =1.0 and η_{2D}=0.637; l_f is the length of the fiber.

6.4 Discussion on reduction factors addressing the fiber orientation factor

As mentioned previously, these guidelines do not directly consider the effect of fiber orientation and dispersion on the structural behavior of K-UHPC and FRSC structures, rather these guidelines used the concept of material reduction factors following JSCE recommendations for HPFRCC (2008) and UFC (2006), which adopted the concept from Eurocode 2 (Final report on FRSC, 2020. SUPER Concrete structural performance verification and Development of design guidelines, Korea Concrete Society). The Final report on FRSC (2020) declares that, due to insufficient experimental data for the reliability analysis and determination of fiber orientation factor, the KCI and KICT recommendation followed the similar concept of safety factors (to apply both the material factor and the member factor) of JSCE.

Table 6.2 Comparison of the design safety factors in different UHPC or UHPFRC guidelines (Final report on FRSC, 2020)

	FRSC (KCI) and K-UHPC (KICT) Design Guidelines (as per Final report on FRSC 2000)	AFGC recommendation (2013)	JSCE recommendation (2006)
Reduction Factors	Member reduction factor ϕ = 0.80 Material reduction factor ϕ_c=0.80	γ_E=Safety factor, $\gamma_c\gamma_E$=1.3 Fiber orientation factor (K_{global})=1.25	Member factor γ_b = 1.3 Material factor γ_c = 1.3
Overall safety factor	0.80×0.80=0.640	1/(1.25×1.3)=0.615	1/(1.3×1.3)=0.592

As indicated in Section 6.3, the Final report on FRSC (2020) revised the values of the material reduction factors to make the overall safety factors comparable to the AFGC recommendation (2013) and JSCE recommendation (2006) (Table 6.1). Table 6.2 presents the comparison of the design safety factors in different UHPC guidelines, e.g., material reduction factor, fiber orientation factor, and material factor for KCI and KICT, AFGC, and JSCE recommendations. The bottom row of the table presents the overall safety factors considering in the case of AFGC recommendations and not considering in the case of KCI, KICT, and JSCE recommendations fiber orientation factor, where the values are very close. For this reason, the Final report on FRSC (2020) states that the effect of the orientation of the steel fibers in K-UHPC and FRSC is reflected by applying a material reduction factor and member reduction factor, as the overall safety factors are pretty close to the AFGC Recommendations (Table 6.2).

7. Swiss Society of Engineers and Architects (SIA), Béton fibré ultra-performant (BFUP); Matériaux, dimensionnement et exécution (2016) (SIA 2052:2016)

7.1 Overview

In December 2014, the Swiss Society of Engineers and Architects (SIA) published SIA 2052: "UHPC: Material, Design, and Construction (Béton fibré ultra-performant [BFUP]: Matériaux, dimensionnement et exécution)". The document provides rules for the design of non-reinforced, reinforced, and prestressed structures with UHPFRC. In addition, it provides a design methodology for composite structures of conventional reinforced concrete with UHPFRC thin bonded overlays. The second edition of SIA 2052 was made available in 2016. The purpose of this technical guide is to regulate the use of ultra-high-performance fiber-reinforced concrete (UHPFRC) in the production project, sizing, and execution of load-bearing structures.

7.2 Definition of UHPFRC

As per SIA 2052 (2016), the Ultra-high performance fiber reinforced concrete (UHPFRC) is a composite material produced from cement, fine aggregates, water, additives, and short fibers. Its high compactness makes it impermeable to liquids. Generally, the characteristic value of its compressive strength is greater than 120 MPa (17,400 psi) at 28 days. Compared to traditional fiber reinforced concrete, UHPFRC is characterized by small aggregate size, a particularly high percentage of fibers, high compactness, and high mechanical properties. The load-bearing structures and the prefabricated elements made of UHPFRC are designed with the aim of minimizing the dimensions of the sections and the dead load. UHPFRCs are highly solicited for long-span roofs, building slabs, bridges, or other structural works, and also facade elements in which the synthetic fibers are frequently used.

7.3 Coefficient related to the orientation of the fibers

The SIA 2052 introduces two coefficients related to the orientation of the fibers in UHPFRC as follows:

η_K =coefficient related to the orientation of the fibers of UHPFRC, depending on the structural element and the manufacturing process (irregular distribution of fibers); and the values are shown below:

- η_K = 0.90 in the case of overall behavior (redistribution of stresses is possible, for example in slabs or hyperstatic systems),
- η_K = 0.75 in the case of localized behavior (no possibility of redistribution of the stresses, for example in the anchoring zones)

η_{hU}=coefficient considering the influence of the thickness of the UHPFRC layer or the thickness of the element as well as the manufacturing process on the orientation of the fibers. Figure 7.1 contains the data for determining the coefficient η_{hU}.

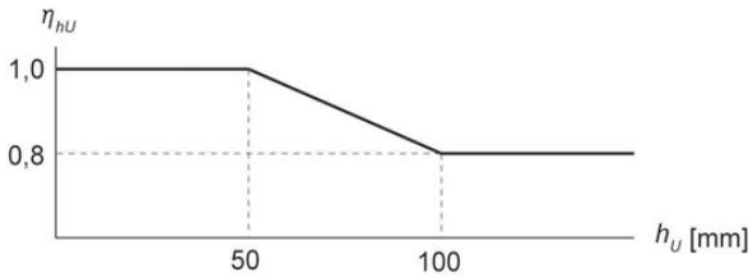

Figure 7.1 Coefficient for taking into account the thickness (h_u) of the element and the manufacturing process (SIA 2052:2016).

The tensile behavior of UHPFRC is characterized by the following material constitutive laws shown in Figure 7.2:

a) A bilinear stress-strain constitutive law for strain-hardening behavior (Figure 7.2a): It describes the elastic behavior of UHPFRC up to f_{Ute} and strain-hardening behavior from f_{Ute} to f_{Utu}, where f_{Ute} and f_{Utu} are the elastic limit under tension and ultimate tensile strength of UHPFRC, respectively, and ε_{Utu} is the ultimate tensile strain of UHPFRC.

b) A stress – crack opening displacement constitutive law for strain-softening behavior (Figure 7.2b): It describes the non-linear softening behavior of UHPFRC. After reaching the tensile strength of f_{Utu}, the stress gradually reduces to zero at maximum softening crack opening in UHPFRC ($w_{Ut,max}$). Here G_{FU} and E_{Ut} are the specific energy of rupture of UHPFRC and modulus of elasticity of UHPFRC under tension, respectively.

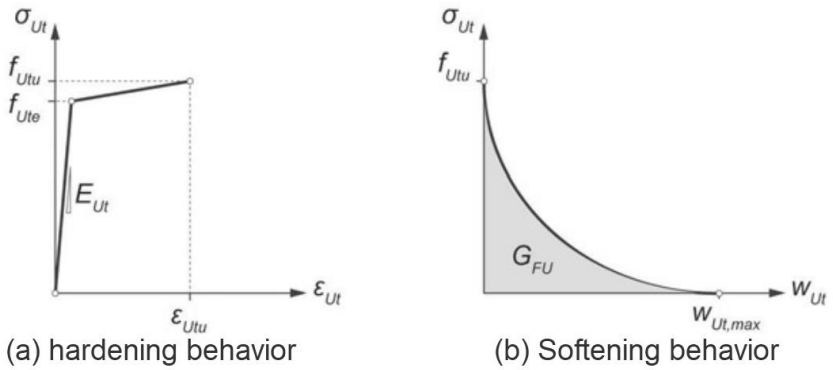

Figure 7.2 Idealized material laws for UHPFRC types (SIA 2052:2016).

In the case of reinforced UHPFRC, the following constitutive law is considered (Figure 7.3). The bilinear behavior of the reinforced UHPFRC under tension is obtained by linear superposition of the constitutive laws of UHPFRC materials and passive reinforcing steel.

All the strength parameters of these constitutive laws are the function of η_{hU} and η_k. Incorporating

these factors, the design tensile strengths of UHPFRC are calculated as follows:

$$f_{Utud} = \frac{\eta_t \eta_{hU} \eta_k f_{Utuk}}{\gamma_U} \qquad \ldots(7.1)$$

$$f_{Uted} = \frac{\eta_t \eta_{hU} \eta_k f_{Utek}}{\gamma_U} \qquad \ldots(7.2)$$

where, f_{Utud} is UHPFRC design tensile strength value, f_{Utuk} is the characteristic value of the ultimate tensile strength of UHPFRC measured by a uniaxial test of dogbone specimens, f_{Uted} is the design value of elastic tensile strength of UHPFRC, f_{Utek} is the characteristic value of the elastic tensile strength of UHPFRC by a uniaxial test of dogbone specimens, η_t is the coefficient considering the duration of loading on UHPFRC, γ_U is the resistance coefficient for structural safety (a design safety factor).

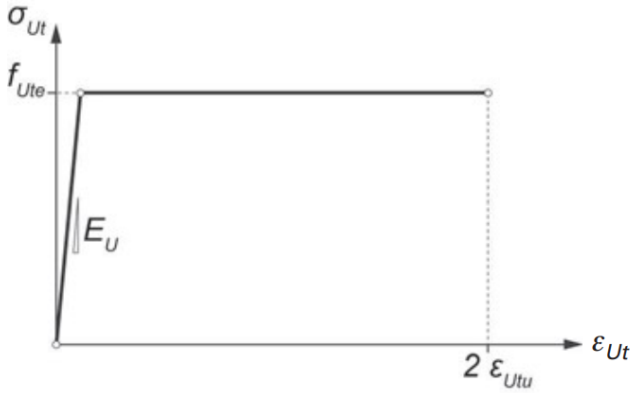

Figure 7.3 Constitutive law of reinforced UHPFRC under tension (SIA 2052:2016).

7.4 Discussion

After reviewing extensive literatures, we are still uncertain about the exact background of the factors discussed in 7.3 from SIA 2052:2016. However, Loser et al. (2018) mentioned the research effort at EMPA (Swiss Federal Laboratories for Materials Science and Technology, Dübendorf, Switzerland), which seems to be concurrent with the development of the code and provides a validation of the code procedures. Therefore, the relevant EMPA experimental studies are documented here for reference.

Figure 7.4 presents one of the important efforts of EMPA, which shows the results of direct tensile tests according to the SIA 2052:2016 guidelines on the same mixture produced by a UHPFRC manufacturer. The different curves were obtained by testing specimens produced with different casting procedures under laboratory and field conditions. The black curves (Figure 7.4) correspond to the first trial, in which the specimens were produced in the manufacturer's laboratory and brought to the testing lab. The measured post-peak behavior has a large scatter, and the curves do not show any clear strain-hardening behavior for all specimens. Based on these results, the composition of the mixtures was adjusted, and the test result of the adjusted mixture casts are presented as the green curves (Figure 7.4). There was still a considerable scatter in the results, with some specimens showing a distinct strain-hardening behavior and others without any strain-hardening, even if the manufacturer paid

special attention when filling the formworks properly. These happened due to the inhomogeneity usually coming from small vortices during casting, in which locally the fibers align perpendicularly to the tensile test direction and resulted in localized cracks instead of multiple cracks as shown in Figure 7.5 (left). To investigate further, the formwork was filled in several layers with a long half-pipe (chute), allowing the UHPFRC to flow very homogeneously into the formwork from one side to another. The filling in several layers should reduce the probability of local inhomogeneities. The modification resulted in the blue curves (Figure 7.4) which show distinct strain hardening behavior. As the last step, the UHPFRC was produced and filled in several layers with a long half pipe again with the identical mixture composition but at the construction site, with disadvantageous production conditions compared to laboratory conditions. The obtained tensile strengths (red curves in Figure 7.4) for these specimens were somewhat lower and with a larger scatter compared to lab conditions (green curves). However, the scatter in the red curves, representing the material properties of the UHPFRC produced under construction site conditions is very limited up to quite large strains and increases only thereafter. In any case, the values are much higher and more homogeneous compared to black and green curves, which emphasizes the importance of the manner of formwork filling. The results show that for the same mixture composition, due to differences in the casting procedure, it could result in different fiber orientations within the specimens (Figure 7.5) and thereby varying mechanical performance. The difference could be significant enough to result in different classifications of UHPFRC per SIA 2052: 2016 (Table 7.1).

Table 7.1 Classes of UHPFRC according to SIA 2052:2016

Class	U0	UA	UB
f_{Utek} (N/mm^2)	≥7.0	≥7.0	≥10.0
f_{Utuk}/f_{Utek}	>0.7	>1.1	>1.2
ε_{Utu} (‰)		>1.5	>2.0
f_{Uck} (N/mm^2)	≥120	≥120	≥120

Note: f_{Utek}: the characteristic value of elastic limit tensile strength; f_{Utuk}: the characteristic value of tensile strength; f_{Utu}: strain-hardening (strain at tensile strength); f_{Uck}: the characteristic value of compressive strength.

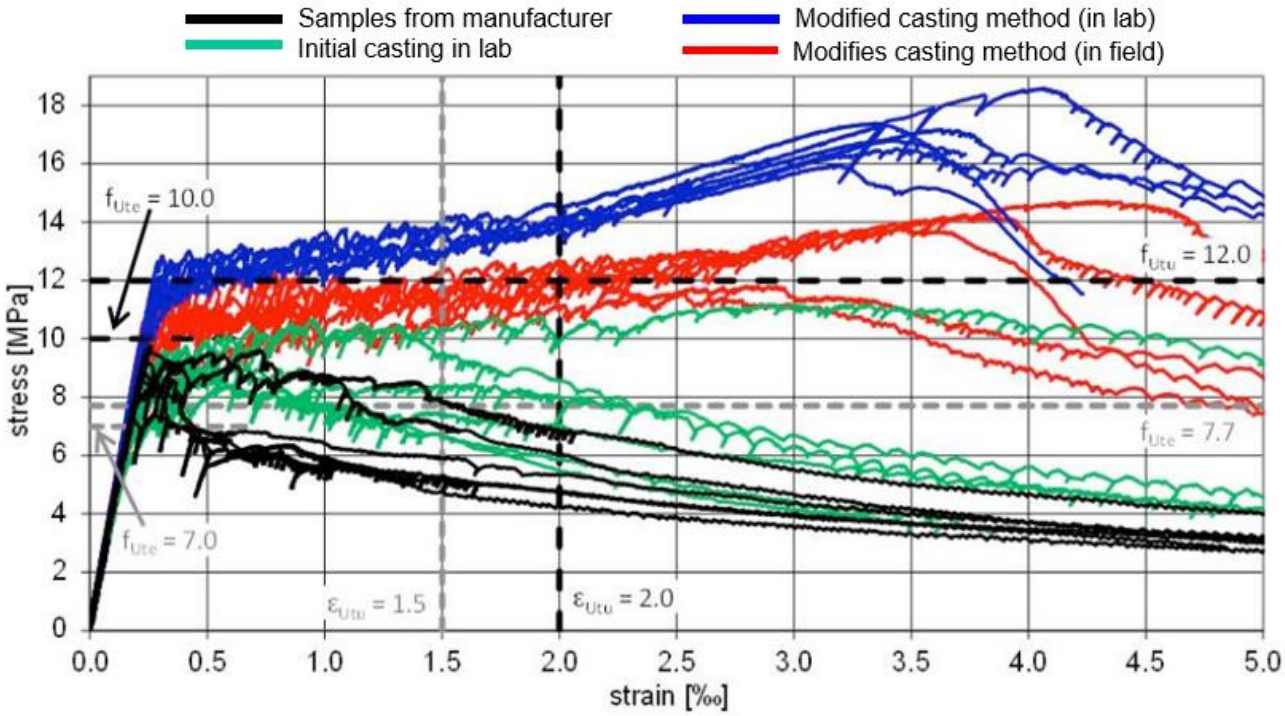

Figure 7.4 Example curves from direct tensile tests according to the SIA 2052 guidelines for the development of a UHPFRC mixture. Series of 6 specimens for every trial. Including limit values for class UA (dashed gray) and UB (dashed black) (Loser et al. 2018).

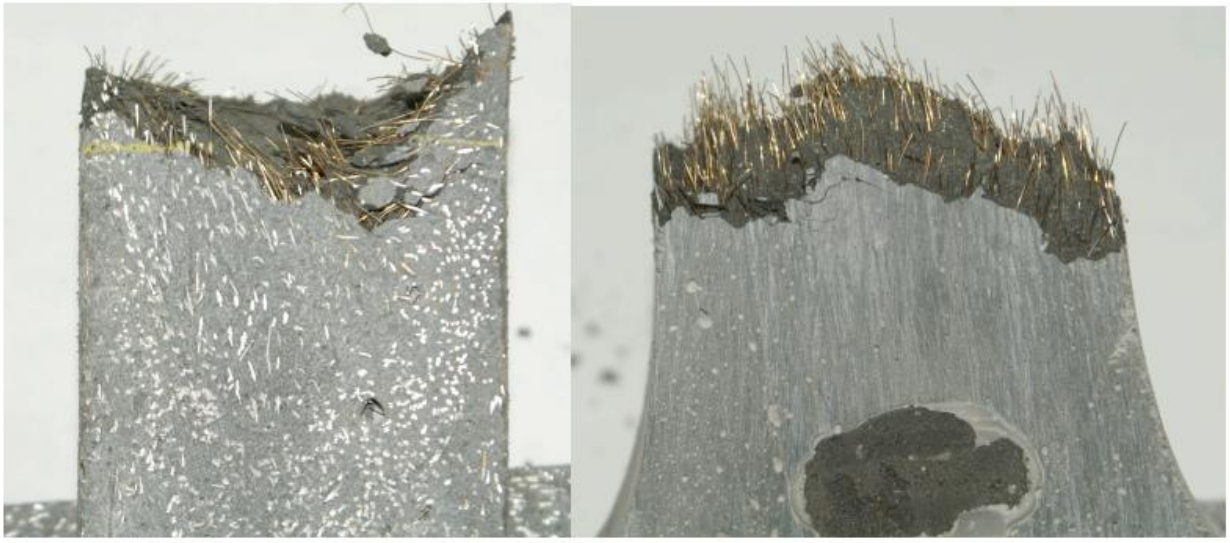

Figure 7.5 Fiber orientation in the fractured cross-section of the final localized crack, shown for two specimens of the same testing series. A specimen without any strain hardening (left) and with distinct strain-hardening (right) (Loser et al. 2018).

The experience demonstrated that only a well-controlled fiber orientation resulted in reproducible and desirable mechanical performance under uniaxial tensile tests. However, these results can only be directly transferred to structures for the case of slender members loaded in tension. In the case of slabs, the fiber orientation is at least 2D, invariably resulting in lower mechanical properties. This confirmed the need for consideration of the fiber orientation of structural members in the design code. Thereby, in the SIA 2052 guidelines, two reducing factors that take into account the fiber orientation are defined as outlined in 7.3. h_k is the fiber orientation factor, which is 0.90 in the case of global load-bearing (redistribution of stresses is possible) and 0.75 in the case of local load-bearing (no stress redistribution is possible). h_{hU} takes into account the influence of the thickness of the component and is going from 1.0 for thicknesses up to 50 mm down to 0.8 for thicknesses up to 100 mm. However, the EMPA study also indicated that comparing these factors with the results in Figure 7.4, a preliminary conclusion can be drawn that they do not appear to be conservative for the case of the specific UHPFRC examined here.

8. Australian Standard, Concrete Structures (2018) (AS 3600)

8.1 Overview

The Concrete structures (2018) (AS 3600) was prepared by Standards Australia Committee BD-002, Concrete Structures, to supersede AS 3600-2009. The principal objective of this Standard is to provide users with nationally acceptable unified rules for the design and detailing of concrete structures and members, with or without steel reinforcement or prestressing tendons, based on the principles of structural engineering mechanics. In this edition, Section 16 (Steel Fibre Reinforced Concrete) and Appendix C (Residual Tensile Strength Test for SFRC) are added to address the specification related to steel fiber reinforced concrete (SFRC). This guideline does not focus on UHPC or UHPFRC, however, it is still reviewed as they provide relevant information on the fiber orientation factors.

8.2 Definition of SFRC

As per AS 3600, the steel fiber reinforced concrete (SFRC) is the mixture of concrete and steel fiber, and SFRC is classified in terms of both its characteristic compressive (cylinder) strength (f'_c) and its characteristic residual tensile strength ($f'_{1.5}$). The characteristic compressive strength of concrete at 28 days (f'_c) shall be either-

(a) taken as equal to the specified strength grade, provided the curing is ensured and that the concrete conforms with AS 1379; or

(b) determined statistically from compressive strength tests carried out in accordance with AS 1012.9. The characteristic compressive strengths of the standard strength grades are 20 MPa, 25 MPa, 32 MPa, 40 MPa, 50 MPa, 65 MPa, 80 MPa, and 100 MPa (2,900 psi, 3,625 psi, 4,640 psi, 5800 psi, 7,250 psi, 9,425 psi, 11,600 psi, and 14,500 psi) for different structural requirements.

The standard characteristic residual tensile strength grades ($f'_{1.5}$) are 0.4 MPa, 0.6 MPa, 0.8 MPa, 1.2 MPa, 1.6 MPa, and 2.0 MPa (58 psi, 87 psi, 116 psi, 174 psi, 232 psi, and 290 psi). The characteristic residual tensile strengths of concrete at 28 days ($f'_{1.5}$) shall be determined statistically from tests carried out by direct tensile testing. Table 8.1 presents the properties of the standard grades of SFRC at 28 days.

Table 8.1 Properties of standard grades of SFRC at 28 days

f'_c	MPa (psi)	20 (2,900)	25 (3,625)	32 (4,640)	40 (5,800)	50 (7,250)	65 (9,425)	80 (11,600)	100 (14,500)
f_{cm}	MPa (psi)	25 (3,625)	31 (4,495)	39 (5,655)	48 (6,960)	59 (8,555)	75 (10,875)	91 (13,195)	110 (15,950)
f_{cmi}	MPa (psi)	22 (3,190)	28 (4,060)	35 (5,075)	43 (6,235)	53 (7,685)	68 (9,860)	82 (11,890)	99 (14,355)
E_c	MPa (psi)	24,000 (3,480,000)	26,700 (3,871,500)	30,100 (4,364,500)	32,800 (4,756,000)	34,800 (5,046,000)	37,400 (5,423,000)	39,600 (5,742,000)	42,200 (6,119,000)

Note: f_{cm} is the mean value of cylinder strength (compressive strength) and f_{cmi} is the mean value of the in situ compressive strength of concrete.

8.3 Fiber orientation factors

There are three fiber orientation factors introduced in this standard, e.g., K_s, k_{3Dt}, and k_{3Db}. The term K_s is defined as fiber orientation casting bias factor and the value is taken as 0.64. The value of K_s is considered a constant in this standard. This factor is only used when calculating the contribution of the fibers to the ultimate shear strength (V_{uf}) of an SFRC beam as follows:

$$V_{uf} = K_s k_g d_v b_v f'_w cot\theta_v \quad \ldots(8.1)$$

where k_g is defined as member size factor determined by the equation 8.2 and A_{ctu} is the area of concrete within the tensile zone and A_o is a reference area taken as 15,600 mm^2, f'_w is the characteristic residual tensile strength of SFRC corresponding to crack opening displacement, i.e. COD, here, the crack opening displacement (COD) is the width of a single localized crack, taken as an average on four sides, for a direct tensile test on a strain-softening SFRC dog-bone shaped specimen (Figure 8.1 presents strain softening and strain hardening SFRC based on the stress-COD relation), d_v is the effective shear depth of member which shall be taken as the greater of 0.72D or 0.9d, where d is the distance from the extreme compression fiber to the centroid of the longitudinal tension reinforcement in the half-depth of the section containing the flexural tension zone and D is the overall depth of a cross-section in the plane of bending, b_v is the effective width of a web for shear, θ_v is the angle between the axis of the concrete compression strut and the longitudinal axis of the member calculated as $\theta_v = (29 + 7000\varepsilon_x)$ where ε_x is the longitudinal strain of concrete for shear.

$$k_g = 1 + \frac{0.0067A_{ctu}}{A_o} \leq 1.6 \quad \ldots(8.2)$$

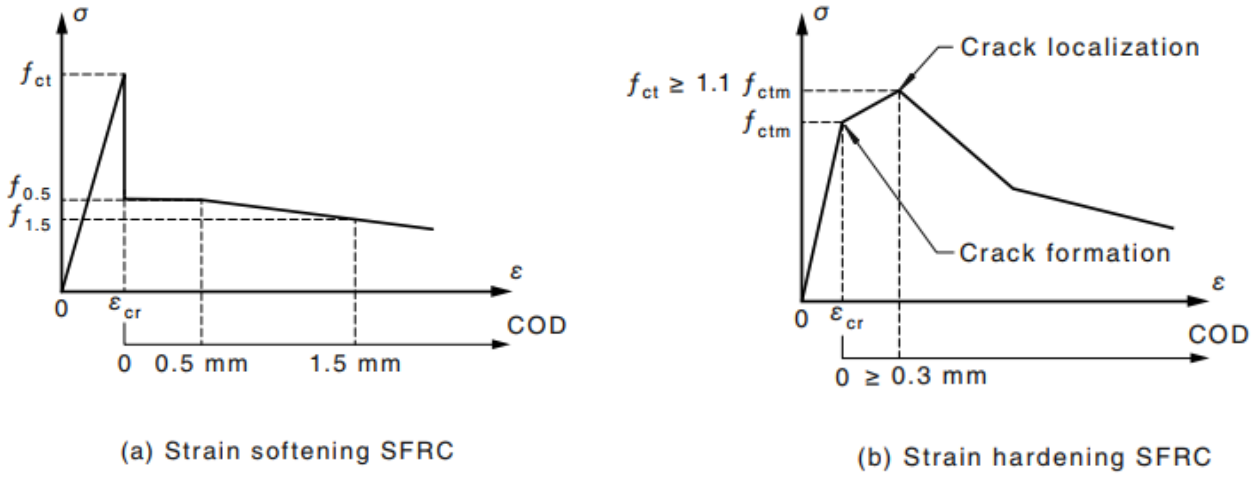

Figure 8.1 Classification of SFRC (AS 3600:2018).

The term k_{3Dt} is the three-dimensional orientation factor which is calculated using the following formula based on the dimension of the fibers and the specimen:

$$k_{3Dt} = \frac{1}{0.94+0.6l_f/b} \leq 1 \qquad \ldots(8.3)$$

where l_f is the length of steel fiber and b is taken as the average of the width and depth of the specimen at the critical section. During the determination of residual tensile strength of strain-softening SFRC by direct tension test, strength results are multiplied by the three-dimensional orientation factor k_{3Dt}. This factor removes the influence of the boundaries on the fiber distribution and converts the results of the test to a state where the fibers can be considered to be randomly orientated in three-dimensional space. The testing should be performed in a laboratory accredited by the National Association of Testing Laboratories (NATA). In the case of testing using an independently approved and verified testing method, the residual tensile strength results obtained from the direct tension test shall be multiplied by the three-dimensional orientation factor k_{3Dtb}, where-

$$k_{3Db} = \frac{1}{1+0.19l_f/b} \leq 1 \qquad \ldots(8.4)$$

The design procedures in this standard are for SFRC with a softening classification only (Figure 8.1a). The strain hardening SFRC and the use of synthetic fibers are beyond the scope of the standard (Figure 8.1b) and the structural design of UHPC and UHPFRC are beyond the scope of the standard as well. In the case of softening response of SFRC, the direct tensile stress-strain relation shows a linear behavior up to f_{ct} (uniaxial tensile strength of concrete), followed by a drop at ε_{cr} which is the tensile strain at the crack, and at $f_{0.5}$ (residual tensile strength of concrete at 28 days at a COD of 0.5 mm). Then a plateau continues up to COD of 0.5 mm and linearly reduces to COD of 1.5 mm to $f_{1.5}$ (residual tensile strength of concrete at 28 days at a COD of 1.5 mm). When determining the characteristic values of $f_{0.5}$ and $f_{1.5}$, i.e., $f'_{0.5}$ and $f'_{1.5}$, the fiber orientation factors k_{3Dt} (and k_{3Db}) need to be incorporated. For example, they can be calculated as follows:

$$f'_{0.5} = k_{3Db}(-0.04f'_{R,4} + 0.37f'_{R.2}) \leq k_{3Db}0.36\sqrt{f'_c} \qquad \ldots(8.5)$$
$$f'_{1.5} = k_{3Db}(0.04f'_{R,4} - 0.07f'_{R.2}) \leq k_{3Db}0.36\sqrt{f'_c} \qquad \ldots(8.6)$$

where, $f'_{R,2}$ = characteristic residual flexural tensile strengths corresponding to a CMOD of 1.5 mm (0.06 in), $f'_{R,4}$= mean residual flexural tensile strengths corresponding to a CMOD of 3.5 mm (0.14 in), f'_c = characteristic compressive strength of concrete at 28 days. Here, CMOD (crack mouth opening displacement) is the width of a crack measured at its mouth in a flexural tensile test undertaken in accordance with EN 14651:2005, which is a three-point notched bending test on 150 mm (5.91 in) square section prisms with a span length of 500 mm (19.7 in.) and notch depth of 25 mm (0.984 in.). Figure 8.2 presents the load-CMOD relation for residual flexural tension of SFRC specimen. Here, the $F_{R.1}$, $F_{R.2}$, $F_{R.3}$, $F_{R.4}$ are the recorded loads corresponding to $CMOD_1$, $CMOD_2$, $CMOD_3$, $CMOD_4$ respectively, i.e. 0.5 mm (0.01 in), 1.5 mm (0.06 in), 2.5 mm (0.1 in), 3.5 mm (0.14 in) respectively.

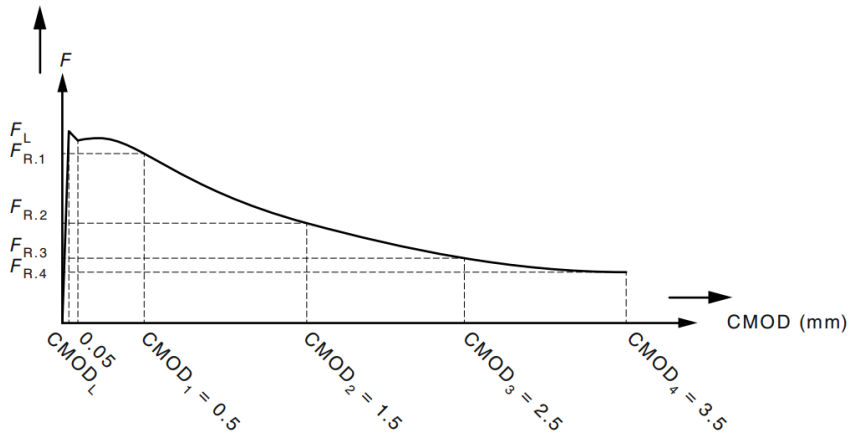

Figure 8.2 Load versus CMOD for residual flexural tension of SFRC (AS 3600:2018).

8.4 Background and discussion

There is a significant contribution of the research by Frank J. Vecchio and S.J. Foster on steel fiber reinforced concrete to enrich the steel fiber reinforced concrete part of the Australian standards on Concrete structures (AS 3600: 2018) and design of concrete bridges (AS 5100). Their analyses and formulation of the fiber orientation factors based on the experimental data of the four-point flexure test and direct tensile test helped to estimate the influence of boundary surface in SFRC structures. The AS 3600:2018 describes three fiber orientation factors. In this effort, we are able the find out the background of two factors (K_s and k_{3Dt}). We are still in search of the background of the third factor (k_{3Db}).

Background of K_s

The fiber orientation varies in regions where the distance to a boundary surface is less than the fiber length because the fiber inclination angle herein is affected by the surface (Lee et al. 2011a). The fiber orientation factor, K_s is determined by the probability of the fiber crossing the fracture plane and is affected by the shape of the domain. Figure 8.3 shows the orientation of a fiber crossing a 2D space. The probability density function of a fiber, the K_s factor can be derived as (Ng et al. 2012):

$$K_s = \frac{\int_{-\pi/2}^{\pi/2} \cos\theta \, d\theta}{\int_{-\pi/2}^{\pi/2} d\theta} = \frac{\pi}{2} \qquad \ldots(8.7)$$

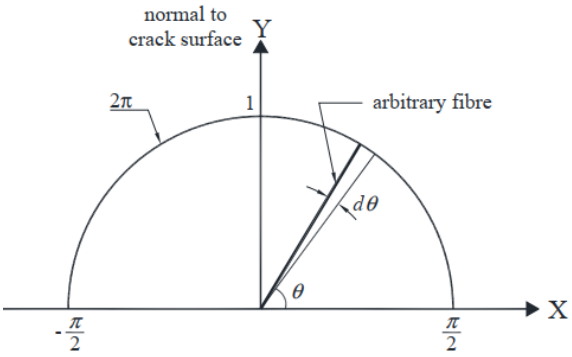

Figure 8.3 Polar coordinates and averaging for orientation in two-dimensional (2D) space (Ng et al. 2012).

At the boundary surface, because out-of-plane fiber inclinations are assumed not to be allowed, the fiber orientation is assumed to be 2D ($K_s = 0.64$) (Ng et al. 2012; Aveston and Kelly, 1973; Lee et al. 2011a, b), which was adopted in the AS 3600:2018 (discussed in Section 8.3). This factor is only found to apply to shear design in the code.

The $K_s = 0.64$ may be too conservative. After analyzing the shear behavior of steel fiber reinforced concrete beam from flexure tests (due to lack of shear test data), it was shown in Foster et al. (2018) that the value of K_s could be taken as 1.0 if there was no bias between the prism bending test results and structural behavior. Taking K_s as 0.82 (as adopted in Amin and Foster, 2016) provides a reasonable degree of conservatism and Foster et al. (2018) further reported that a value of 0.70 provided more appropriate conservatism for design.

Background of k_{3Dt}

The term three-dimensional orientation factor, k_{3Dt} (Equation 8.3) was applied to the direct tension tests to adjust for the wall (boundary) effect. This factor was adapted from Lee et al. (2011a, b) for a square cross-section (Foster, 2014) as:

$$k_{3Dt} = \frac{1}{0.94+0.6l_f/b} \leq 1 \qquad \ldots(8.3)$$

Lee et al. (2011a and b) used a similar procedure as the fib MC2020 (in progress) detailed in Section 3.4 (which followed Dupont and Vandewalle, 2005) to model the distribution of the fibers in different sections. They consider that the fiber orientation varies in regions where the distance to a boundary surface is less than the fiber length because the fiber inclination angle is affected by the surface. They also proposed a Diverse Embedment Model (DEM) for modeling the behavior of FRC in tension which considered the pullout behavior of fibers and the fiber distributions and verified their model with experimental results. From this work, they also evaluated the average fiber orientation factors in 3D sections as a function of l_f/b. Foster (2014) mentioned that this work was the basis of Equation 8.3.

9. DAfStb Guideline on Steel Fibre Reinforced Concrete (2012 and 2019)

9.1 Overview

The German Committee for Reinforced Concrete (Deutscher Ausschuss für Stahlbeton – DAfStb) published the first draft of the DAfStb Guideline on Steel fibre reinforced concrete in 2012 and the second draft in 2019. The guideline regulates the properties and applications of the material "steel fiber reinforced concrete" that are not covered by DIN EN 1992-1-1 (Eurocode 2: Design of concrete structures - Part 1-1: General rules and rules for buildings; German version EN 1992-1-1:2004 + AC: 2010) in conjunction with DIN EN 1992-1-1/NA (Eurocode 2), (DIN, E., 2001. 206-1: Concrete. Specification, performance, production and conformity.) in conjunction with DIN 1045-2 (Concrete, reinforced and prestressed concrete structures - Part 2: Concrete - Specification, properties, production, and conformity - Application rules for DIN EN 206-1) and DIN EN 13670 (Execution of concrete structures.) in conjunction with DIN 1045-3 (Concrete, reinforced and prestressed concrete structures - Part 3: Execution of structures - Application rules for DIN EN 13670) or by the DAfStb guidelines on concrete exposed to water-contaminating substances or those on concrete structures that are impermeable to water.

9.2 Definition of SFRC

In this document, steel fiber reinforced concrete refers to concrete according to DIN EN 206-1/DIN 1045-2, to which steel fibers are added to achieve certain properties. Together with Part 1-1 of Eurocode 2, this guideline covers the design and construction of load-bearing structures (including civil engineering structures) made from SFRC and SFRC with reinforcement up to compressive strength class C50/60 (characteristic compressive cylinder strength 50 MPa or 7,230 psi and characteristic compressive cube strength 60 MPa or 8,700 psi).

The guideline includes a classification of the steel fiber concrete based on the post-crack flexural strength Performance classes. There are two performance classes:
- Performance class L1 for small deformations (0.5 mm or 0.02 in);
- Performance class L2 for larger deformations (3.5 mm or 0.14 in).

The designer defines the performance classes. The composition of the concrete, including the type and amount of fiber, is determined by the manufacturer of the steel fiber concrete.

9.3 Fiber orientation factor

German Committee for Structural Concrete (Deutscher Ausschuss für Stahlbeton – DAfStb) guideline (2012 and 2019) for steel fiber reinforced concrete also introduces κ_F^f factor to take into account the fiber orientation. The value of κ_F^f=0.5 in the case of flat, horizontal, or planar components (e.g. b > 5h, where b is the width and h is the thickness of the member). In the case of beams in their longitudinal direction, κ_F^f = 1.0 is assumed for bending and tensile loads. These factors are used in the calculation of centric post-cracking tensile strengths obtained from post-cracking tensile strengths as follows, which will be later used to define the tensile constitutive laws of SFRC for design:

$$f^f{}_{ctR,L1} = \kappa_F^f \cdot \kappa_G^f \cdot f^f{}_{ct0,L1} \quad \ldots(9.1)$$

$$f^f{}_{ctR,L2} = \kappa_F^f \cdot \kappa_G^f \cdot f^f{}_{ct0,L2} \quad \ldots(9.2)$$

$$f^f{}_{ctR,u} = \kappa_F^f \cdot \kappa_G^f \cdot f^f{}_{ct0,u} \quad \ldots(9.3)$$

$$f^f{}_{ctR,s} = \kappa_F^f \cdot \kappa_G^f \cdot f^f{}_{ct0,s} \quad \ldots(9.4)$$

where,

κ_G^f = factor taking into account the effect of member size on the coefficient of variation; and κ_G^f= $1.0+0.5A_{ct}^f \leq 1.70$, where A_{ct}^f is the area of tension zones in the concrete of the cracked cross-sections or plastic hinges (in m^2). In the case of components with pure bending without normal force, the term A_{ct}^f can be estimated at $0.9A_c$ where A_c is the cross-section area of concrete.

κ_F^f = factor taking into account the fiber orientation

$f^f{}_{ctR,L1}$ = calculated centric post-cracking tensile strength when using the stress-strain curve of uniaxial tension test of dogbone specimen (Performance class L1).

$f^f{}_{ctR,L2}$ = calculated centric post-cracking tensile strength when using the stress-strain curve of uniaxial tension test of dogbone specimen (Performance class L2).

$f^f{}_{ctR,u}$ = calculated centric post-cracking tensile strength at the ultimate limit state when assuming the rectangular stress block and using reinforcement

$f^f{}_{ctR,s}$ = calculated centric post-cracking tensile strength in the serviceability limit state when using reinforcement

$f^f{}_{ct0,L1}$= basic value of centric post-cracking tensile strength obtained using the stress-strain curve of uniaxial tension test of dogbone specimen (Performance class L1)

$f^f{}_{ct0,L2}$ = basic value of centric post-cracking tensile strength obtained using the stress-strain curve of uniaxial tension test of dogbone specimen (Performance class L2)

$f^f{}_{ct0,u}$= basic value of centric post-cracking tensile strength at the ultimate limit state when assuming the rectangular stress block and using reinforcement

$f^f{}_{ct0,s}$ = basic value of centric post-cracking tensile strength in the serviceability limit state when using reinforcement

The stress-strain constitutive law of SFRC in the tensile area for analysis and deformation calculation using non-linear methods is shown in Figure 9.1(a). The curve increases linearly up to f_{ctm} followed by a drop to $1.04f^f{}_{ctR,L1}$ and maintains a plateau until 0.35% strain, and then decreases linearly to $1.04f^f{}_{ctR,L2}$ at 2.5% strain. A simplified stress-strain relation can be derived where the stress shows plastic rigid behavior up to $1.04f^f{}_{ctR,u}$ and a plateau up to 2.5% strain.

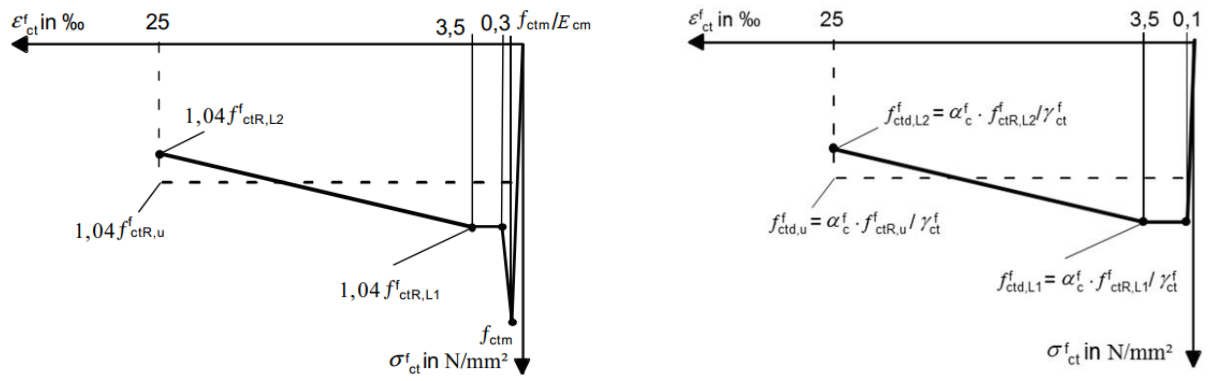

(a) (b)

Figure 9.1 (a) Stress-strain curve of SFRC in the tensile area for analysis and deformation calculation using non-linear methods; (b) Stress-strain curve of SFRC in the tensile area for cross-section design at the ultimate limit state, except for non-linear methods (DAfStb guideline 2012).

In the case of stress-strain constitutive law of SFRC in the tensile area for cross-section design at the ultimate limit state, except for non-linear methods (Figure 9.1b), the curve rises linearly to $f^f{}_{ctd,L1}$ (= $\alpha^f_c . f^f{}_{ctR,L1}/\gamma^f_{ct}$) and maintains a plateau value up to 0.35% strain, and then decreases linearly to $f^f{}_{ctd,u}$ (= $\alpha^f_c . f^f{}_{ctR,L2}/\gamma^f_{ct}$). Again, a simplified stress-strain relation can be derived where the stress shows plastic rigid behavior up to $f^f{}_{ctd,u}$= $\alpha^f_c . f^f{}_{ctR,u}/\gamma^f_{ct}$ and a plateau up to 2.5% strain. Here f_{ctm} is the post-cracking tensile strength of steel fiber reinforced concrete, $f^f{}_{ctd,L1}$ is the design centric post-cracking tensile strength in performance class L1 when using the complete stress-strain curve, $f^f{}_{ctd,L2}$ is the design centric post-cracking tensile strength in performance class L2 when using the complete stress-strain curve, $f^f{}_{ctd,u}$ is the design value of centric post-cracking tensile strength at the ultimate limit state when using the rectangular stress block and reinforcement, $f^f{}_{ctd,s}$ = design value of centric post-cracking tensile strength at the serviceability limit state when using the rectangular stress block and reinforcement, α^f_c is the reduction factor for calculating concrete compressive strength due to long-term effects on the post-cracking tensile strength of steel fiber reinforced concrete and is equal to 0.85, γ^f_{ct} is the partial safety factor for steel fiber reinforced concrete with or without reinforcement at ultimate limit states and is equal to 1.25, ε^f_{ct} is the strain in the steel fiber reinforced concrete. These constitutive models for SFRC design are based on the post-cracking tensile strength of SFRC which are influenced by the fiber orientation factor.

9.4 Background

In the DAfStb Heft 614-2016 (Commentary on the DAfStb Guideline "Steel Fibre Reinforced Concrete"), the orientation factors described in DAfStb Guideline on Steel fibre reinforced concrete (2012) are further clarified. According to DAfStb Heft 614-2016, the factor k^f_F takes into account the orientation of the fibers in the direction of the flow of the concrete (see Figure 9.2). A factor k^f_F = 1.0

means that the fiber orientation in the structural element is comparable to that in the standard beam test (dimensions of 150 mm x 150 mm x 700 mm or 6 in x 6 in x 27.5 in as specified in EN 12390-1, i.e., “Testing hardened concrete–Part 1: Shape, dimensions and other requirements for specimens and molds”).

The orientation of fibers in a member is influenced to a great extent by the consistency of the concrete and the method of concreting. A fiber orientation perpendicular to the direction of concreting and compaction occurs most frequently, while a fiber orientation parallel to the surfaces of the formwork predominates in small test specimens. The fiber orientation in standard beam specimens as well as for horizontally cast plane members subjected to bending is generally favorable because it is in direction of the principal tensile stresses. The residual tensile strengths determined on standard beams according to this guideline may be applied to such members without reduction (k_F^f =1.0). On the other hand, if the specimens are cast such that the fiber orientation is unfavorable with respect to the structural stresses acting on a member, k_F^f shall be taken as 0.5. This is the case for vertically cast walls that are subjected to bending around the horizontal axis, where the fiber orientation is perpendicular to the tensile stress direction (Figure 9.2).

This code considers only two values for the fiber orientation factor, which represent the very basic conditions. Researchers and engineers have later commented that it is necessary for the scientific committee of the DAfStb guideline (2019) to consider other parameters (wall effects, concrete flowability, casting and compaction processes, fiber material, and structure geometry) that control the fiber orientation and revise the fiber orientation factors (Conforti et al. 2021, Schuler et al. 2017).

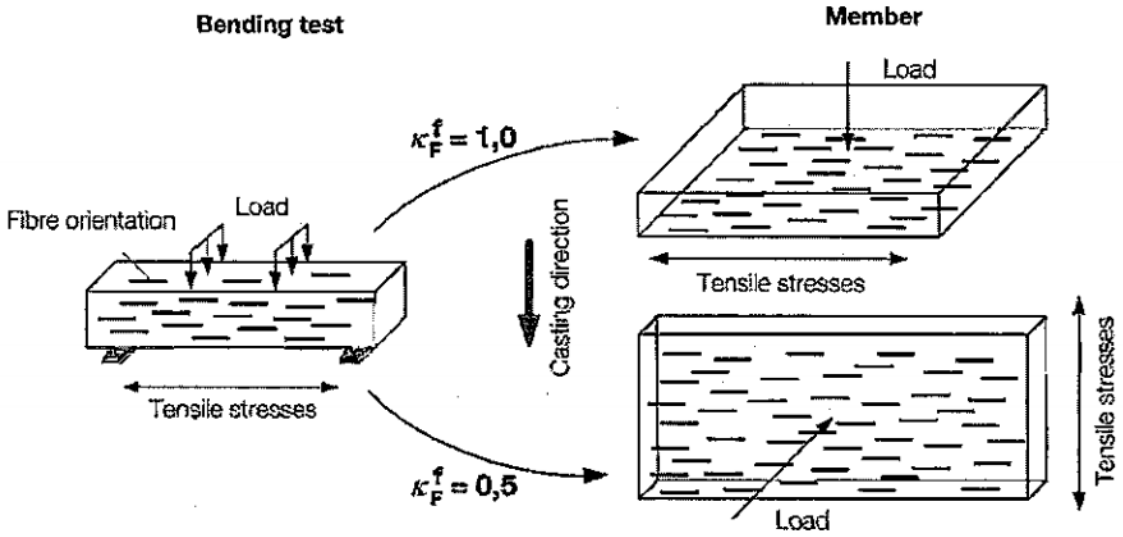

Figure 9.2 Explanation of factors k^{f}_{F} (DAfStb Heft 614-2016).

10. JSCE Recommendations

(1) Recommendations for the Design and Construction of Ultra High Strength Fiber-Reinforced Concrete (UFC) of JSCE (2006) (In English)
(2) Recommendations for Design and Construction of High Performance Fiber Reinforced Cement Composites with Multiple Fine Cracks (HPFRCC) (2008)

10.1 Overview

In 2004 the Concrete Committee of the Japan Society of Civil Engineers (JSCE) published the "Recommendations for Design and Construction of Ultra High Strength Fiber Reinforced Concrete Structures (Draft)" in Japanese language (JSCE recommendation 2004) and the English version was published in 2006. The publication of the recommendations aimed to promote the utilization of Ultra High Strength Fiber Reinforced Concrete (UFC) as an innovative construction material in the 21st century. Taking the examined results of Sakata-Mirai Bridge, Japan into account and also referring to the guidelines published in France (AFGC guidelines, 2002), the subcommittee on the research of UFC published the recommendations for design and construction of UFC in 2004 (JSCE recommendation 2004 in Japanese).

The JSCE Recommendations for Design and Construction of High-Performance Fiber Reinforced Cement Composites with Multiple Fine Cracks (HPFRCC) (2008) was published by the Japanese Society of Civil Engineers (JSCE) in 2008. The document provides basic provisions capable of satisfying the performance requirements of structures such as safety, serviceability, recoverability, and compatibility to the environment when designing and constructing structures of high-performance fiber-reinforced cement composites with multiple fine cracks (HPFRCC).

10.2 Definition of HPFRCC

HPFRCC is a composite material comprising a cement-based matrix and organic short reinforcing fibers and is a highly ductile material exhibiting multiple fine cracks and pseudo-strain-hardening characteristics under uniaxial tensile stress. In this recommendation, the term pseudo strain-hardening is defined as a subsequent increase in tensile stress after the first cracking under uniaxial tensile stress (Figure 10.1). On the other hand, plain concrete and low fiber reinforced concrete show a brittle or strain-softening effect after first cracking strength along with single crack formation.

Some ductile fiber reinforced concrete materials do not exhibit pseudo strain-hardening characteristics but show an increase in flexural stress with an increase in flexural deformation – deflection-hardening characteristics. The ultra-high strength fiber reinforced concrete is a major example of deflection-hardening materials. The deflection-hardening materials show damage localization at a relatively early stage of deformation depending upon the size of the member and loading conditions, and control of crack widths is difficult. This is a distinct difference in material property from HPFRCC that exhibits pseudo strain-hardening solely by the material and has a crack width control capability under

increasing deformation, and a different method is required when verifying its durability. Thus, the "Recommendations" document only deals with HPFRCC and excludes deflection-hardening materials. It is worth noting that this document does not focus on UHPC or UHPFRC, as unlike the definition of UHPC or UHPFRC, HPFRCC does not necessarily exhibit a high compressive and tensile strength. However, this document is still reviewed for its relevance to fiber orientation and dispersion considerations.

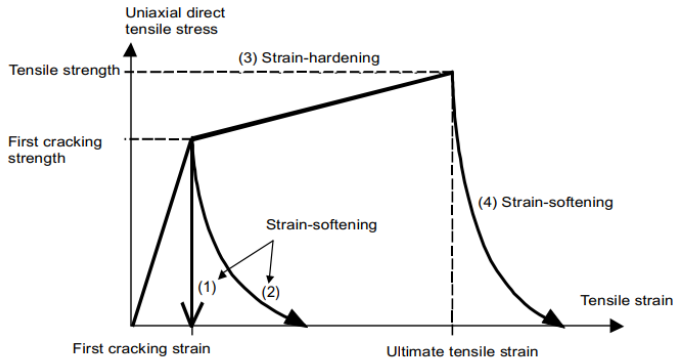

Figure 10.1 Concept of strain-hardening and strain-softening under tensile stress (JSCE recommendations 2006).

10.3 Consideration of fiber orientation

The JSCE recommendation for HPFRCC (2008) does not provide any fiber orientation factor for the structural design of HPFRCC. Instead, it is considered that the placement method and construction procedure influence the fiber dispersion and orientation in the matrix and suggested the following steps:

(1) In placing HPFRCC, the execution plan shall be formulated in consideration of the fact that the placement method affects the dispersion and orientation of reinforcing fiber.
(2) HPFRCC is usually placed by buckets or similar devices. A detailed plan for placement locations and methods shall be formulated in advance, in order to allow the placement work to be performed continuously until the whole section is completed.
(3) The placement speed shall be properly determined to suit the member configurations and steel arrangements based on existing field data or tests.
(4) Any locations that have overlaying placement on previously placed layer or merging may become weak points in HPFRCC, and thus shall be avoided where possible in principle. Shall such a placement procedure become inevitable, proper treatments shall be given, such as in the form of roiling with tamping rods.
(5) Where there is a construction joint, it shall be created by a test-proven proper method or procedure.

Similarly, the JSCE recommendation for UFC (2006) does not provide any factor to explicitly consider the orientation of fiber in the design of UFC structures.

10.4 Discussion on reduction factors addressing the fiber orientation

The above mentioned JSCE guidelines do not directly consider the effect of fiber orientation and dispersion on the structural behavior of HPFRCC and UFC structures, rather they consider an overall material factor (material reduction factor) and member factor (member reduction factor) as safety factors, which is similar to the approach of partial safety factor in the Eurocode 2 (EN 1992, 2004).

The JSCE recommendation (2006) introduces the concept of material factors for UFC structural design. The recommendation stated that the material factor of the tensile strength shall be determined taking into account the orientation of the reinforcing fibers, which was inspired by AFGC recommendation (2002). However, this recommendation does not mention the process of determining the material factors. It provides the following points to be considered when setting the material factors:

- Variation of data going in undesirable directions (disparity and shortage of test data, etc.).
- Differences in material characteristics between test specimens and the concrete in the actual structure
- Influence of material characteristics on limit states
- Aging of materials, etc.
- Differences between test specimens and the concrete in the actual structure from construction procedures.
- Effects from aging of materials and continuous loading.

From the list, the material factor may have included the effect of fiber orientation, however, they are lumped with other effects.

After reviewing the concept of partial safety factor in Eurocode 2, it can be said that the JSCE recommendation adopted the concept of material factor and member factor from Eurocode 2 (which is named as partial safety factor as per Eurocode 2), although the Eurocode 2 does not consider the contribution of fibers in FRC.

In general, the material factor (γ_c) of the UFC can be set to 1.3 to evaluate ULS, and 1.0 to evaluate SLS. The JSCE recommendation suggests that in designing a structure using UFC, setting the material factor $\gamma_c = 1.3$ is sufficient enough to secure the safety of the UFC structure. However, in actual practice to implement the value on the construction site, the material factor (γ_c) may be determined through a variety of tests using either actual concrete or models, and a close study of the orientation factor (here, the recommendation referred to the concept of suitability test in the AFGC recommendation, 2002). Table 6.2 shows that the overall reduction factor of the JSCE recommendations (2006 and 2008) is also close to the overall factor of AFGC recommendations (2013).

11. Canadian Standards

(1) Concrete materials and methods of concrete construction/Test methods and standard practices for concrete (2019) (CSA A23:19)
(2) Canadian Highway Bridge Design Code (2019) (CSA S6:19)

11.1 Overview

The Canadian Standards Association (CSA) provides two separate standards for UHPC and FRC, (1) Canadian Highway Bridge Design Code (2019) (CSA S6:19) and (2) Concrete materials and methods of concrete construction/Test methods and standard practices for concrete (2019) (CSA A23:19). CSA S6:19 (2019) is based on limit states design principles and defines design loadings, load combinations and load factors, criteria for earthquake resistant design, and detailed design criteria for various materials. CSA A23:19 provides the requirements for materials and methods of construction for cast-in-place concrete, concrete precast in the field, and residential concrete used in the construction of buildings. The Annex U of CSA A23:19 provides information for materials and methods of construction for the use of UHPC in cast-in-place concrete and precast concrete.

The latest version of the Canadian Highway Bridge Design Code (CSA S6:19) which was published in November 2019, introduced Annex A8.1 (informative) titled “Fibre-reinforced concrete (FRC)”. This Annex specifies the requirements for the design of structural components that are made of precast or cast-in-place FRC with prestressed or non-prestressed steel. The Annex covered the prestressed members with pre-tensioned steel, grouted post-tensioned steel, or both. The Annex also covered the behavior of tension softening FRC (TSFRC) and tension hardening FRC (THFRC). This Annex covers the use of steel fibers only, except in Clause A8.1.21, where the use of synthetic fibers is specifically indicated.

11.2 Definition of UHPCs and FRCs

As per CSA A23:19 (Annex U), Ultra-high performance concrete (UHPC) is a cementitious composite material with enhanced strength, durability, and ductility compared to high performance concretes. UHPC can contain fibers for post-cracking ductility, have a specified compressive strength of at least 120 MPa (17,400 psi) at 28 days, and are formulated with a modified multi-scale particle packing of inorganic materials of less than 0.6 mm (0.02 in) diameter.

As per CSA S6:19, fiber-reinforced concrete (FRC) is defined as a composite material characterized by a concrete matrix and discrete (discontinuous) fibers. This guideline categorizes FRCs in two types, e.g., (1) tension hardening FRC (THFRC) is a fiber-reinforced concrete that shows an increase in tensile strength after cracking up to a specific deformation while subjected to uniaxial direct tensile forces; and (2) tension softening FRC (TSFRC) is a fiber-reinforced concrete that shows a decrease in tensile strength after cracking while subjected to uniaxial direct tensile forces. Also, two categories of UHPC are defined. Tension hardening UHPC (THUHPC) is an ultra-high performance concrete in accordance with CSA A23, Annex U that shows an increase in tensile strength after cracking up to a

specific deformation while subjected to uniaxial direct tensile forces, tension softening UHPC (TSUHPC) is an ultra-high performance concrete in accordance with CSA A23:19 Annex U that shows a decrease in tensile strength after cracking while subjected to uniaxial direct tensile forces.

11.3 Fiber efficiency factor

The CSA A23:19 does not provide any factors for considering fiber dispersion or orientation in structural design.

However, in the Annex A8.1 of CSA S6:19, the fiber efficiency factor γ_F is introduced. The γ_F is similar to the inverse of K factors of AFGC recommendations, and CSA S6:19 states that the post-cracking tensile properties shall be multiplied by the fiber efficiency factor γ_F to account for the actual fiber orientation and dispersion in structural components relative to the direction of applied tensile stresses. It is worth noting that this factor is only applicable to FRC, not UHPC.

As per CSA S6:19 (Clause A8.1.4.5.4), the tensile strength properties of FRC shall be determined on a minimum of 30 consecutive four-point flexural prism tests of specimens coming from a minimum of 3 separate batches of a single mix design. A minimum of 3 and a maximum of 10 specimens per batch shall be used. As per CSA A23:19, the prism samples shall have a length at least 50 mm (2 in) greater than three times their depth; they shall be formed with their long axes horizontal; the ratio of width to depth, as molded, shall not exceed 1.5; and the cross-section shall be not less than 150 mm x 150 mm (6 in x 6 in) or three times the maximum size of aggregate, whichever is larger. Unless stated otherwise, characteristic values (10^{th} percentile value equal to the average value minus 1.4 times the standard deviation) shall be used for design.

The values of γ_F shall be determined in accordance with one of the following approaches:

(a) from experimental results:

The fiber efficiency factor γ_F shall be equal to the ratio of the characteristic post-cracking tensile property value obtained from the four-point flexural test on prism samples sawn or cored from a mock-up structure identical to the actual structural member to the characteristic post-cracking tensile property value obtained from four-point flexural tests on cast prism samples (dimensions of the specimens are stated above). Samples shall be sawn or cored such that the fibers in the test samples are acting in the same direction as that in the in situ member. As per CSA A23:19, the sawn flexural test specimens shall be not less than 150 mm x 150 mm (6 in x 6 in) or three times the maximum size of aggregate, whichever is larger. Where constrained by element section, the cross-section of sawn samples shall be not less than 75 mm x 75 mm (3 in x 3 in). The test specimen shall have a span length, as nearly as practicable, that is three times its depth as tested. The minimum specimen length shall be equal to the span length plus 50 mm. The flexural samples shall be tested by four-point flexural prism test. The sample post-cracking tensile strength shall correspond to the characteristic value, defined as the 10% fractile value, computed with a minimum of six tests on samples obtained from a maximum of two cast members identical to the designed elements.

(b) from the following values:

i) for elements cast horizontally in which a mostly two-dimensional fiber dispersion is expected, such as decks and slabs: γ_F = 0.8 for flexure and beam shear; γ_F = 0.6 for two-way action shear

ii) for elements cast vertically in which a mostly two-dimensional fiber dispersion is expected, such as walls: γ_F = 0.5 for flexure and beam shear; γ_F = 0.5 for two-way action shear,

iii) for bond and development length of reinforcement: γ_F = 0.5,

iv) for large structural components and elements in which three-dimensional fiber dispersion is expected, such as beams, girders, footings: γ_F = 0.4, and

v) for local effects, such as anchors: γ_F = 0.3.

When using approach (a), it is important to ensure that the samples are taken from the members at representative locations for the fiber dispersion and at critical sections for the member behavior. These critical sections could include maximum moment and shear locations, and locations where the fiber dispersion can be altered due to sectional geometry changes or other casting-related influences. The data should be checked for outlying observations, which are test results that are abnormally high or low. The cause for any outlier test results should be carefully investigated to ensure that the suspected outlier is not a valid result that reflects irregular fiber distribution because of casting procedures or other detrimental influences. If the fiber dispersion is irregular over even a small portion of the member, this can govern the overall member strength and behavior, and outlier results can govern the fiber efficiency in the member.

The fiber efficiency factor γ_F shall not be larger than 1.0. As per the Annex A8 of CSA S6:19, when the isotropic material behavior of FRC is assumed, the fiber efficiency factor shall be the minimum factor obtained for all properties. On the other hand, when orthotropic material behavior is assumed for FRC, the fiber efficiency factors specific to the direction of loading and loading type may be used.

The fiber efficiency factor shall be applied to post-cracking strength (f_{Fs}, f_{Fm}, and f_{Fu}) and strain (ε_{tu}) properties in SLS (serviceability limit state), FLS (fatigue limit state), and ULS (ultimate limit state) design plastic stress-strain models of TSFRC and THFRC as shown in Figures 11.1 and 11.2 respectively. The required properties for TSFRC for the post-cracking region shall be determined with the simplified stress-crack width model presented in Figure 11.3.

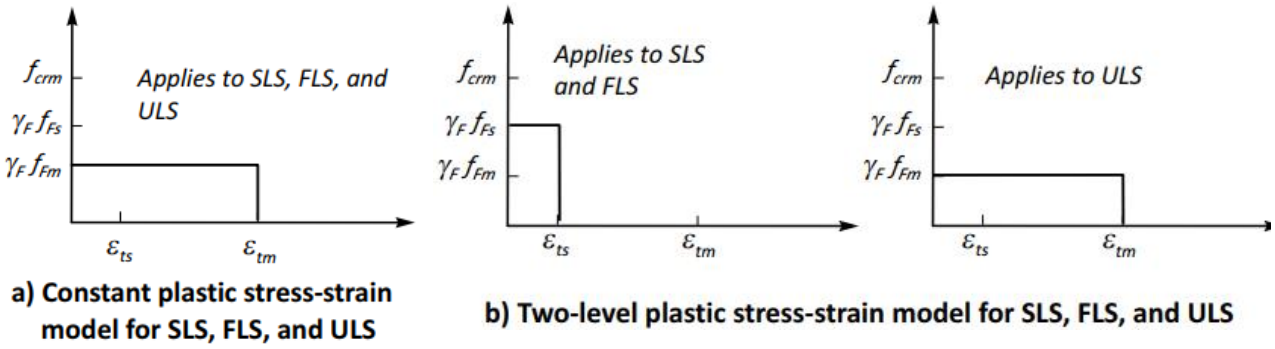

a) Constant plastic stress-strain model for SLS, FLS, and ULS

b) Two-level plastic stress-strain model for SLS, FLS, and ULS

Figure 11.1 Design plastic stress-strain models for TSFRC (CSA S6:19).

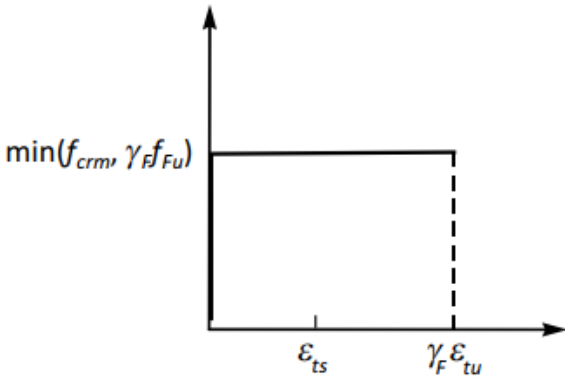

Figure 11.2 Design stress-strain model for THFRC at ULS (CSA S6:19).

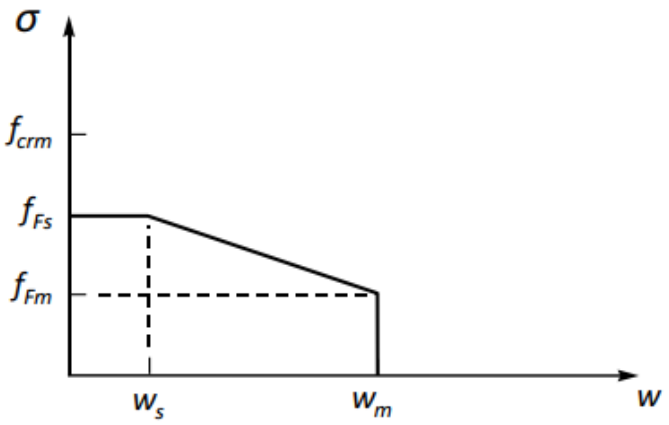

Figure 11.3 TSFRC post-cracking properties (CSA S6:19).

For TSFRC, the design tension constitutive model of TSFRC can be characterized by either of the two simplified equivalent stress-strain models shown in Figure 11.1 (i.e., Figure 11.1a or 11.1b). The first model (Figure 11.1a) shows a rigid perfectly plastic behavior where the stress maintains at $\gamma_F f_{Fm}$ up to the strain of ε_{tu} for SLS, FLS, and ULS. The second model shows a rigid perfectly plastic behavior where the stress maintains at $\gamma_F f_{Fs}$ up to the strain of ε_{ts}, for SLS and FLS; and a rigid perfectly plastic behavior where the stress maintains at $\gamma_F f_{Fm}$ up to the strain of ε_{tm}. Here, f_{Fm}= specified post-

cracking tensile strength at ULS for TSFRC at crack width w_m and f_{Fs} = specified post-cracking tensile strength at SLS and FLS for TSFRC at crack width w_s; ε_{ts} is the strain associated with crack width w_s ; and ε_{tm} is the strain associated with crack width w_m (Figure 11.3). w_s is taken as 0.5 mm and the value of w_m shall not exceed the lesser of 3.5 mm (0.14 in) or l_F/4, where l_F is the length of the longest fiber corresponding to a minimum of 50% of the total fiber content.

In the case of THFRC at ULS (Figure 11.2), the model shows a plastic rigid behavior up to a stress level equal to the minimum of f_{crm} and $\gamma_F f_{Fu}$, and the stress is maintained up to a strain of $\gamma_F \varepsilon_{tu}$. Here, f_{crm} = average cracking strength of the FRC matrix; f_{Fu} = specified ultimate tensile strength for THFRC; ε_{tu} = the specified maximum design strain at ULS for THFRC. At SLS and FLS, THFRC shall only resist tension up to a design strain: $\varepsilon_{ts} = 0.5\gamma_F \varepsilon_{tu}$ instead of $\gamma_F \varepsilon_{tu}$. Fiber contribution for strains larger than the design strain shall not be considered.

All the above-specified values can be obtained from the aforementioned four-point flexural tests as per CSA S6:19 (Clause A8.1.4.5.4). For example, f_{Fs}, f_{Fm} shall be determined as the minimum characteristic tensile strength up to the crack width w_s and w_m, respectively.

The CSA A23:19 provides the following model for TSUHPC and THUHPC as shown in Figure 11.4. However, the fiber efficiency factor is not considered in this document. The THUHPC in accordance with CSA A23.1, Annex U shows an increase in tensile stress (up to f_{fu}=maximum direct tensile strength of the fiber reinforced UHPC) after cracking (f_{cr}=direct tensile strength of the cementitious UHPC matrix and ε_{cr}=tensile strain corresponding to f_{cr}) until reaching a specific deformation (strain reaches ε_{fu}=tensile strain corresponding to f_{fu}) under uniaxial direct tensile forces (Figure 11.4a). After that, crack localization occurs, and the stress starts to decrease. For TSUHPC in accordance with CSA A23:19 Annex U, it shows a decrease in tensile strength after cracking under uniaxial direct tensile forces and the tension constitutive model is shown in Figure 11.4b. A minimum of 3 points in the elastic range and a minimum of four intermediate $w_i - f_{ti}$ points ($w_1 - f_{t1}$ to $w_4 - f_{t4}$) with f_{ti} corresponding to 80%, 60%, 40%, and 20% of f_{tu} respectively shall be provided in accordance with Figure 11.4(a), for a THUHPC. A minimum of 3 points in the elastic range and a minimum of six intermediate $w_i - f_{ti}$ points ($w_1 - f_{t1}$ to $w_6 - f_{t6}$) corresponding to w_1 = 0.15 mm, w_2 = 0.25 mm, w_3 = 0.50 mm, w_4 = 1.5 mm, w_5 = 2.5 mm, and w_6 = 3.5 mm respectively shall be provided in accordance with Figure 11.4(b) for a TSUHPC.

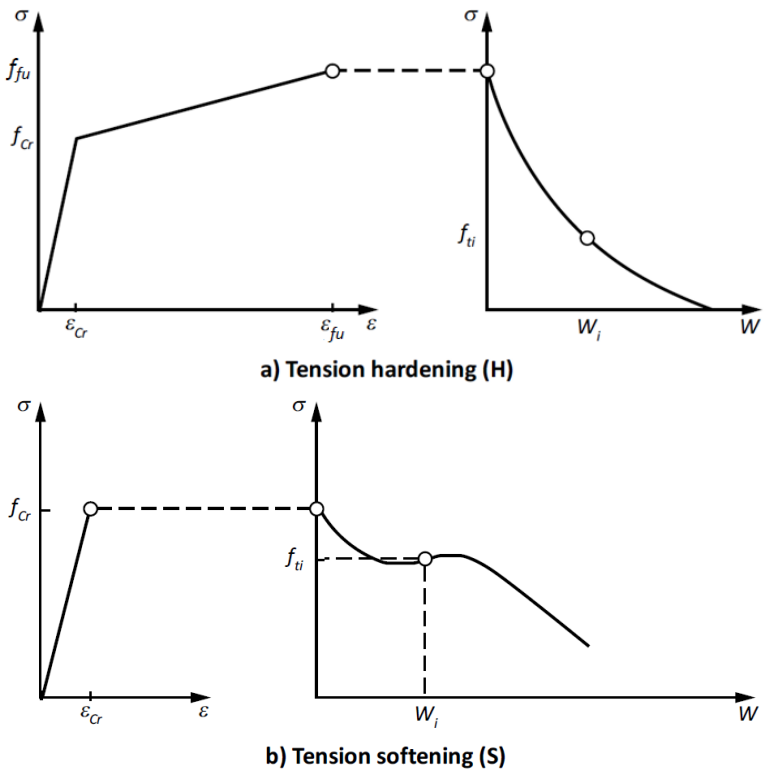

Figure 11.4 Stress-strain and stress-crack width diagrams: (a) THUHPC; (b) TSUHPC (CSA A23:19 Annex U).

11.4 Background of fiber efficiency factor and discussion

The Commentary to CSA S6:19 referred to the following literatures (Casanova and Rossi, 1997; Laranjeira et al., 2011; Abrishambaf et al., 2013; etc.) which proposed the fiber efficiency factor. The concept is quite similar to the fiber orientation factor K in AFGC recommendation and the fib MC2010, with some differences in the actual formulation. Also, the AFGC recommendation only determines the fiber orientation factor for post-cracking tensile strength or flexural strength, but the efficiency factor in CSA S6:19 guideline is applicable for all post-cracking tensile properties including tensile strains.

CSA S6:19 states that the casting and consolidation methods, as specified in CSA A23:19, Annex U, should ensure a uniform dispersion, and thereby the fiber efficiency factor is not used. However, when uniform fiber dispersion is not achieved, fiber efficiency factors need to be used to account for unfavorable fiber orientation relative to the expected direction of stresses.

The Commentary of CSA S6:19 referenced a few literatures that helped to determine the aforementioned values of γ_F in absence of experimental data. Design of FRC Structures - fib International TG4.1 suggested that in cases with unfavorable fiber orientation, the fiber efficiency factor can be as low as 0.30 or possibly even lower for FRC with a low fiber content where localized areas can have few contributing fibers (Commentary of CSA S6:19). Local effects (such as anchors)

are typically applicable to elements of small dimensions such as bond or anchorage. Abrishambaf et al. (2013) reported from the experimental investigation that, the fiber efficiency factor values for components in which preferential 2D (where the fibers are parallel to the flow of concrete) fiber orientation factor can be expected are ranging from 0.77 to 0.87. They also reported that fiber efficiency factors ranging from 0.57 to 0.76 for 2D components where unfavorable fiber orientation was expected (where the fibers are perpendicular to the flow of concrete). Laranjeira et al. (2011) reported a fiber efficiency factor value of 0.64 for unfavorable fiber orientation (at the edges), which is also suggested by the AFGC recommendation (2013) as fiber orientation factor for edge effect (α2D). In some instances, such as for large members where the failure mechanism involves a large area (such as deck slabs under flexure), the calculated efficiency factor could be larger than 1.0, indicating that the characteristic values are conservative. While values of γ_F greater than 1.0 are proposed in some standards or guidelines (Commentary of CSA S6: 19, Design of FRC Structures - fib International, TG 4.1), indicating that the tensile member behavior may be more favorable than the material characterization value, but the CSA S6:19 Annex A8 does not allow for values larger than 1.0.

12. AASHTO LRFD Guide Specification for Structural Design with Ultra-High Performance Concrete, Version 1.0, 2021 (Proposed Version)

12.1 Overview

The proposed version of AASHTO (2021) (AASHTO LRFD guide specification for structural design with ultra-high performance concrete, Version 1.0, 2021, proposed version) is developed in consultation with AASHTO CBS T-10 (Structural Concrete Design) and developed by researchers at the FHWA Turner-Fairbank Highway Research Center. The provisions in this document apply to the design of the bridge and ancillary structures constructed by UHPC.

This document does not intend to supplant proper training or independent judgment of the Design Professional, and only identifies the minimum requirements necessary to ensure public safety. There may be a requirement that higher standards are set for the level of sophistication or quality of materials and construction by a Design Professional or Owner. AASHTO (2020) (AASHTO LRFD Bridge Design Specifications, Ninth Edition, LRFDBDS-9, 2020) as well as conventional reinforced and prestressed concrete structures must be familiar to the design professional.

12.2 Definition of UHPC

As per AASHTO LRFD guide specification, the UHPC materials exhibits a strain-hardening behavior and have the following minimum property values for use in design:

- Minimum compressive strength, f_c', of 18.0 ksi,
- Minimum effective cracking strength,$f_{t,cr}$, of 0.75 ksi,
- Minimum localization stress, $f_{t,loc}$, greater or equal to the effective cracking strength, $f_{t,cr}$,
- Minimum localization strain, $\varepsilon_{t,loc}$, of 0.0025,
- The average uniaxial electrical resistivity value shall meet or exceed the threshold value, i.e., 1500 Ω.m, as per AASHTO TP 119-21 (Standard Method of Test for Electrical Resistivity of a Concrete Cylinder Tested in a Uniaxial Resistance Test) as a requirement for minimum durability criteria.

12.3 Consideration of fiber orientation

The Proposed Draft Version of AASHTO LRFD Guide Specification for Structural Design with Ultra-High Performance Concrete (Version 1.0) does not consider the orientation of fiber in the design of UHPC structural members. However, it discusses the following issues regarding the fiber orientation and dispersion in the UHPC structure:

- The tensile resistance behavior of UHPC is dependent on the distribution and orientation of the fiber reinforcement in the UHPC which relies on the use of appropriate construction methods to ensure that the fiber reinforcement is evenly dispersed through the member and does not exhibit an undesirable orientational preference.
- In this context, the contract documents should require the use of appropriate construction methods and the casting processes should be considered by the Design Professional to ensure that the

member can be constructed.

- The disturbance of fiber distribution, as would occur at a cold joint or when fiber flow is restricted from reaching a part of the member, will affect the structural performance of the member and should be avoided.

Figures 12.1(a) and 12.1(b) shows the idealized tensile stress-strain model of UHPC for $f_{t,loc}$<1.20$f_{t,cr}$ and $f_{t,loc}$≥1.20$f_{t,cr}$ respectively. In the case of $f_{t,loc}$<1.20$f_{t,cr}$, the tensile stress-strain curve increases linearly up to $\gamma f_{t,cr}$ and $\varepsilon_{t,cr}$, and maintains a plateau up to $\varepsilon_{t,loc}$. Here, $\varepsilon_{t,cr}$ is the elastic tensile strain limit of UHPC corresponding to a tensile stress of $\gamma f_{t,cr}$, and γ is the reduction factor to account for the variability in the UHPC tensile parameter and it shall not be greater than 0.85. The reduction factor γ accounts for the variability in tensile stress parameters with respect to the average values and provides a level of conservatism to the methods adopted to identify the tensile stress parameters used in the design. Again, in the case of $f_{t,loc}$≥1.20$f_{t,cr}$, the tensile stress-strain curve increases linearly up to $\gamma f_{t,cr}$ and $\varepsilon_{t,cr}$, and again increases to $\gamma f_{t,loc}$ and $\varepsilon_{t,loc}$.

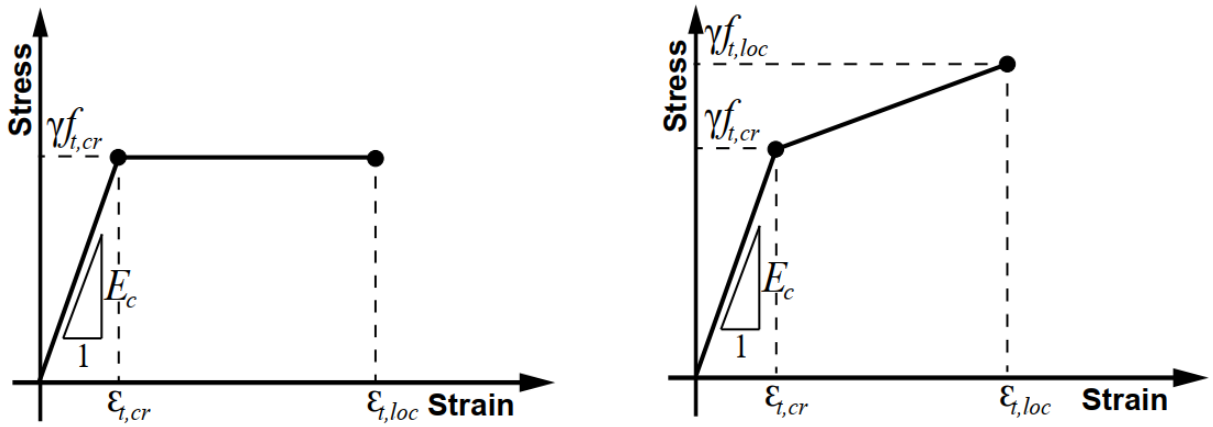

(a) (b)

Figure 12.1 Idealized tensile stress-strain model of UHPC: (a) $f_{t,loc}$<1.20$f_{t,cr}$; (b) $f_{t,loc}$≥1.20$f_{t,cr}$ (AASHTO LRFD guide specification 2021, proposed version).

13. Summary Chart

Table 12.1 briefly presents the fiber orientation factors considered in different recommendations, guidelines, codes, and standards on UHPC, UHPFRC, or SFRC.

Table 12.1 Summary of fiber orientation factors from different recommendations, guidelines, codes, and standards on UHPC, UHPFRC, or SFRC

Serial No.	**Recommendation, guidelines, codes, and standards on UHPC, UHPFRC, or SFRC**	**Fiber orientation factor**
1	AFGC Recommendation on Ultra-High Performance Fiber-Reinforced Concrete (UHPFRC) (2002 and 2013)	$K_{global} = \frac{\overline{M_{m,max,\iota}}}{\overline{M_{s,max,\iota}}}$ $K_{local} = \frac{\overline{M_{m,max,\iota}}}{(M_{s,max,i})_{min}}$ $K_{global} = \frac{\overline{F_{m,max,\iota}}}{\overline{F_{s,max,}}}$ $K_{local} = \frac{\overline{F_{m,max,\iota}}}{(F_{s,max,i})_{min}}$ Without suitability test, K_{global} = 1.25 K_{local} = 1.75
2	fib Model Code for Concrete Structures (fib MC2010 and in progress fib MC2020)	$K = \frac{\alpha_0}{0.58}$ α_0 = 0.5 in the case of 3D random fiber orientation; α_0 = 0.64 in the case of 2D random fiber orientation (for any sectional plane perpendicular to the fiber plane) α_0 = 0 in the case of 2D random fiber orientation (for a sectional plane parallel to the fiber plane) α_0 = 1 in the case of 1D aligned fibers (for a sectional plane perpendicular to the fiber direction) α_0 = 1 in the case of 1D aligned fibers (for a sectional plane perpendicular to the fiber direction) K >1 (favorable condition) K <1 (unfavorable condition) K = 0.5 in a local check without any experimental investigation should be considered as an unfavorable effect.

Table 12.2 Summary of fiber orientation factors from different recommendations, guidelines, codes, and standards on UHPC, UHPFRC, or SFRC (continued)

Serial No.	**Recommendation, guidelines, codes, and standards on UHPC, UHPFRC, or SFRC**	**Fiber orientation factor**
3	French National Standards: (1) NF P18-710, National addition to Eurocode 2 - Design of concrete structures: specific rules for Ultra-high performance fibre-reinforced concrete (UHPFRC) (2016), (2) NF P 18-470, Concrete - Ultra-high performance fibre-reinforced concrete- Specifications, performance, production and conformity (2016), (3) NF P 18-451, Concrete - Execution of concrete structures - Specific rules for UHPFRC (2018)	$K_{global} = \frac{\overline{M_{m,max,\iota}}}{\overline{M_{s,max,\iota}}}$ $K_{local} = \frac{\overline{M_{m,max,\iota}}}{(\overline{M_{s,max,\iota}})_{min}}$ $K_{global} = \frac{\overline{F_{m,max,\iota}}}{\overline{F_{s,max,}}}$ $K_{local} = \frac{\overline{F_{m,max,\iota}}}{(\overline{F_{s,max,\iota}})_{min}}$ Without suitability test, K_{global} = 1.25 K_{local} = 1.75
4	ACI 239C Emerging Technology Report (ETR) (2018 and 2019) (Draft copy)	K_G = 1.3 K_L = 1.7
5	Korean Guidelines: (1) KICT Design Guideline for K-UHPC (2014) (2) KCl-M-19-006, The Structural Design Guidelines of Fiber Reinforced SUPER Concrete (2019)	Not applicable.

Table 12.3 Summary of fiber orientation factors from different recommendations, guidelines, codes, and standards on UHPC, UHPFRC, or SFRC (continued)

Serial No.	**Recommendation, guidelines, codes, and standards on UHPC, UHPFRC, or SFRC**	**Fiber orientation factor**
6	Swiss Society of Engineers and Architects (SIA), Béton fibré ultra-performant (BFUP); Matériaux, dimensionnement et exécution (2016) (SIA 2052)	η_K = 0.90 and 0.75 and η_{hU}= 0.8 to 1.0 (geometry factor)
7	Australian Standard of Concrete structures (2018) (AS 3600)	$K_s = 0.64$ (for shear only) $k_{3Dt} = \frac{1}{0.94+0.6l_f/b} \leq 1$ (for behavior other than shear) $k_{3Dtb} = \frac{1}{1+0.19l_f/b} \leq 1$ (for behavior other than shear)
8	DAfStb Guideline on Steel fibre reinforced concrete (2012 and 2019)	κ_F^f=0.5 (flat, horizontal, or planar components) κ_F^f= 1.0 (for beams in their longitudinal direction for bending and tensile loads)
9	JSCE Recommendations (a) Recommendations for Design and Construction of High Performance Fiber Reinforced Cement Composites with Multiple Fine Cracks (HPFRCC) (2008) (b) Recommendations for the Design and Construction of Ultra High Strength Fiber-Reinforced Concrete (UHSFRC) of JSCE (2006)	Not applicable.

Table 12.4 Summary of fiber orientation factors from different recommendations, guidelines, codes, and standards on UHPC, UHPFRC, or SFRC (continued)

Serial No.	**Recommendation, guidelines, codes, and standards on UHPC, UHPFRC, or SFRC**	**Fiber orientation factor**
10	Canadian standards: (1) Concrete materials and methods of concrete construction/Test methods and standard practices for concrete (2019) (CSA A23.1:19) (2) Canadian Highway Bridge Design Code (2019) (CSA-S6:19)	As per CSA S6:19: γ_F= fiber efficiency factor, which is the ratio of characteristic tensile properties obtained by four-point flexural test on a sawn sample from real or mockup structures and that of laboratory cast sample, or, following value: i) for elements cast horizontally in which a mostly two-dimensional fiber dispersion is expected, such as decks and slabs: γ_F = 0.8 for flexure and beam shear; γ_F = 0.6 for two-way action shear ii) for elements cast vertically in which a mostly two-dimensional fiber dispersion is expected, such as walls: γ_F = 0.5 for flexure and beam shear; γ_F = 0.5 for two-way action shear, iii) for bond and development length of reinforcement: γ_F = 0.5, iv) for large structural components and elements in which three-dimensional fiber dispersion is expected, such as beams, girders, footings: γ_F = 0.4, and v) for local effects, such as anchors: γ_F = 0.3.
11	AASHTO LRFD guide specification for structural design with ultra-high performance concrete 2021, Version 1.0 (proposed version)	Not applicable.

PART 2: Literature Review of Other Studies on the Effect of UHPC Casting Procedure on Fiber Orientation and Mechanical Performances

14. Introduction

The unique tensile response of ultra high performance concrete (UHPC) is affected not only by the material composition but also by the casting method, pouring processes, direction of flow, element construction process, which have a tremendous effect on fiber dispersion and orientation, and ultimately on the mechanical and structural performance of UHPC. In addition, the fiber orientation and distribution may also be affected by the flow properties of the UHPC mixture, the size, geometry of the formwork, and the presence of rebars and prestress tendons. In this deliverable, the effect of the casting procedure on fiber orientation and dispersion, as well as mechanical performance, are critically reviewed.

Based on the scale of the investigation, we grouped the relevant available literature into two categories. In the first category, the investigations on the structural-scale (large-scale) members are reviewed, in which the researchers applied realistic casting procedures and then either measured fiber orientation employing different methods or performed mechanical testing to verify fiber orientation or both. In the second category, studies on small-scale lab specimens are reviewed. In our review, we found that extensive studies have been conducted in the second category. Many special casting procedures or casting devices have also been developed to control the fiber orientation in a desirable manner at this scale. However, there are very limited investigations on quantifying the actual fiber orientation and distribution of UHPC or on the influence of casting procedure to control the fiber orientation and dispersion in realistic large-scale structural members. Also, there exists a big knowledge gap on the scalability of the casting procedures or devices developed at a small scale for large-scale structures. The detailed reviews will be provided in the following sections.

In this document, the term “UHPC” is used consistently. In many literatures, especially from European researchers, the term ultra-high performance fiber reinforced concrete (UHPFRC) is used. There exists a slight difference between these two terms by definition, which is not relevant to this discussion. Therefore, for simplicity, in this document, the term “UHPC” is used when referring to all similar materials with steel fibers.

15. Effect of Casting Procedure on Fiber Orientation and Mechanical Properties for Large Scale UHPC Structure

In this section, different UHPC casting procedures for the realistic large-scale structural members and their effects on fiber orientation are discussed. This section provides a review of the effects of casting flow, casting devices, rebar arrangement on the fiber orientation, and structural performance of UHPC structures.

15.1 Effect of casting procedure in longitudinal members

In this section, the effect of different casting procedures, especially different casting flow directions, on the fiber orientation and structural properties of longitudinal members (e.g., beams, piles) are reviewed. The casting flow for long structures can be categorized as (i) casting from one end (of the beam) and letting the material flow to the other end, and (ii) casting from the middle (of the beam) and letting the material flow to the ends. The self-consolidation property of the UHPC mix allows it to flow in the formwork, which tends to align the fibers in the flow direction, but the exact fiber orientation may vary depending on many factors, e.g., size of structures, flow distance, the geometry of structure and formwork, rebar arrangement, etc. In addition, several researches also reported using special casting procedures, which are also discussed in this section. Due to the limited number of studies, we found in this category, many other studies, which did not focus on the influence of casting procedure but reported the casting procedure as part of their experimental approach, are also included.

Kang and Kim (2012) summarized the orientation of fibers resultant from different flow patterns of the mixtures (Figure 15.1). These flow patterns are the results of the changes in formwork geometry and size, placement position and direction, and rheology of the mixtures. For example, placing UHPC from one end of a confined geometry (e.g., a beam) and letting it flow can result in the confined shear flow of the mixture (Figures 15.1a-c). Fibers tend to align along the flow direction of the mixture. There exists a similar, increased, and decreased shear stress for parallel sides (Figure 15.1a), converging sides (Figure 15.1b), and diverging sides (Figure 15.1c), respectively, which provides moderate, high, and low fiber alignment, respectively. Fiber orientation can be improved with the increase of the distance of flow of the UHPC mixture, leading to a higher extent of fiber alignment with increasing flow distance. On the other hand, placing UHPC at one point of the slab and letting it flow outwards in an unconfined condition can lead to the radial flow (Figures 15.1d and 15.1e), such as in the case of the center casting of slabs. Such flow of mixture can drive fibers to align perpendicularly to the flow direction (Figures 15.1d and 15.1e). The extent of fiber alignment also increases with increasing flow distance. This is consistent with all the research findings discussed in Sections 2.1, 2.2, and 3.1.

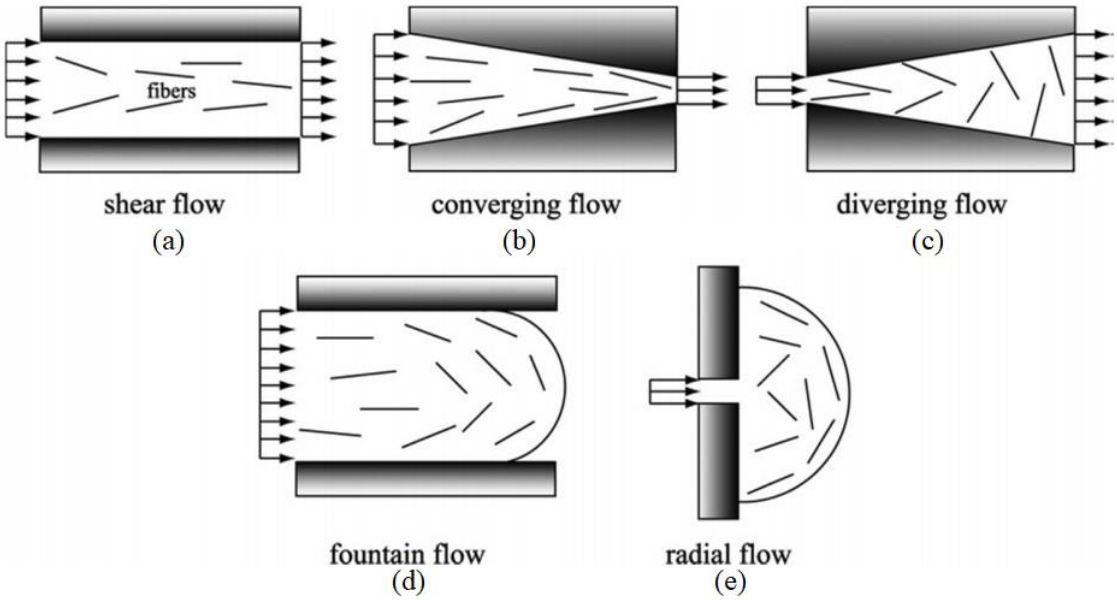

Figure 15.1 Orientation of fibers in different flow patterns (Kang and Kim 2012).

Yang et al. (2010) examined the influence of casting flow on the flexural behavioral characteristics on 14 reinforced UHPC beams (180 x 270 x 2,900 mm [7 x 10.6 x 114.2 in.]) with rebar ratios ranging 0-0.02 and 2% steel fibers (straight steel fibers with a diameter of 0.2 mm [0.0078 in.] and a length of 13 mm [0.51 in.]). The flexural capacity was found to be affected by the placing method of the UHPC even for identical cross-sections and rebar ratios. The UHPC was placed using two methods, i.e. (1) placed from one end of the form and allowed to flow to the other end to complete the filling process, (2) placed from the midspan and allowed to flow to both ends of the form (Figure 15.2). The authors reported that placing the UHPC from the end of the beam provided better structural performance than placing the UHPC from midspan. When casting from one end, the UHPC flow along the longitudinal direction orienting the fiber towards the flow direction (i.e., principal tensile stress direction under bending) at midspan where the bending stress is highest. On the other hand, the outward flow from the midspan during midspan casting partially disturbed the fiber orientation at the midspan. As a result, the beam cast from one end showed 5-15% higher bending load capacity compared to the beam cast at midspan. This result further confirmed that the alignments of the steel fibers were influenced by the UHPC placing direction.

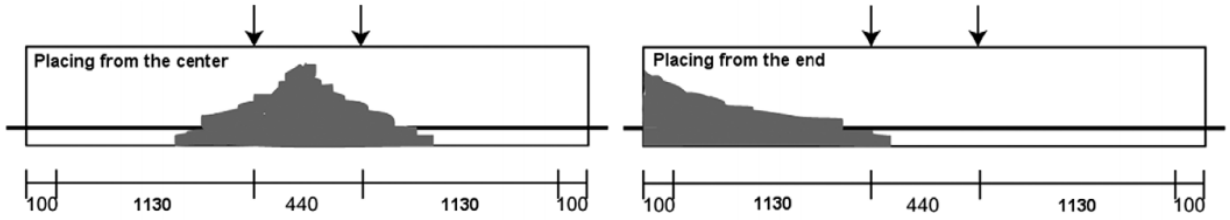

Figure 15.2 Procedure for placing the UHPC (Yang et al. 2010)

The following studies did not evaluate the impact of different casting procedures; however, they reported the casting procedure and reported the corresponding fiber orientation.

Groeneveld et al. (2017a) investigated the effect of fiber alignment on dynamic strength and ductility of a UHPC (using 0.55 mm [0.022 in.] diameter and 30 mm [1.2 in.] long hooked-end fibers with 3.15% volume fraction) with varying casting flow directions. They constructed a beam specimen measuring roughly 200 mm wide, 610 mm high, and 3050 mm long (8 in. wide, 24 in. high, and 10 ft long) as a representative structural element. The beam was cast from one end, and concrete was allowed to flow (along x-axis) and fill the formwork. Vibration was applied to the formwork walls, but not to the UHPC itself, to achieve reasonable consolidation without fiber segregation. The narrow beam was intended to give a realistic assessment of fiber alignment due to flow. Figure 15.3 shows the schematic view of the beam and scheme of cutting the cores. The cores were extracted and observed under x-ray Micro CT to determine the fiber orientation. The x-ray CT scans were performed at the University of Florida's Advanced Materials Characterization Laboratory (AMCL). The image analysis was performed in MATLAB (The MathWorks 2014) using the methodology and code established by Oesch (2015). The measured mean fiber orientation angles are 39-degrees, 71.2-degrees and 62.2-degrees with respect to x-, y- and z- axes of the beam respectively (Groeneveld et al. 2017b). The x-ray Micro CT imaging showed that the highest fiber alignment was along the direction of flow.

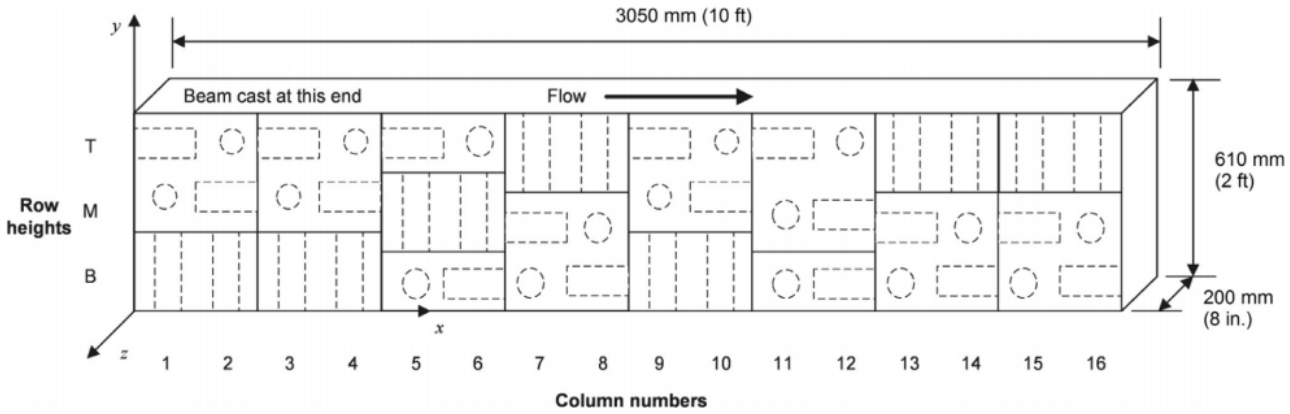

Figure 15.3 Schematic view of the beam. Cores are shown with dashed lines; cuts for blocks or prisms are shown with solid lines. Not to scale (Groeneveld et al. 2017a).

de Andrade et al. (2021) evaluated the fiber orientation in a UHPC mock-up specimen of Class I-B Motorway in Brazil. The bridge structure was comprised of a single carriageway made of eight parallel box girders as shown in Figure 15.4. The UHPC mix used 1.5% hooked steel fiber with a length of 60 mm (2.36 in.) and diameter of 0.75 mm (0.0295 in.). The UHPC was cast manually using a bucket (Figure 15.5a). Figure 15.5 shows the casting sequence and casting flow (vertical for webs and horizontal for the deck as shown in Figures 15.5 b and 15.5c). Figure 15.5(d) shows the mock-up specimen. After the image analysis of sawn samples from different locations of mock-up specimen, the authors reported that there was a tendency of 2D alignment of fiber when the thickness of

formwork reduces due to the wall effect. The authors calculated the global fiber orientation factor (K_{global}) as per AFGC recommendation (2013), which are 1.15-1.44 for sidewalls and 0.53-1.11 for top flanges in the principal stress direction (longitudinal direction).

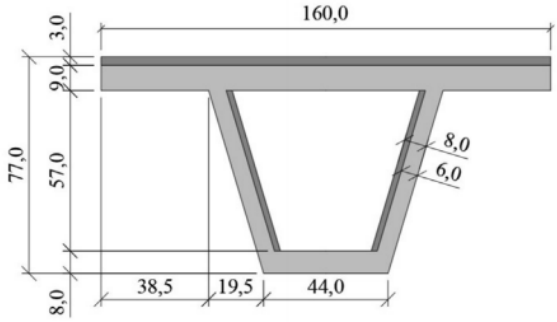

Figure 15.4 Cross-sections (all parts are UHPC) and dimensions of the elements of the girder for the carriageway of a Class I-B Motorway in Brazil. (units in cm) (de Andrade et al. 2021).

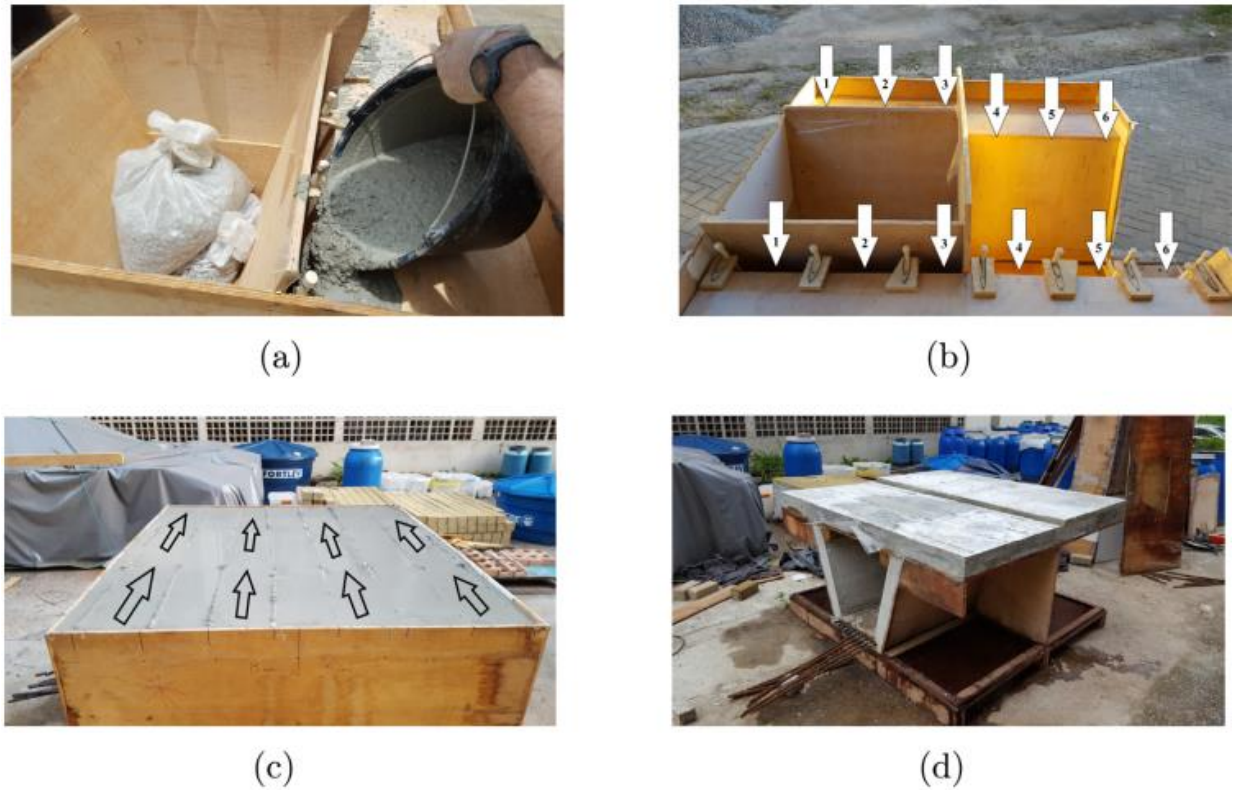

Figure 15.5 Casting method: (a) UHPC pouring using a plastic bucket; (b) pouring sequence in the webs (vertical flow); (c) pouring direction in the top flange (horizontal flow); (d) mock-up demolding (de Andrade et al. 2021).

The following studies did directly report the fiber orientation, however, they assumed certain fiber orientation (e.g., K=1.0 or other values, or random fiber orientation) for flexural analysis and obtained good agreement with the experimental results. This may indicate that they had achieved the assumed fiber orientation at critical sections. However, this correlation is very indirect and not reliable.

Khalil and Tayfur (2013) investigated the flexural behavior of ten 150×150×1950 mm (6×6×76.7 in.) reinforced UHPC beams containing hooked and crimped steel fibers (length of 30 mm [1.18 in.] and diameter of 0.6 mm [0.023 in.]) with different volume fractions (0.5%, 0.75%, and 1%) and compared with a control beam of the same size with no fibers. They prepared two types of beams, e.g., full depth UHPC beams and partial (bottom half) depth UHPC beams. Figure 15.6 shows the rebar arrangement and loading setup of the beams. The UHPC mix in full depth UHPC beams was placed in three equal layers; each batch was prepared to have a volume of about one-third of the beam volume. Each layer was compacted by means of internal vibration for about 40-60 seconds. Partial-depth UHPC beams were cast for the bottom and top half parts in two layers with the same vibrator. The authors considered a uniform fiber orientation and numerically calculated the moment capacities considering the random 3D fiber orientation factor of 0.41 which showed a good agreement with the experimental result.

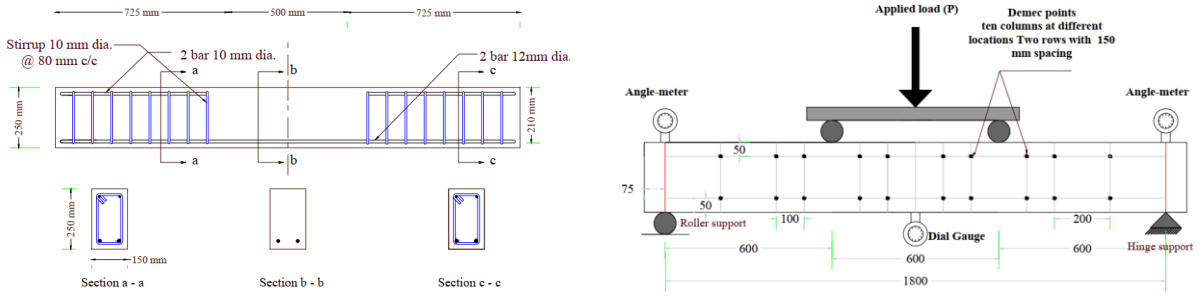

(a) (b)

Figure 15.6 (a) Details of reinforcement for beam specimens; (b) schematic drawing showing the general flexural test setup for beam specimens (Units: mm) (Khalil and Tayfur 2013).

Yoo and Yoon (2015) tested a total of ten large reinforced UHPC beams (Figure 15.7) of size 150 mm x 220 mm x 2500 mm (6 in x 9 in x 100 in) with 2% steel fibers and reinforcement ratios of 0.94% and 1.5%. Three different fibers with lengths of 13 mm (0.51 in.), 19.5 mm (0.77 in.) and 30 mm (1.18 in.), respectively, and corresponding diameters of 0.2 mm (0.0078 in.), 0.2 mm (0.0078 in.) and 0.3 mm (0.0118 in.), respectively, were used. and two different shapes (i.e., straight smooth, and straight twisted). The fresh UHPC mix was cast from one end of the formwork and allowed to flow to the other end and fill completely. They suspected that the fiber orientation and dispersion were poorer for the reinforced beams with longer steel fibers owing to the interruption of stirrups and longitudinal steel rebars compared to those of the fibers with shorter lengths. They also reported that the assumed fiber orientation factor K=1.25 (as per AFGC recommendation 2002, 2013) showed quite good agreement with the experimental results and better prediction of the flexural response of the UHPC beams, compared to that without consideration of fiber orientation coefficient (i.e., K=1.0).

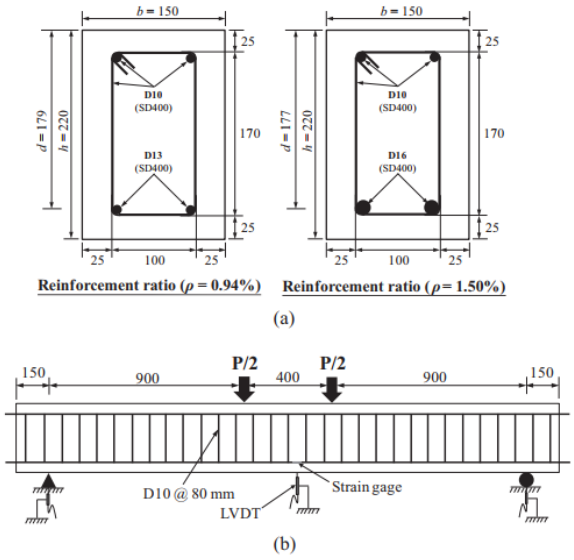

Figure 15.7 Details of test program (unit: mm): (a) cross-section details of test beams; (b) details of test setup (Yoo and Yoon 2015)

Singh et al. (2017) cast four UHPC simply supported beams, as shown in Figure 15.8 using UHPC with 2.25% by volume of hooked steel fibers. The length and diameter of the hooked steel fibers were 35 mm (1.38 in.) and 0.55 mm (0.0216 in.), respectively. In this study, the authors claimed that the presence of shear reinforcement restricted the free flow of the UHPC mix, due to this reason, the beams were fabricated by placing the UHPC mix horizontally using the back-and-forth placement method along the span of the beam. They modeled the beams in a finite element platform to back estimate the fiber orientation. They observed that the ultimate load capacity of the FE models was overestimated by more than 25%, when the global fiber orientation coefficient as per AFGC recommendation (2002, 2013) was taken as K=1.0. However, the coefficient K = 1.25 was adopted to account for the disturbed fiber orientation in the beam specimens and observed that ultimate capacity was underestimated by 4%. They concluded that a higher fiber alignment along the principal stress direction can be achieved by the back-and-forth placement method compared to casting from one end and the use of a fiber orientation factor of 1.25 (as per AFGC recommendation 2013) was found appropriate considering the influence of rebar arrangements.

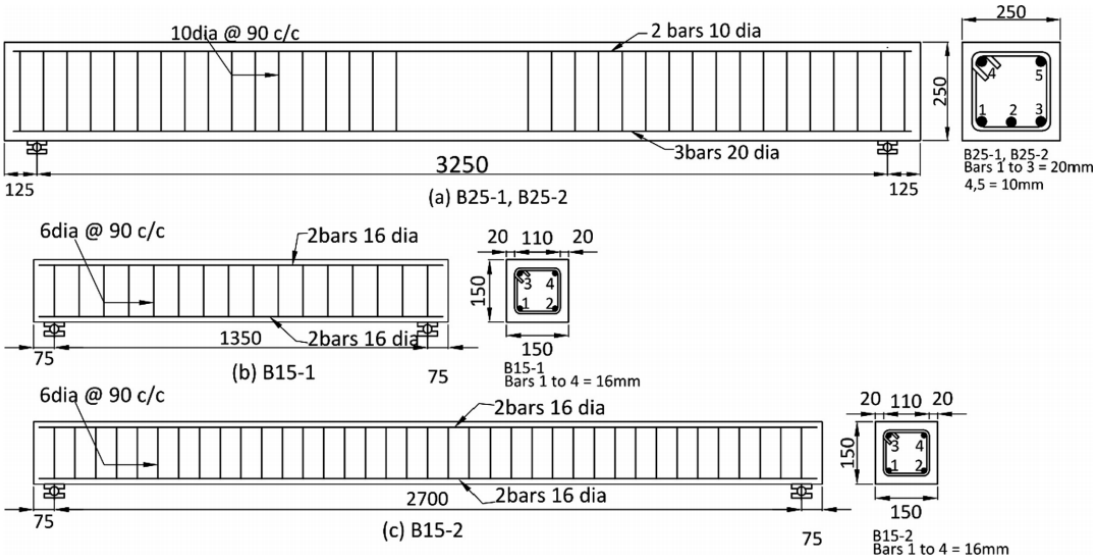

Figure 15.8 Reinforcement detail of beams, B25-1 and B25-2 are identical (Singh et al. 2017)

Yoo et al. (2017) experimentally and numerically investigated the flexural behavior of reinforced UHPC beams with varying reinforcement ratios. They fabricated and tested four UHPC beams with different reinforcement ratios (0%-1.71%). The UHPC mix had 2% by volume of straight steel fibers with a diameter of 0.2 mm (0.0078 in.) and a length of 13 mm (0.51 in.). For all test beams, UHPC mix was carefully placed from one end of the beam and allowed to flow to fill the molds completely. The details regarding the geometry and reinforcement of the beams are shown in Figure 15.9. The study reported that AFGC recommendations (2002, 2013) well predicted the flexural behavior assuming the global fiber orientation factor K=1.0, which refers to uniform fiber orientation.

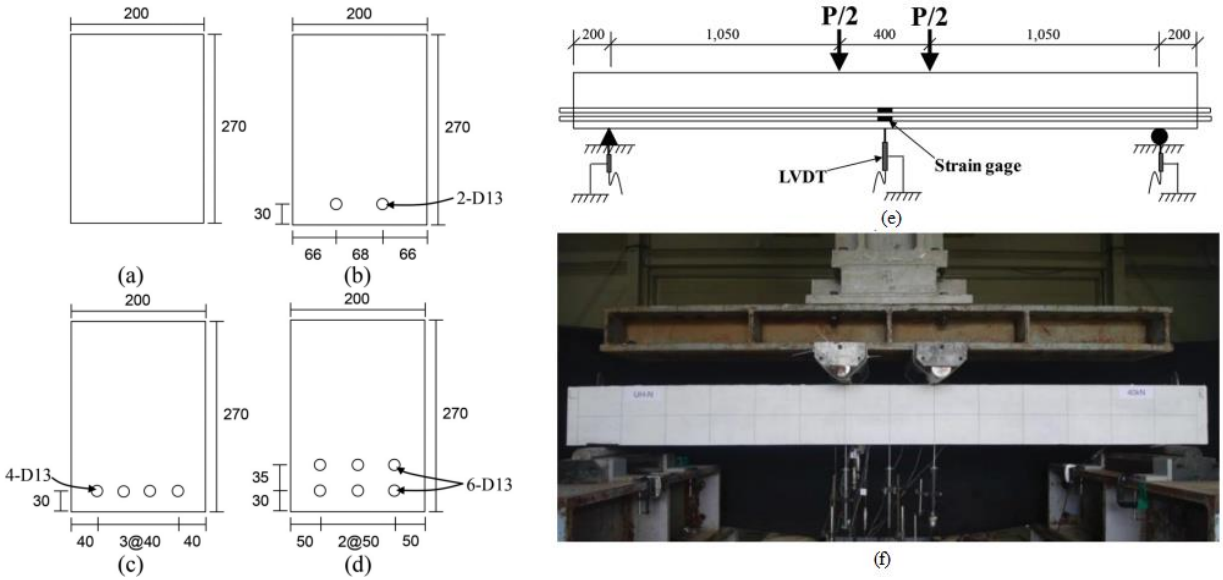

Figure 15.9 (a)-(d) Section details of flexure test program (unit: mm); (e), (f) details of test setup (unit: mm) (Yoo et al. 2017).

Hasgul et al. (2018) experimentally investigated the deflection and curvature ductility, moment capacities, flexural stiffness, and cracking behaviors of UHPC beams (using 1.5% by volume of straight micro-steel fibers with a diameter of 0.16 mm [0.0063 in.] and length 13 mm [0.51 in.]). Eight singly reinforced beams with four tensile reinforcement ratios (0.009, 0.019, 0.028, and 0.043) were tested under four-point loading (Figures 15.10a and 15.10b). The fresh UHPC mix was cast from the midspan of the beam and allowed to flow to the ends (Figure 15.10c). They reported that the use of UHPC provides increases between 23% and 50% for the moment capacities compared to the non-fiber reinforced beams. The authors considered a random fiber orientation in 3D space and numerically calculated the moment capacities considering the fiber efficiency factor of 0.41 which showed a good agreement with the experimental result.

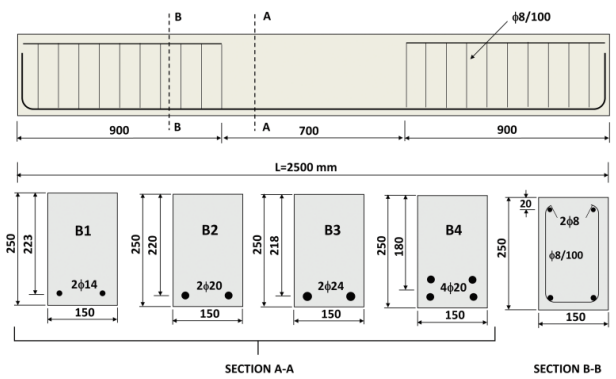

(a)

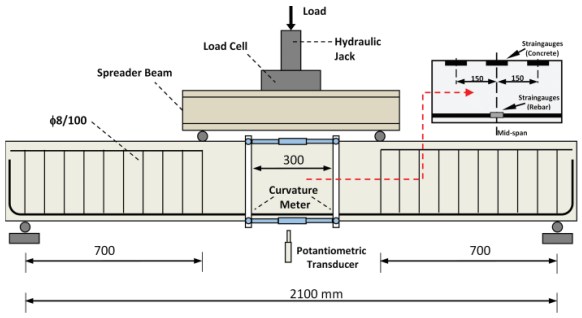

(b)

(c)

Figure 15.10 (a), (b) Reinforcement details and loading setup of the beams, dimensions are in mm; (c) casting procedure of the beams (Hasgul et al. 2018)

In Turker et al. (2019) study, eight UHPC beams and four reference beams (without fibers) with four different tensile reinforcement ratios (0.009, 0.019, 0.028, and 0.043) were tested (Figure 15.11). Two groups of fibers were used to prepare the UHPC beams (using monofiber of 1.5% by volume of short-straight steel fibers of length 13 mm [0.51 in.] and diameter of 0.16 mm [0.0063 in.], and hybrid steel fibers consisting of 1% of short-straight fiber and 0.5% of long-hooked fiber of length of 60 mm [2.36 in.] and diameter of 0.75 mm [0.0295 in.]). They placed the UHPC from mid-span and allowed it to flow to the ends. They also considered a uniform fiber orientation and numerically calculated the

moment capacities considering the 3D fiber efficiency factor of 0.41 (same as Hasgul et al. 2018), which also showed a good agreement with the experimental result.

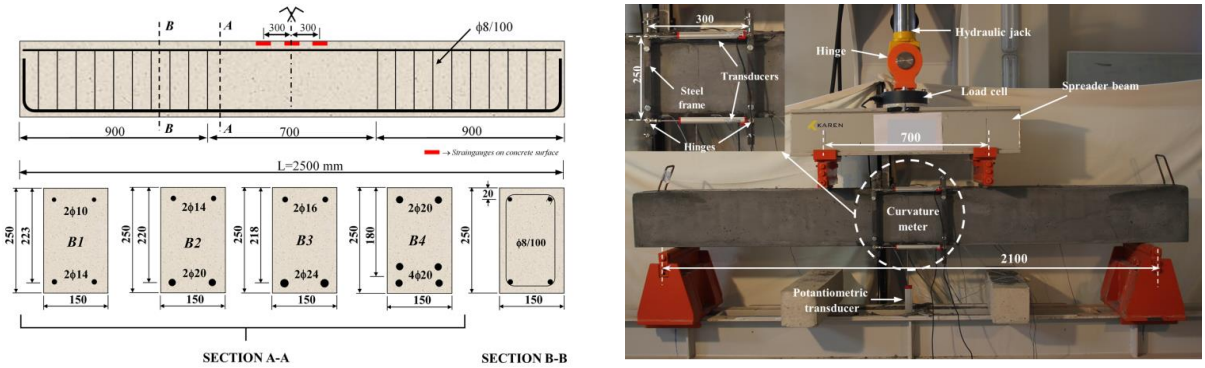

(a) (b)

Figure 15.11 (a) Beam geometries and reinforcement details; (b) four-point bending test setup (Turker et al. 2019)

It should be noted that some of the above-mentioned studies assume K=1.0 or random fiber orientation in the analysis and obtained results that agreed well with experimental results. This is contradictory to UHPC construction project experiences following AFGC recommendations (2002, 2013) reported in deliverable 2, which reported measured K factors to be much higher. The reason may be that the studies reviewed in this section are of relatively small size compared to that of the project experience reported in deliverable 2. In this case, the fiber tends to align in the longitudinal direction leading to desirable flexural performance.

Several other investigations on the structural behavior of UHPC members also reported their casting procedure but did not attempt to identify the fiber orientation in any way. For example, Graybeal (2006) tested AASHTO Type II UHPC girders, and they reported that the girders were cast from one end of the formworks and were externally vibrated on an intermittent basis using a formwork vibrator during the casting. Sritharan et al. (2011) and Voort et al. (2008) constructed and tested UHPC pile that were cast from one end and internal vibration was applied to ensure complete filling. Shao and Billington (2019) tested steel-rebar-reinforced UHPC beams, in which the UHPC was also placed from one end of a beam mold. Kahanji et al. (2017) also tested UHPC beams subjected to four-point loading, and they reported that the molds were placed on a vibrating table during casting and UHPC was cast from one end, and no specific dominating fiber orientation was observed. Chen et al. (2018) also investigated reinforced UHPC beams under pure bending and combined bending and shear, in this study, the UHPC mixture was placed from mid-span and allowed to flow both ends.

15.2 Effect of casting procedure in slabs and panels

In this section, the casting procedure, especially the casting flow direction of UHPC mix in the slabs or panels of circular or rectangular shapes is discussed. Compared to realistic large-scale slabs, the scale of the following reviewed research is still on the smaller side, however, these researches provide representative data to understand the UHPC flow behavior in flat members and their effect on fiber orientation and mechanical performances of UHPC.

Kim et al. (2008) evaluated the effect of the filling method on fiber orientation and dispersion and mechanical properties of UHPC. They prepared unreinforced structural-level UHPC slab (1320 x 1320 x 100 mm [52 x 52 x 4 in.]) with 2% short steel fibers as shown in Figure 15.12. UHPC placing was done by free fall from a height of about 200 mm (8 in.) from the center of the plate. The fresh UHPC was let to flow radially by itself. The complete filling was realized without additional finishing work except surface finishing. Figure 15.12(a) depicts the placing and flow directions during the manufacture of the plate structure. Specimens were cut from the slab as illustrated in Figure 15.12(b) and tested for flexural behavior to investigate the effect of casting flow on fiber orientation. The result revealed that the flexural strength increased when the flow of UHPC was oriented perpendicularly to the direction of the principal tensile stress. This showed that the alignment of the fibers tends to be normal to the flow at a larger flow distance from the pouring site as shown in Figure 15.12(c).

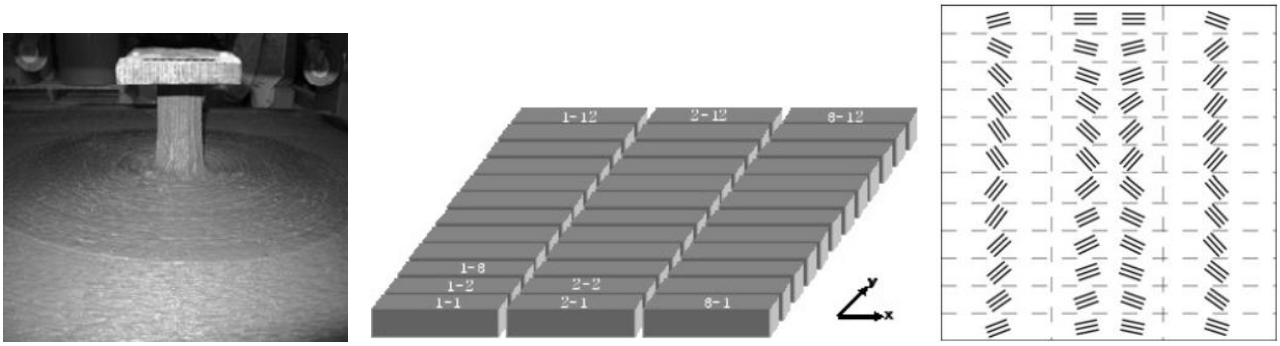

(a) (b) (c)

Figure 15.12 (a) UHPC flow direction; (b) labeling and cutting scheme of slab element and shape of plate pieces; (c) relative orientation of fiber by position in the plate (plan view of the slab element) (Kim et al. 2008).

Barnett et al. (2010) conducted an experimental investigation on casting UHPC circular panels of 550 mm (21.6 in.) in diameter using three placement methods, i.e., (i) placing UHPC from a single point at the center of the slab, (ii) placing UHPC from several points around the perimeter of the slab, and (iii) placing UHPC from several points randomly (Figure 15.13). The UHPC used 2-4% of straight 13 mm (0.51 in.) long steel fibers with a diameter of 0.2 mm (0.0078 in.). The authors reported that from the image analysis of the x-ray computed tomography (CT), for panels poured from the center, the fibers tend to align perpendicular to the radius of the panels, i.e., perpendicular to the flow of the fresh UHPC. In the case of panels poured at the edge, the fibers were aligned along the radius of the panels.

For panels poured randomly, the fibers were oriented randomly. In the case of flexural strengths under center point loading with 3 point support equally spaced near periphery, panels poured from the center, in which the fibers tended to align perpendicular to the radius, was the strongest (maximum load carried 78.7 kN or 17.7 kips); panels poured at the edge, where the fibers tended to lie more parallelly to the radius, was the weakest (maximum load carried 42.8 kN or 9.6 kips), and panels poured randomly, where the fiber orientation seemed to be more random, had an intermediate strength (maximum load carried 62.2 kN or 13.9 kips). It is clear from this research that the center casting orients the fibers tangentially (perpendicular to the flow direction) and casting from the periphery of the edge aligns the fibers parallel to the radius (along flow direction).

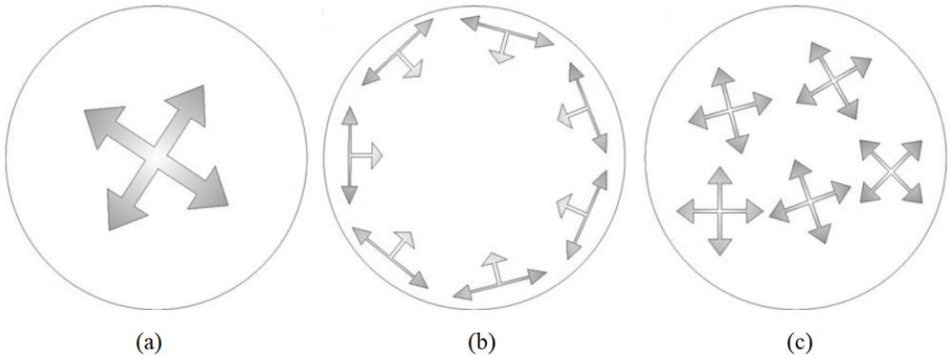

Figure 15.13 Schematic showing the flow of concrete according to casting method: (a) center; (b) perimeter; (c) random (Barnett et al. 2010).

Zhou and Uchida (2017) also cast circular UHPC panels of a diameter of 1200 mm (47 in.), using UHPC with 2% steel fibers that are 15 mm (0.51 in.) long and 0.2 mm (0.0078 in.) in diameter, from its center point to investigate the orientation and distribution of fibers along the radial direction (Figure 15.14a). The authors also constructed a 1.0 m (3.28 ft.) square panel cast from its center using a visualization model UHPC as shown in Figure 15.14(b) to better visualize the fiber orientation. They also observed that fibers in a panel cast from the center tended to orient perpendicular to the radial direction, especially at locations farther away from the center. To verify the flexural behavior, specimens were cut from the panels at different locations and directions as shown in Figure 15.14(a), and tested under flexure. Figure 15.15 shows the flexural stress-crack mouth opening displacement (CMOD) curves of the sawn specimens. The result indicated that even at the same cutting angle, there was a clear decrease in the post-cracking flexural strength of the specimens cut with flow distances (Figures 15.15a and 15.15b) for angles below 60 degrees. Due to the radial flow, the fibers get more aligned perpendicular to the flow direction with increasing flow distance. Moreover, the peripheral boundary wall aligned the fibers perpendicular to the flow near the boundary of the formwork due to the wall effect. This research's outcomes also support the findings of Barnett et al. (2010) as discussed above. In summary, the fiber aligned tangentially (perpendicular to the radial flow) while casting from the center of a panel, and the bending capacity along the tangential direction is significantly higher compared to the radial direction and along the radial direction. The fibers are more aligned at a longer flow distance from the casting point.

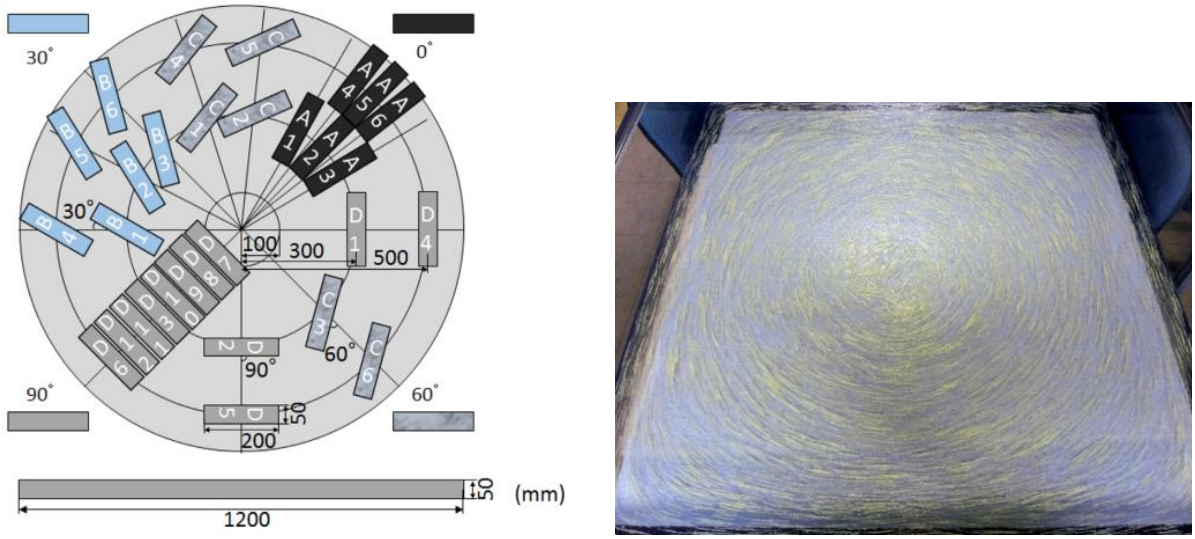

(a) (b)

Figure 15.14 (a) Saw cutting locations and orientations of specimens in circular UHPC panel, dimensions are in mm; (b) fiber orientation in the 1.0 m (3.28 ft.) square panel cast from its center using a visualization model concrete (Zhou and Uchida 2017).

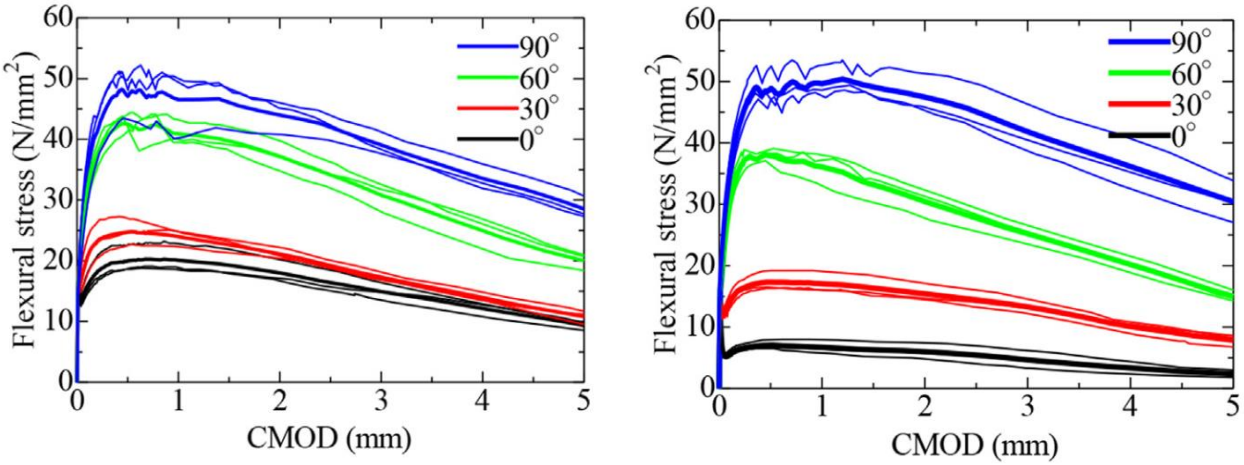

(a) (b)

Figure 15.15 Stress-crack mouth opening displacement (CMOD) curve at: (a) 300 mm (11.8 in.); (b) 500 mm (19.68 in.) from the center (Zhou and Uchida 2017).

Ferrara et al. (2011) investigated the effect of longitudinal and transverse casting flow on the mechanical properties and fiber orientation of rectangular UHPC slabs with short steel fibers (13 mm [0.5 in.] long and 0.16 mm [0.006 in.] in diameter with 1.27% fiber volume fraction). Figure 15.16 presents the case of longitudinal and transverse casting. Flexural specimens were cut from slabs along the longitudinal direction and transverse direction and tested for their flexural performance. For slab with casting flow along the longitudinal direction, the average flexural capacity of beams parallel to flow was 178% higher than beams perpendicular to flow, but in the case of the slab with casting flow

along the transverse direction, the average flexural capacity of beams parallel to flow is 23% higher than beams perpendicular to flow. These results indicate that fibers tend to align parallel to the flow direction in this case. For the larger casting of the flat specimen, the transverse casting may lead to more random fiber orientation and less fiber alignment in any particular direction, while longitudinal casting leads to more fiber alignment along the flow direction.

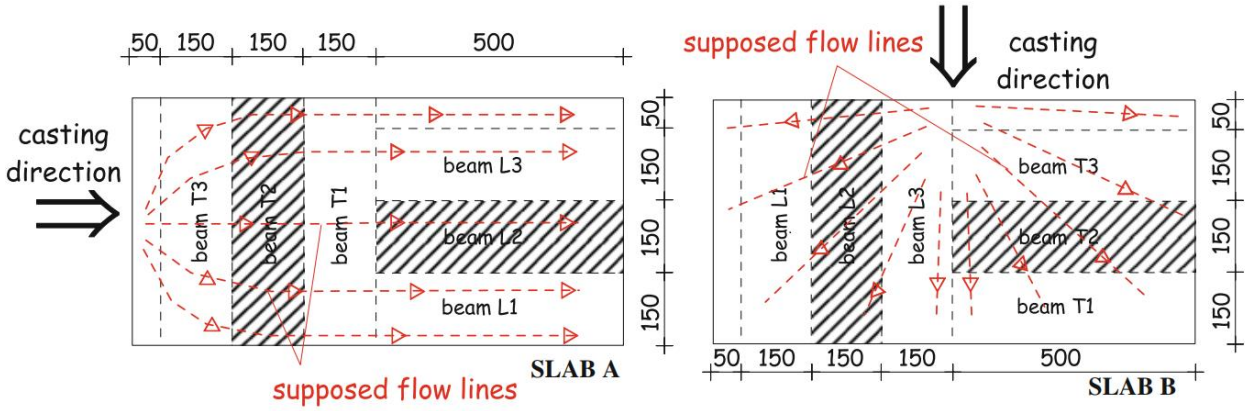

Figure 15.16 Schematic of slab-specimen (thickness 30 mm or 1.18 in.) casting flow and beam cutting (dashed specimens were further used for fiber orientation analysis) (Unit: mm) (Ferrara et al., 2011).

Duque and Graybeal (2017) also investigated the effect of casting direction for rectangular slabs. They cast UHPC (using 2% steel fibers of diameter 0.2 mm [0.008 in.] and length of 12.7 mm [0.5 in.]) slabs of 3048 x 914 x 50.8 mm (120 x 36 x 2 in.) with flow from one end to the other end in the longitudinal direction (Figure 15.17a). They collected sawn specimens from 0, 45, and 90 degrees (Figure 15.17b) to the direction of the casting flow and tested them under direct tension to evaluate the influence of casting direction on the fiber orientation and tensile behavior. Beam specimens of the same size were also directly cast in the lab and tested for comparison purposes. The 0-degree specimen showed higher strength and ductility followed by the mold cast specimen, 45-degree specimens, and 90-degree specimens. Figure 15.18 shows the tensile response of prismatic specimens. In summary, the experiment proved that there exists a strong influence of casting flow direction on the fiber orientation and corresponding mechanical properties of UHPC. The fibers tend to align along the flow direction.

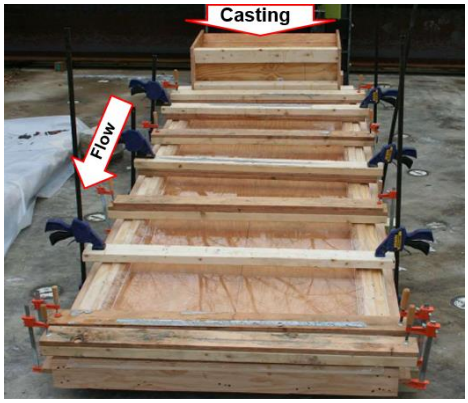

(a)

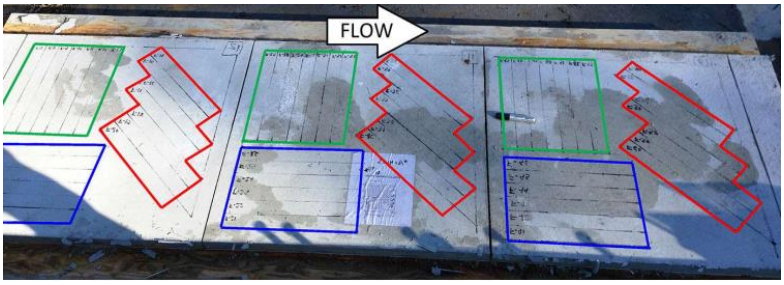

(b)

Figure 15.17 (a) The formwork of the slab element for casting; (b) layout of prismatic elements cut from UHPC slab (Duque and Graybeal, 2017)

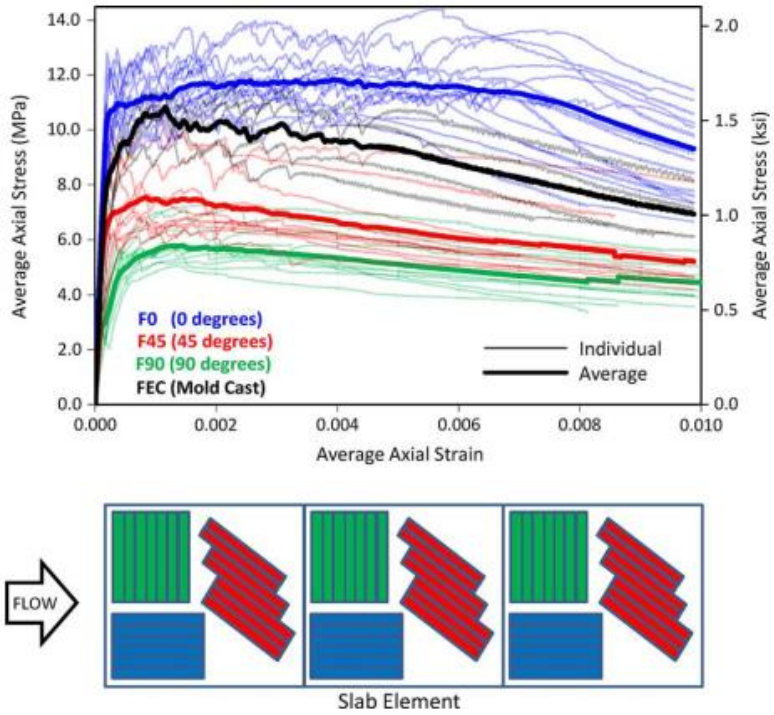

Figure 15.18 Tensile response of prismatic specimens, the thick lines are the averages for each specimen set (Duque and Graybeal, 2017).

When steel reinforcement is included in slabs, the flow of UHPC could be affected by the steel reinforcement, which also alters the fiber orientation. Nguyen et al. (2017) analyzed the relationships between the casting positions, casting flow directions, the fiber volume ratios, the slab thickness, and the reinforcement ratios on the punching shear capacity of 8 thin slabs (1000 x 1000 x 60 mm [39.4 x 39.4 x 2.4 in.]) made of UHPC. The UHPC mix used steel fibers of 13 mm (0.51 in.) in length and 0.20 mm (0.0078 in.) in diameter with volume fractions of 0, 0.8, and 1.6%. They followed three casting methods, e.g., from the center of the slab, from one side of the slab, and from one corner of the slab, as shown in Figure 15.19(a). To ensure good casting repeatability and align the fibers before entering the mold, a chute was used in this research. The chute with a flat bottom was made of steel and had an inclined angle of 20 degrees with respect to the horizontal plane. The chute length is approximately 1.6 m (5.25 ft). The arrangement of the casting equipment is shown in Figure 15.19(b). Based on the load-deflection curves of the slabs, the authors reported that the best position for casting UHPC depended on the volume fraction of fibers. At 0.8% of fiber, casting from the center of the slab showed the best performance, while at 1.6% of fiber, casting from one side of the slab showed outstanding punching shear behavior. The slabs prepared by casting from a corner presented good performance in both cases. The authors reported that the fibers nearby steel bars were blocked or reoriented by the rebars. Moreover, the narrow space in the concrete cover zone (between rebar and formwork base) could be inadequate for the flow of fibers. Hence, the number of fibers could be reduced, or the fiber orientation could be disturbed with increasing flow distance. Due to this issue, a fresh mix with a higher percentage of fiber such as 1.6% may cause a negative effect as mentioned.

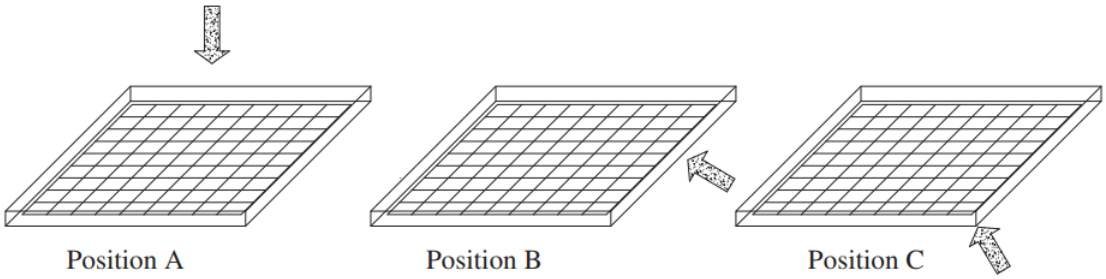

(a)

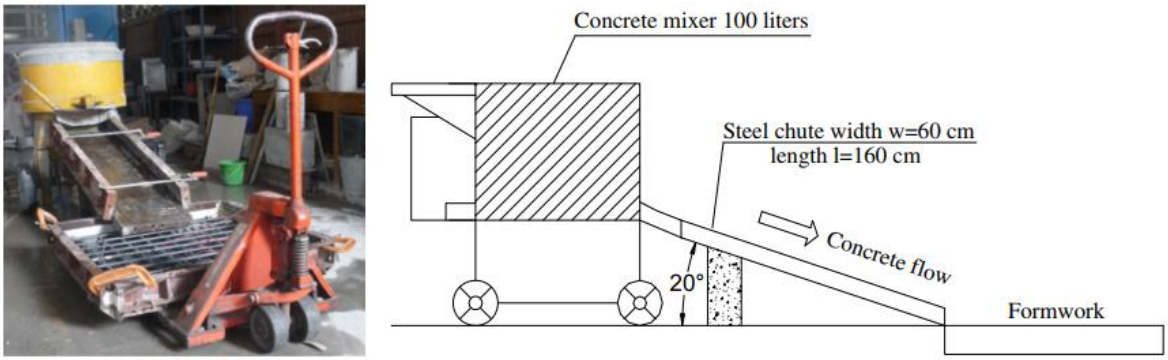

(b)

Figure 15.19 (a) UHPC casting positions; (b) the casting equipment and casting procedure (Nguyen et al. 2017).

In brief, for slabs, when casting from the center, the fibers tend to align perpendicular to the flow direction and when casting from one side, the fibers tend to align along the flow direction. This could be further explained by the mechanism detailed in Section 15.1. The presence of rebars may disturb the flow of fibers, making the fiber orientation more complex.

15.3 Effect of rebar arrangement

There is no clear study on the effect of rebar arrangement other than some studies pointed out the observed negative effect of the rebars on the fiber orientation. More studies are needed to quantify or measure the fiber orientation when there are complex geometries of rebar arrangement since the fibers do not only affect the mechanical property but also influence the rebar pullout out behavior, which will be discussed later. The following researchers reported mixed experiences on the effect on fiber orientation due to the rebar arrangements.

Several studies reviewed in earlier sections mentioned the rebars affect fiber orientation and distribution. For example, Yoo and Yoon (2015) suspected that the fiber orientation and dispersion were poorer for the reinforced beams with longer steel fibers owing to the interruption of stirrups and longitudinal steel rebars compared to those of the fibers with shorter lengths. Singh et al. (2017) claimed that the presence of shear reinforcement restricted the free flow of the UHPC mix and that the fiber orientation factor K was greater than 1.0 because of this. Nguyen et al. (2017) also reported that for reinforced UHPC slabs, the fibers nearby steel bars were blocked or reoriented by the rebars, the space in the concrete cover zone could be inadequate for the flow of fibers due to the thin geometry.

In addition, Shao and Billington (2021) investigated the bond between steel reinforcement and UHPC (using steel fibers of 0.2 mm [0.0078 in.] in diameter and 13 mm [0.51 in.] in length) using beam-end specimens (discussed in detail in Section 5). Figures 15.20(a) and 15.20(b) present the casting flow direction and location of the core sample collected for image analysis. Micro-computed tomography (Micro-CT) scan results of core samples revealed that when the casting flow was parallel to the longitudinal rebar, fibers were mostly aligned parallel to the bar, and there existed a fiber-free zone with a thickness of around 1.9 mm [0.075 in.] around the bar (Figure 15.20c).

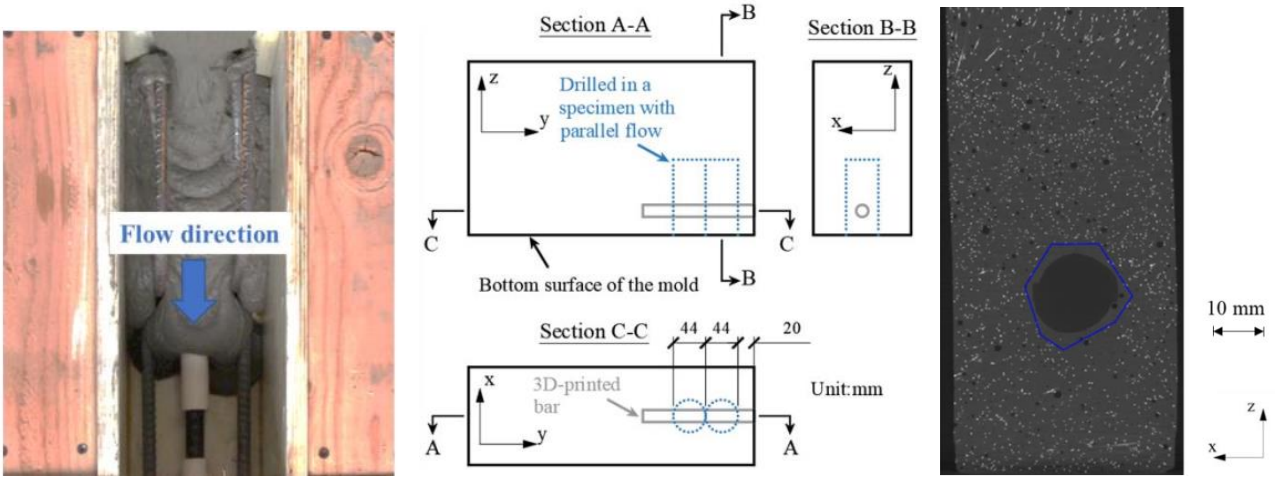

(a) (b) (c)

Figure 15.20 (a) Casting method; (b) core sample locations; (c) fiber orientation and dispersion around rebar in 2D CT image of the core sample in X-Z plane (Shao and Billington 2021).

Miletić et al. (2017) investigated the fiber orientation in the structural member with and without reinforcement using dynamic X-ray radiography. In order to more accurately observe the fiber orientation within the matrix, a viscous grain-laden fluid, consisting of glass beads, glycerol, and steel fibers were used instead of actual UHPC. The steel fibers used in the study were short straight wires and had a length of 11-14 mm [0.4-0.55 in.] and a diameter of 1.0 mm [0.0394 in.]. The total volumetric fiber content adopted in this experimental study was 2 %. Figure 15.21(a) shows the prototype mold for casting with reinforcement. Figure 15.21(b) shows a comparison of maps (obtained from analyzing the x-ray images) of the principal fiber orientation within the structural member with and without reinforcement. The color on the plots indicates the angle between the fiber major axis, and the horizontal plane in a counter-clockwise direction. It can be seen from Figure 15.21(b) that the fiber orientation was substantially affected by the presence of reinforcement, and local disturbance of the fiber orientation was observed near the rebars. However, the casting direction (from the top) of this specimen was not representative of regular beams due to the short length of the specimen, therefore, the actual fiber orientation may not be representative as well.

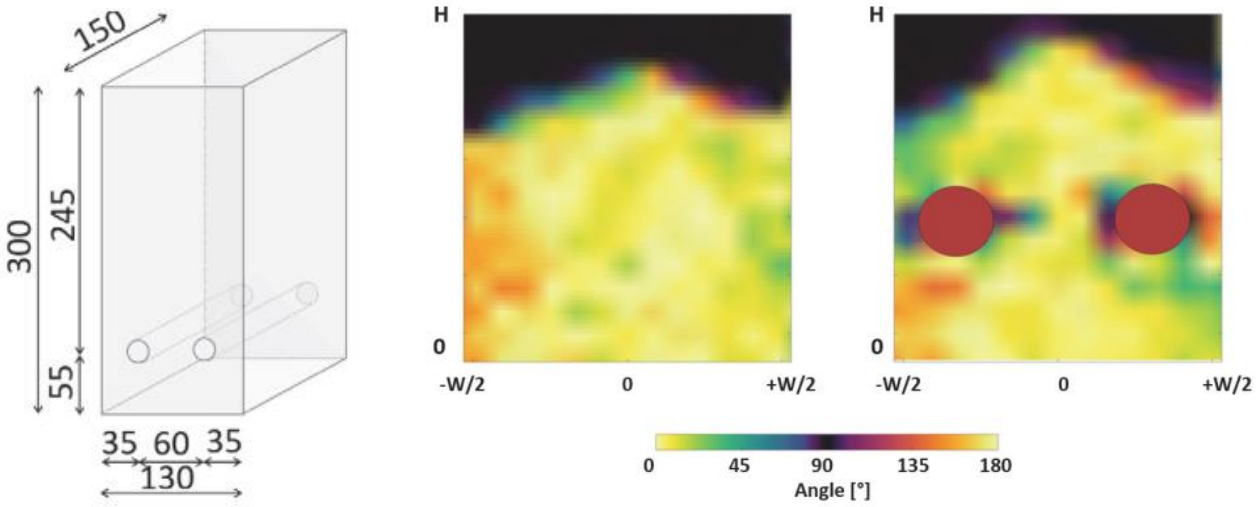

(a) (b)

Figure 15.21 (a) Schematic diagram of the experimental setup (all dimensions are in mm); (b) principal fiber orientation within the structural member (by analyzing dynamic x-ray images): without reinforcement at left, with reinforcement at right (Miletić et al. 2017).

Walsh et al. (2018) investigated the fiber orientation within a field-cast reinforced UHPC (using 2% steel fiber of 0.2 mm [0.008 in.] and length of 12.7 mm [0.5 in.]) shear key (Figure 15.22a) replica (Figure 15.22b). The goal of the research was to examine the interaction of the fibers with the rebar (12.5 mm diameter [#4 bar], made of resin for better visualization using CT scanning images) as the UHPC flowed through the key. In this case, the flow direction is perpendicular to the bars. Figure 15.22(b) presents the plan and section view of the core sample locations in shear key replicas and UHPC flow direction. Figures 15.22(c) and 15.22(d) show fiber orientation around the rebar from the CT scanning image analysis at locations 4A and 6A (Figure 15.22b) and Figures 15.22(e) and 15.22(f) shows the CT images of samples 4A and 6A, with the direction of UHPC flow being right to left. It was observed that fibers tended to collect upstream of the rebars, resulting in a higher fiber density at this location. Furthermore, the immediate downstream side of the rebar was observed to be relatively fiber-free.

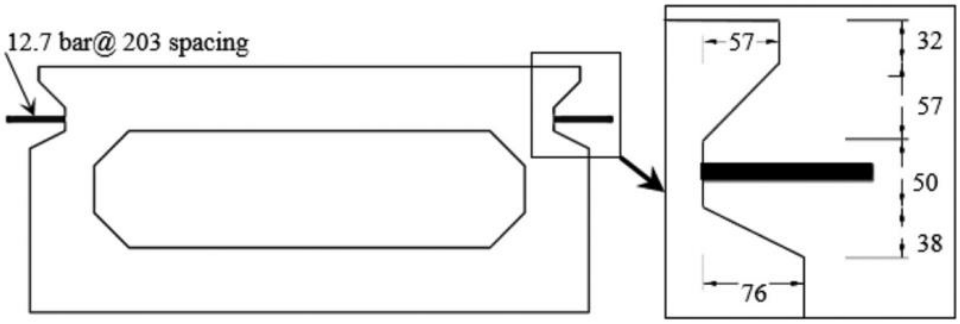

(a)

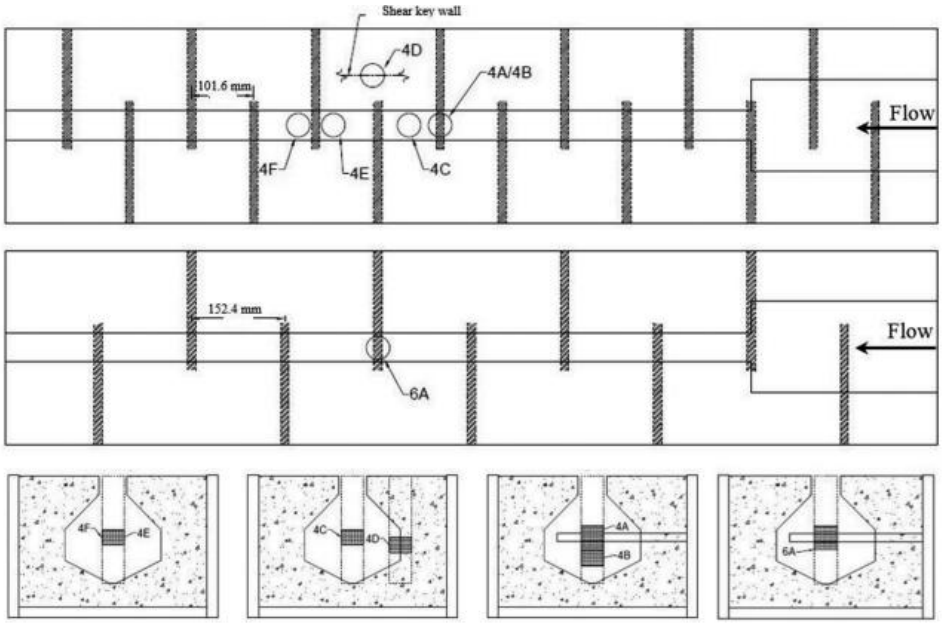

(b)

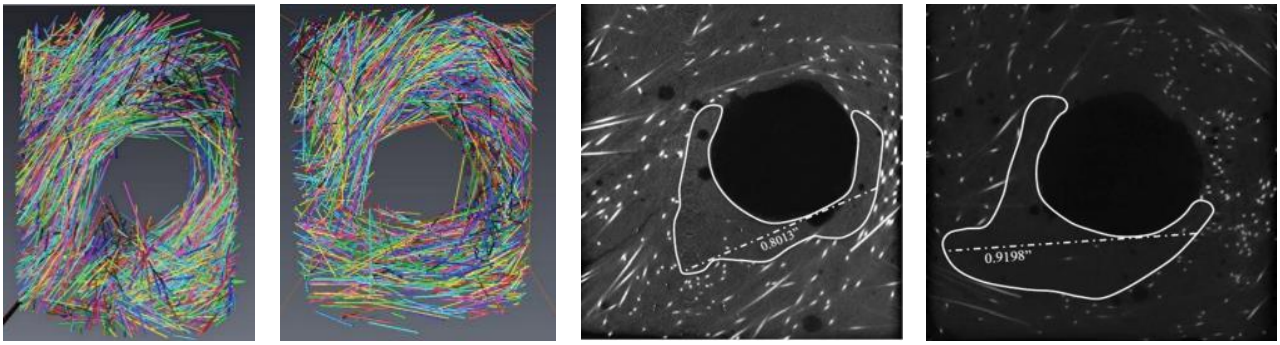

(c) (d) (e) (f)

Figure 15.22 (a) New adjacent-box-beam shear connection using UHPC and transverse rebar; (b) plan and section view of the core sample locations in shear key replicas and UHPC flow direction; (c), (d) sample 4A and 6A respectively: fiber approximation from CT scanning image analysis (flow direction is right to left); (e), (f) CT image showing disruption of flow caused by rebar in sample 4A and 6A, respectively (Walsh et al. 2018).

In brief, there is no systematic study on the influence of rebar arrangement in large-scale UHPC members on the fiber orientation, however, it is suspected by the researchers that rebar arrangement could disrupt the fiber alignment along with the flow directions. Studies also suggest that when UHPC flow is parallel to the rebars, fibers tend to be mostly aligned parallel to the bar and there existed a thin fiber-free zone around the rebars. When the UHPC flow is perpendicular to the rebar, fibers tended to collect upstream of the rebars, resulting in a higher fiber density at this location, while the immediate downstream side of the rebar was observed to be relatively fiber-free.

16. Effect of Casting Procedure on Fiber Orientation and Mechanical Properties for Small-Scale UHPC Specimens

The effect of construction procedures and casting processes on fiber orientation in UHPC has been one of the research epicenters in recent years (Huang et al. 2021a). The earlier sections provide a detailed review of the large-scale UHPC construction. In the following sections, the advancements, and outcomes of the research on small-scale (or prototype) UHPC casting processes and their effects on fiber orientation are reviewed.

16.1 Effect of casting flow direction

In continuation of the discussion on large-scale UHPC casting at Section 15.1, the fiber orientation in UHPC specimens is significantly influenced by the flow directions, which is in turn affected by the size and geometry of the specimens.

Many studies were conducted to evaluate the influence of different casting directions on the fiber orientation and mechanical performance of various small-scale specimens in order to find the best casting process. Kang et al. (2011) investigated the impact of the fiber distribution and orientation, which results from different placing directions of small-scale beams (100 x 100 x 400 mm [4 x 4 x 16 in.]), on the flexural behavior of UHPC (using steel fiber of length 13 mm [0.5 in.] and 0.2 mm [0.0078 in.] diameter with 2% volume fraction). They manufactured the specimens with two different placing directions (Figure 16.1) and flexural behaviors including cracking and ultimate flexural strengths were then measured. The casting processes are (a) placing material parallel to the longitudinal direction of the specimen and (b) placing material transversely to the longitudinal direction of the specimen using scoops. The parallelly placed specimens showed significant fiber alignment along the longitudinal direction by image analysis on the sawn cross-sections. The authors reported achieving 61% higher flexural strength (by four-point bending test) for parallelly placed specimens compared to transversely placed specimens. Kang and Kim (2011) repeated the investigation (casting as shown in Figure 16.1) for direct tension of dogbone specimens. They achieved a higher fiber alignment along the longitudinal direction along with 33% higher direct tensile capacity for parallelly placed specimens compared to transversely placed specimens. In summary, placing UHPC mix parallel to the longitudinal direction and in layers orient the fibers along the casting direction more efficiently and improve the flexural and tensile performance significantly.

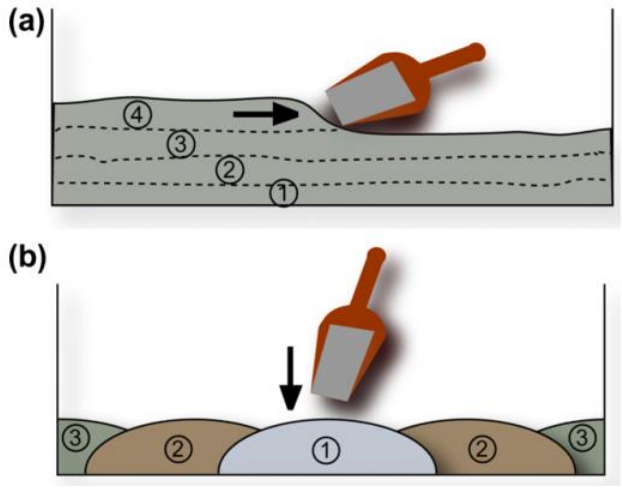

Figure 16.1 Specimen preparation by: (a) placing material parallel to the longitudinal direction of the specimen (PL Specimens); (b) placing material transversely to the longitudinal direction of the specimen (TL Specimens) (note: the material was placed in numerical order) (Kang et al., 2011).

Yoo et al. (2014) investigated the effect of casting flow on fiber orientation in small-scale beams (100 x 100 x 400 mm [4 x 4 x 16 in.]). They reported that when casting from the center, the flexural capacity of the beams increased due to the higher number of fibers present at the mid-span. In this study, they performed a three-point bending test of UHPC. The UHPC was made of 2% fibers with various lengths, i.e. 13 mm (0.51 in.), 16.3 mm (0.64 in.), 19.5 mm (0.77 in.), 30 mm (1.12 in.) with diameters of 0.2 mm (0.0078 in.), 0.2 mm (0.0078 in.), 0.2 mm (0.0078 in.), 0.3 mm (0.0118 in.), respectively. Two casting directions have been experimented with, e.g., (a) placing UHPC from one end, and (b) placing UHPC from the center, using a customized hoper, as shown in Figure 16.2. They reported that center casting led to more uniform fiber dispersion and fiber alignment along the flow direction, as determined by image analysis of the cross-section at the center and corner of the beam, compared to end casting. They also observed that the number of fibers decreased as the flow distance increased due to the boundary effect of the end wall. Therefore, center casting leads to more fibers at the midspan, which improves flexural performance. In addition, the fiber orientation at the center of the specimen was barely affected by the fiber length when placing UHPC from the center but decreased with increasing fiber length up to 19.5 mm (0.77 in.) when casting from the end. This happened due to the short flow distance, which could not effectively align the longer fibers along the flow direction (Kang and Kim (2012)) as well as the end wall effect. However, for very long fibers (e.g., 30 mm [1.12 in.]), the effect of formwork sidewall may be more dominant, leading to a higher level of alignment in the flow direction again. In brief, the small-scale specimens with UHPC placed in the center exhibited higher flexural strength because more fibers were present at the crack plane compared to the specimen cast from the end.

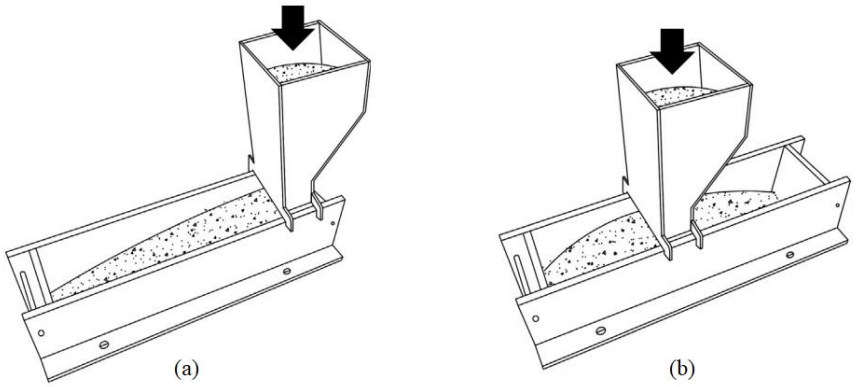

Figure 16.2 Two different placing methods using customized hopper: (a) placing concrete at one end; (b) placing concrete at the center (Yoo et al. 2014).

Huang et al. (2020) also investigated the fiber orientation in small scale UHPC beams (70 mm x 70 mm x 630 mm [2.75 in. x 2.75 in. 24.8 in.]) with different placement methods, e.g. (a) placing UHPC from one end, (b) from the middle and (c) from two ends of the formwork (Figure 16.3). The UHPC used 2% steel fibers with a length of 13 mm (0.51 in.) and a diameter of 0.22 mm (0.0086 in.). They studied the steel fiber motion and orientation during these placement procedures by using the smoothed particle hydrodynamics (SPH) simulation approach, which was also verified by image analysis of specimens. For example, Figure 16.3 shows the SPH simulation results of placing UHPC from one end of the formwork. From the simulation and image analysis result, the fibers were found better aligned with the direction of flow at the place of casting, and fibers were less aligned at a longer distance from the casting point, probably due to the end wall effect in the short flow distance. As a result, higher flexural strengths are observed at the casting places and lower for regions at a distance from the casting position. These findings are opposite of the hypothesis by Kang and Kim (2012) but similar to Yoo et al. (2014). Figure 16.4 shows the fiber orientation angle distribution of specimens cast in the three methods where the higher angle of fiber are found away from the casting location due to end wall effect (Figures 16.4a and 16.4b) and collision of UHPC flows at the center cast from both ends (Figure 16.4c).

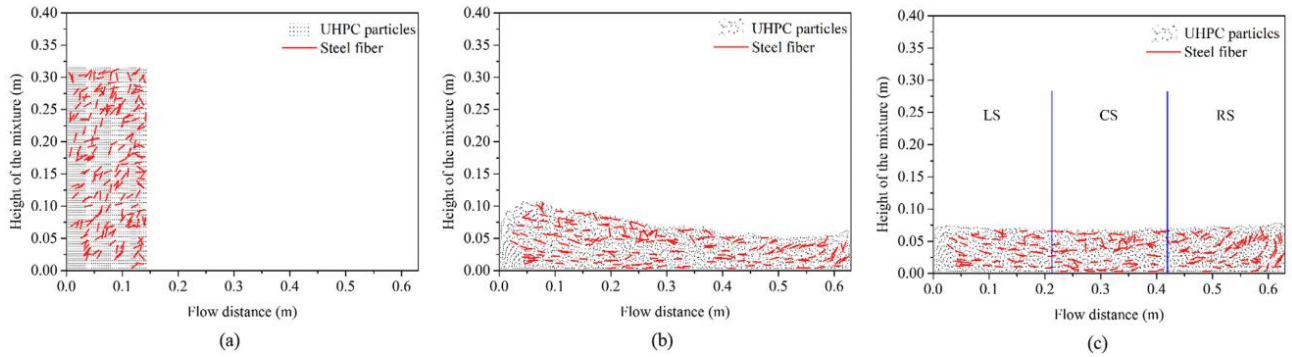

Figure 16.3 Smoothed particle hydrodynamics (SPH) simulation results of placing UHPC at one end of the formwork at: (a) time, t = 0 s; (b) t = 0.5 s; (c) t = 2 s (Huang et al. 2020).

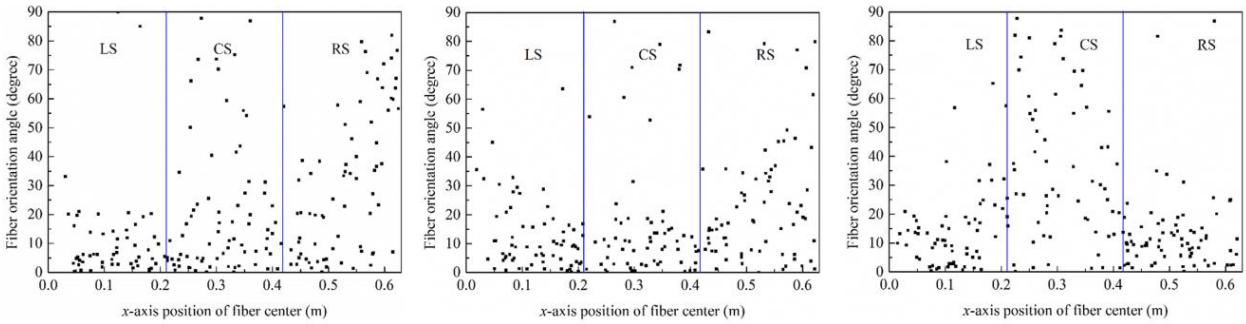

(a) (b) (c)

Figure 16.4 The fiber orientation angle distribution of specimens cast by: (a) placing UHPC at one end;, (b) placing at the middle; (c) placing at two ends of the formwork (Huang et al. 2020).

In brief, for small-scale beam casting, studies found that, unlike large-scale specimens, due to shorter flow distance, the fibers are not aligned along the flow direction properly, and casting from one end could cause the middle sections to have fewer fibers along the flow direction. The end wall effect also influences the fiber alignment in small-scale specimens. Therefore, casting from the center of the beam could be preferred.

16.2 Effect of casting devices

Many researchers have developed different casting devices to align the fibers to achieve the best performance of UHPC material. By employing different casting devices, it can optimize flow patterns of mixtures, thus promoting fiber alignment along the direction of principal tensile stress. To this end, the research on the performance of different casting devices for different geometry of structure and formwork is mostly on small-scale prototype specimens. A great concern is the scalability of those devices to be used in large-scale UHPC structures. Further investigations on the scalability of these devices are in critical need. Nevertheless, the relevant literatures are reviewed in this session.

As reviewed in Section 16.1, Kang et al. (2011) and Kang and Kim (2011) used a conventional scoop for casting UHPC specimens (Figure 16.1) by placing material parallel to the longitudinal direction of the specimen. They were able to align the fibers along the longitudinal direction and achieved 33% higher flexural capacity compared to placing material transversely to the longitudinal direction of the specimen. The efficient way of using a conventional scoop for casting in layers improved the fiber alignment and flexural capacity.

Wille and Parra-Montesinos (2012) used a chute (length of 1.0 m [40 in.]) with an inclination of approximately 30-degrees to cast UHPC beam specimens of 102 x 102 x 406 mm (4 x 4 x 16 in.) and 152 x 152 x 508 mm (6 x 6 x 20 in.) according to RILEM TC 162-TDF (2002) (Test and Design Methods for Steel Fibre Reinforced Concrete, Recommendations) and ASTM C1609/C1609M-06 (Standard Test Method for Flexural Performance of Fiber-Reinforced Concrete (Using Beam with Third-Point Loading). They used various UHPC with straight, hooked, and twisted fibers of lengths 13 mm (0.51 in.), 30 mm (1.18 in.), and 30 mm (1.18 in.), respectively and diameters of 0.20 mm

(0.008 in.), 0.38 mm (0.015 in.), and 0.30 mm (0.012 in.) respectively with volume fraction of 1.5-2.5%. They followed the respective casting processes. For RILEM TC 162-TDF (2002), UHPC was cast at the middle and let the flow reach both ends. The UHPC flow in the middle of the specimens followed a funnel-like shape during casting. They reported that the high workability of the UHPC mixtures led fibers to align following the UHPC flow (i.e., fiber alignment along the funnel radius, shown in Figure 16.5). On the other hand, as per ASTM C1609/C1609M-06, the beam was filled layer by layer by moving the chute back and forth as shown in Figure 16.5. Moreover, three casting speeds, e.g., slow, medium, and high, were employed to cast specimens, and Figure 16.5 (b at the right) shows the casting patterns for these speeds. In this case, the chute speeds (0.13 m/s [5 in./s] to 0.5 m/s [20 in./s]) were limited such as to avoid a break of the flow. They found that the slow movement of the chute caused a snake-like pattern, leading to areas where fibers tended to orient vertically, and increased speeds led to a thin layer of casting with more preferred fiber alignment along the beam axis. They reported that the flexural strength for fast-moving chute casting was approximately 144%, 30%, 100% higher than that of beams cast using a slow chute moving speed, medium chute moving speed, and middle cast beam, respectively.

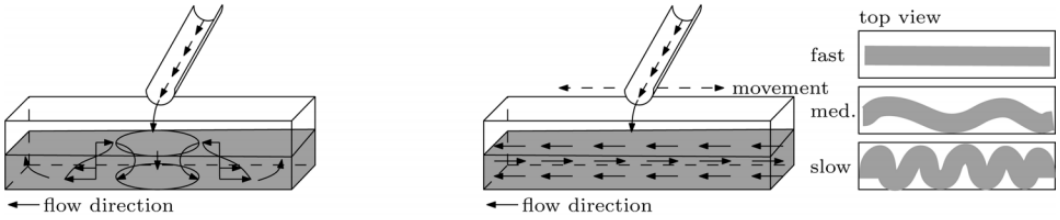

(a) middle casting (RILEM TC 162-TDF)

(b) layer casting (ASTM C1609/C1609M) with different chute speeds

Figure 16.5 Middle and layer casting and corresponding flow direction (Wille and Parra-Montesinos 2012).

Teng et al. (2020) also cast UHPC mix (using 2% steel fiber of 13 mm [0.51 in.] in length and 0.2 mm [0.0078 in.] in diameter) from one end of the beam using a chute inclined at 30-degrees and let it flow (Figure 16.6). The authors reported a 15%-45% improvement in fiber alignment in the longitudinal direction, compared to the conventional casting method (casting randomly using scoop or bucket).

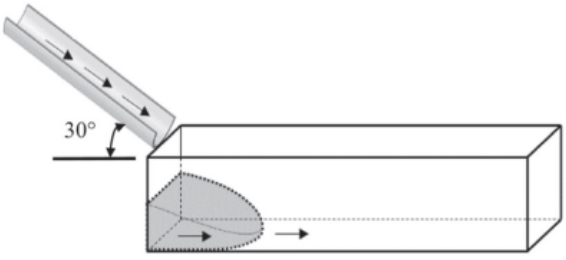

Figure 16.6 Casting UHPC using 30-degree chute (Teng et al. 2020).

Huang et al. (2018, 2019a, 2019b, 2021a, 2021b, 2021c) developed a flow-induced casting device (L-shape device) and cast UHPC (using steel fiber of 13 mm [0.51 in.] in length and 0.2 mm [0.0078 in.] in diameter with a volume fraction of 2%) layer by layer to promote fiber alignment as shown in Figure 16.7. Such a casting method can lead to a converging flow of the mixture. The authors reported that the proposed casting method using an L-shape device led to a 10%-40% increase in fiber orientation (measured by image analysis) along casting flow direction, compared to the conventional casting method (casting randomly using scoop or bucket) that typically results in random fiber orientation.

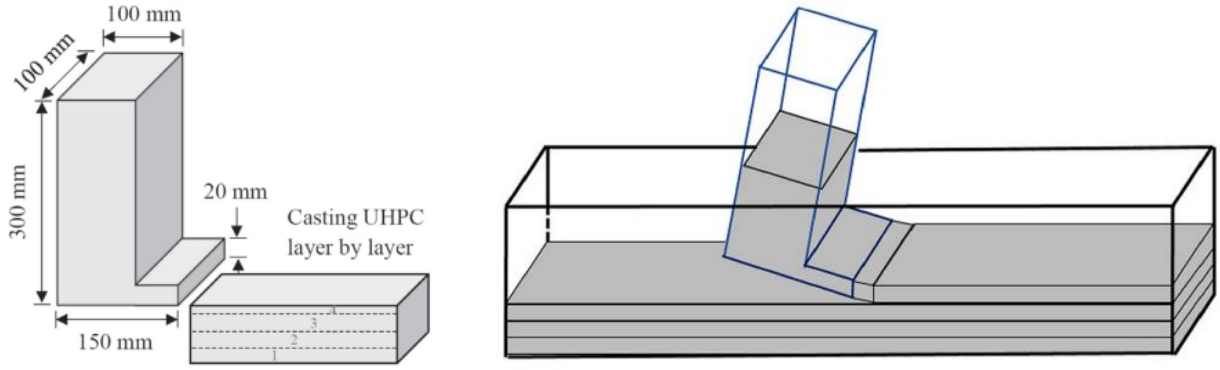

Figure 16.7 Casting UHPC using L-shape device (Huang et al. 2018, 2019a, 2019b, 2021a, 2021b).

Zhang et al. (2020) and Qu et al. (2020) cast UHPC (made with 2% steel fibers of 13 mm [0.51 in.] in length and 0.2 mm [0.0078 in.] in diameter) by a fiber aligning channel and a vibration table to promote fiber alignment during the placement of the mixture, as illustrated in Figure 16.8(a). As shown in Figure 16.8(b), after starting the vibration table, the UHPC mix was poured onto the channels. The vibration increased the fluidity of the mix, which began to flow at a speed between 0.068-0.083 m/s (0.21-0.27 ft/s). The applied vibration can overcome the high yield stress of UHPC and enable the mixture to flow into the fiber aligning channel, which aligned the fibers in the flow direction. The mold was moved back and forth to fill the majority part of the mold in layers and then the edges were filled manually. Each 100 mm (4 in.) high mold was filled in 14-17 layers with a layer thickness of 5.88-7.14 mm (0.23-0.28 in.). The results showed that such a casting method can lead to a 25% increase in fiber alignment along casting flow direction compared to the conventional method (casting randomly using scoop or bucket).

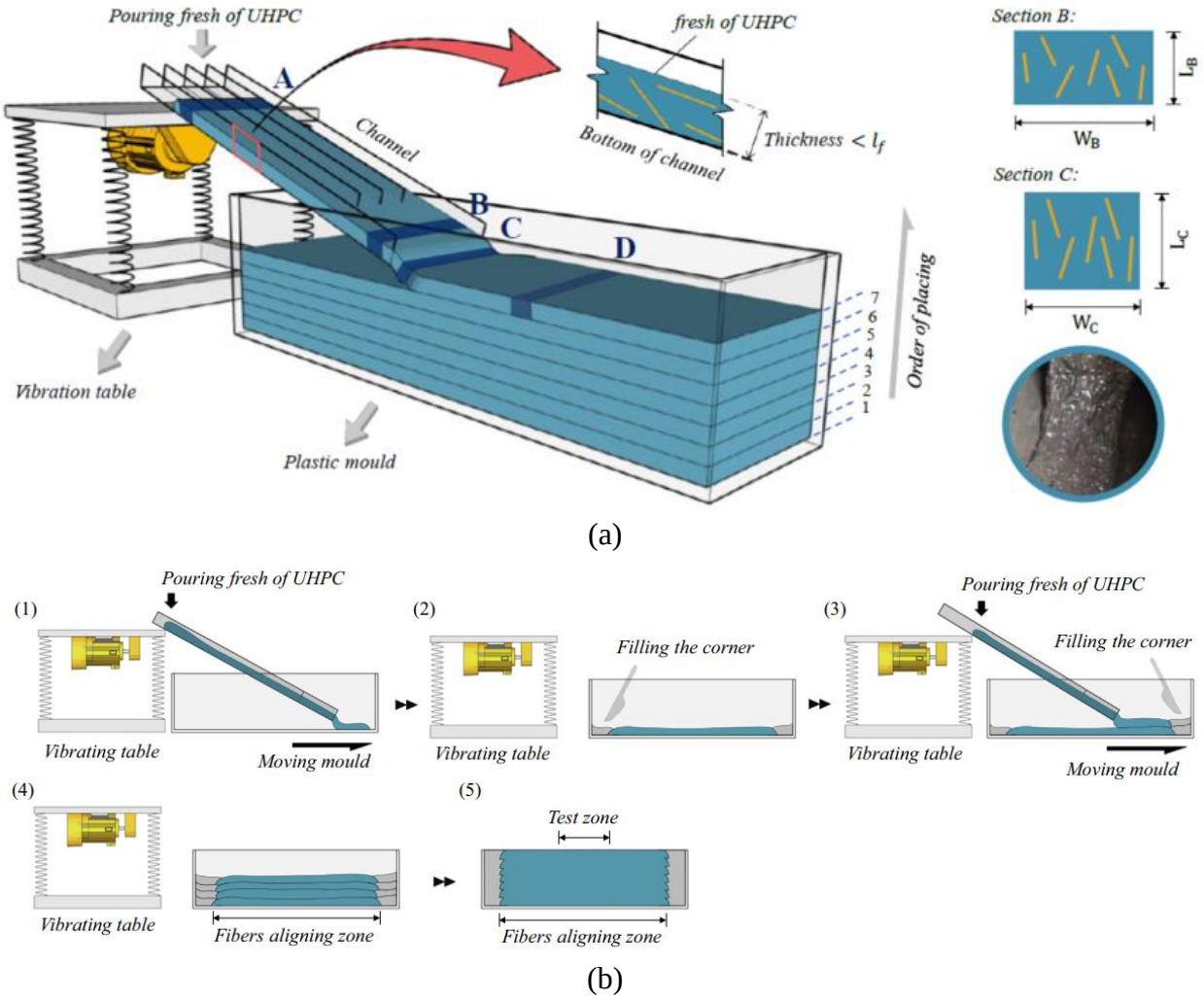

Figure 16.8 (a) Schematic descriptions of the apparatus of fiber aligning (Qiu et al. 2020, Zhang et al., 2020); (b) detailed procedures for aligning steel fibers in UHPC using channeled casting device (Zhang et al., 2020)

Comparing these devices, for small-scale specimens, 30-degree chute, and L-shape devices can secure a relatively high improvement in fiber alignment compared to the channelized device, or conventional methods (e.g., scoop) of casting. However, the risk of blockage increases with the increase of fiber length and volume, given the limited outlet height of the L-shape device (Huang et al. 2021a, b, c). This is not the case for the 30-degree chute, which has no limitation on fiber length and volume. The other two casting methods, i.e., placing UHPC parallelly to the tensile direction (Kang and Kim 2011; Kang et al. 2011) using a conventional scoop and casting UHPC using a fiber aligning channel and vibration table (Zhang et al. 2020; Qu et al. 2020), can be used for mixtures with low and high fluidity, although the improvement in fiber orientation was relatively low, compared to the L-shape device and 30-degree chute. A summary of the advantages and disadvantages of different casting devices is provided in Table 16.1. The scalability is also briefly discussed.

Table 16.1 Different UHPC casting methods and their advantages, disadvantages, and suitability for scalability

Casting device	**Advantages**	**Disadvantages**	**Suitability for large scale construction**
L-shape device	No limitation on formwork geometry, high improvement in fiber orientation	High mixture fluidity is required to prevent blockage, especially when long fibers and high fiber volume are used.	Low up-scalability; if a larger opening is needed for more rapid placement, then the fiber alignment effect will be reduced.
30-degree chute	No limitation on fiber length and volume	High mixture fluidity is required.	Suitable for large-scale structures in the field construction and precast sections in labs. Currently a popular method for large-scale casting.
Conventional scoop (by placing UHPC parallelly to the tensile direction)	Both for low and high mixture fluidity; no limitation on fiber length and volume	Low improvement in fiber orientation	Not suitable to handle large volume casting for large-scale structures.
Fiber aligning channel and vibration table	Both for low and high mixture fluidity	Low improvement in fiber orientation and low casting efficiency	Not suitable for large-scale structures due to low efficiency and that the beam needs to move back and forth.

There is no research available on evaluating special casting devices for the large-scale construction of UHPC members. Usually, the large-scale UHPC members are precast or cast-in-place members that are manufactured by casting using half-pipe or chute from mixing trucks or carrying trucks, hopper hanging from a crane, wheelbarrows, buckets, etc. Figure 16.9 shows different casting devices for UHPC large-scale casting. However, the existing literature which used these devices for large-scale specimens did not investigate or evaluate the effects of the casting devices on the fiber orientation in UHPC.

(a)

(b)

(c)

(d)

(e)

(f)

(g)

(h)

Figure 16.9 Different casting device for UHPC large scale construction: (a) inclined chute or half-pipe from concrete mixing truck in the field; (b) inclined chute or half-pipe from concrete mixing truck in the lab; (c), (d) vertical flow from a chute or half pipe from UHPC mix carrying Tuckerbilt buggy; (e) casting using an inclined channel; (f) casting using a wheelbarrow; (g) casting using hopper hanging from a crane in the field; (h) casting using a plastic bucket.

16.3 Effect of formwork wall, specimen size, and fiber length

The formwork geometry has a significant effect on the fiber orientation, especially for the small-scale testing specimens, as the formwork sidewalls and base tend to orient the fibers parallel to them during casting. As per AFGC recommendations (2002, 2013) fibers near formwork walls are naturally aligned parallel to the formwork, which is called the wall effect. It only occurs when the distance from the formwork is less than or equal to the length of the fibers.

Since the wall effect occurs near the formwork walls, the effect of the formwork sidewalls on the fiber alignment is higher for smaller specimens than for large-scale specimens. This leads to a "size effect", which indicates that specimens with different sizes perform differently due to differences in fiber orientation. In large-scale specimens, the advantage of the wall effect on fiber alignment along the longitudinal direction is lower and the flexural performance is generally lower compared to the small-scale specimens. However, if the large-scale structures consist of any narrower section (e.g., web of I-girder or pi-girder), it may exhibit local higher fiber orientation and flexural capacity.

Theoretically, fiber orientation and dispersion are also affected by fiber length. If longer fibers are used, the wall effect should be more significant. However, it is also observed that shorter fibers are better aligned along the flow direction in small-scale specimens due to the shorter flow distance not being able to effectively align the longer fibers.

This section reviews the relevant studies on the effect of formwork walls, specimen size, and fiber length on the fiber orientation of UHPC.

Yoo et al. (2016a) investigated the size effect of UHPC beams on fiber orientation and flexural capacity. They prepared three different sizes of beam, e.g., small (50 x 50 x 250 mm [2 x 2 x 10 in.]), medium (100 x 100 x 400 mm [4 x 4 x 16 in.]), and large (150 x 150 x 550 mm [6 x 6 x 22 in.]). They prepared the specimens by placing UHPC mix from the end of the mold. The UHPC contained 2% smooth fibers with a length of 13 mm (0.51 in.) and diameter of 0.2 mm (0.0078 in.), or length of 30 mm (1.18 in.) and diameter of 0.3 (0.0118 mm), or 2% twisted fibers of 30 mm [1.18 in.] in length and 0.3 mm (0.0118 in.) in diameter. They reported a significant decrease of fiber alignment along the longitudinal direction with the increasing size of the beams. The flexural capacity of medium and large beams was reduced up to 27% and 40%, respectively, compared to small beams. They also reported that shorter fibers were more aligned parallel to the flow direction than longer fibers. On the other hand, the fiber dispersion (i.e., number of fibers at different locations) were insignificantly influenced by fiber length.

Wille and Parra-Montesinos (2012) cast UHPC beam specimens of "medium" size of 102 x 102 x 406 mm (4 x 4 x 16 in.) and "large" size of 152 x 152 x 508 mm (6 x 6 x 20 in.) according to RILEM TC 162-TDF (2002), i.e., cast from the middle of the beam using a 30-degree chute. The large beams showed a reduction in flexural strength by up to 6.7% compared to medium beams. However, the reduction in the large beam was not as significant as that found by Yoo et al. (2016). It is probably

due to that the specimens were cast from the center. Therefore, the fiber orientation at the center was less affected by the formwork walls.

More discussions on the formwork wall effect are available in Sections 2.3, 3.4, 8.4, and 11.4. For example, AFGC (2002, 2013) recommend that the edge effect be considered when calculating the K (fiber orientation) factors to remove the influence of boundaries in both cast and sawn prisms. The upcoming fib MC2020 (in progress) included a fiber orientation factor α_0, of which the values can be derived based on the geometry of the specimens (Dupont and Vandewalle, 2005, discussed in Section 3.4). The Australian Standard AS 3600:2018 (Concrete structures) also adopted fiber orientation factor, K_s which is affected by the shape of the specimen (Ng et al. 2012) (discussed in Section 8.4). The Canadian code CSA A23:19 (Canadian Highway Bridge Design Code) also provides different values of fiber orientation coefficient for elements cast horizontally, vertically, or for other local effects (discussed in Section 11.4).

Yoo et al. (2016b) studied the effect of fiber length on the flexural performance and fiber distribution characteristics of UHPC (using smooth steel fibers with an identical diameter of 0.2 mm [0.0078 in.] and three different lengths of 13 mm [0.51 in.], 16.3 mm [0.64 in.], and 19.5 mm [0.77 in.] at a 2% volume fraction). They prepared UHPC beams (100 x 100 x 400 mm [4 x 4 x 16 in.]) for flexure tests which were cast from one end. They reported that the fiber length had little influence on the degree of fiber dispersion (i.e., number of fibers at different locations), but a significant influence on the fiber alignment along the flow direction. A higher fiber alignment along the flow distance was obtained when shorter fibers were used, which means that shorter fibers were more aligned parallel to the flow direction than longer fibers. However, the longer fibers still provided better fiber bridging capacity leading to higher flexural capacity.

Yoo et al. (2014) (reviewed in more detail in Section 3.1) also reported that the fiber orientation coefficient (measured by image analysis) along the flow direction was increased when shorter fibers were used. This is due to the relatively short flow distance in this study, the longer fibers could not be fully aligned along the longitudinal direction. As a result, the fiber orientation coefficient at the center of the specimen was barely affected by the fiber length when placing UHPC from the center, but it decreased with increasing fiber length up to 19.5 mm (0.77 in.) when placing UHPC from the end (Figure 16.3). However, for very long fibers (30 mm [1.12 in.]), the effect of formwork sidewall is more dominant, leading to a higher level of alignment in the flow direction again.

The geometry of specimens and fiber length all have a significant influence on the fiber orientation and mechanical performance of UHPC. As a result, the mechanical strength obtained from small-scale tests may not accurately reflect that of the real structures. As a consequence, many UHPC design specifications consider adjusting fiber orientation based on the geometry of the elements. The influence of fiber length on the fiber orientation is more complex, as it is related to both the flow distance and wall effect.

17. Effect of Rheology and Flow Velocity of Fresh UHPC on Fiber Orientation

In addition to the flow directions, specimen geometry, the orientation and dispersion of fibers in UHPC also depends greatly on the rheology of the fresh UHPC mix (flow properties) and the flow velocity (and its gradient). In this section, the studies on the effect of UHPC rheology on fiber orientation are reviewed. A few research on fiber-reinforced concrete that investigated and explained the effect of the fundamental flow properties on the fiber orientation are also included in this section.

Rheology is the branch of physics that deals with the deformation and flow of matter. Yield stress and viscosity are the two important rheological properties along with the flow velocity to affect the flow of UHPC and therefore fiber orientation within UHPC. Yield stress in rheology is defined as the applied stress at which irreversible plastic flow is first observed across the sample (i.e., the minimum stress needed to initiate flow) and viscosity is a measure of its resistance to flow. The flow velocity is a vector field used to mathematically describe the motion of a continuum (i.e., UHPC mix).

Stähli et al. (2008) and Boulekbache et al. (2010) investigated the effect of the flow velocity field on the fiber alignment as shown in Figure 17.1. They stated that different flow velocity gradient affects the fibers differently and may cause the fibers to rotate in such a way that they align with the flow (confined flow, Figure 17.1a) of the material (Stähli et al. 2008) or reorient perpendicularly (fountain flow or radial flow, Figure 17.1b) to the flow direction (Boulekbache et al. 2010). The effect is stronger at a higher flow velocity gradient or when the velocity can affect the fiber for a longer time (i.e., longer flow distance).

Teng et al. (2021) further analyzed the fiber alignment due to shear-induced flow. He considered that the hydrodynamic stress on the fibers induced by the differential flow velocity, which help to align the fibers, can be determined by Equation 17.1:

$$\tau_s = \mu \frac{dV}{dy} \qquad \ldots(17.1)$$

where τ_s (unit Pa) is the hydrodynamic stress caused by the shear flow of the suspending mortar, μ (unit Pa·s) refers to the plastic viscosity of mortar, and dV/dy (unit s^{-1}) is the gradient of flow velocity between the centerline and side of the prismatic samples. The flow velocity field is also dependent on the rheological properties as well as the geometry of the specimen. Based on Teng et al. (2021), although self-consolidating UHPC has high flow velocity, the mixtures should have an adequate viscosity to drive and align fibers. In general, low yield stress and high viscosity are desirable for fiber alignment. However, they also noted that high viscosity may reduce the flow velocity, which may interfere with fiber alignment along the flow direction. Furthermore, fibers tend to entangle with each other in the mixtures with relatively high yield stress and viscosity, which can also increase the difficulty to align fibers. Therefore, there exists a competing effect about how viscosity and yield stress affect the fiber alignment in UHPC casting flow. The optimum range of these rheological properties

for fiber alignment may be case-specific.

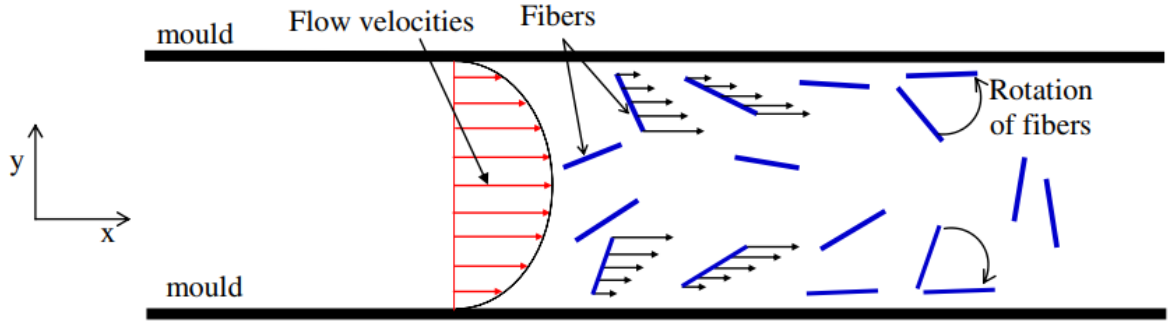

(a)

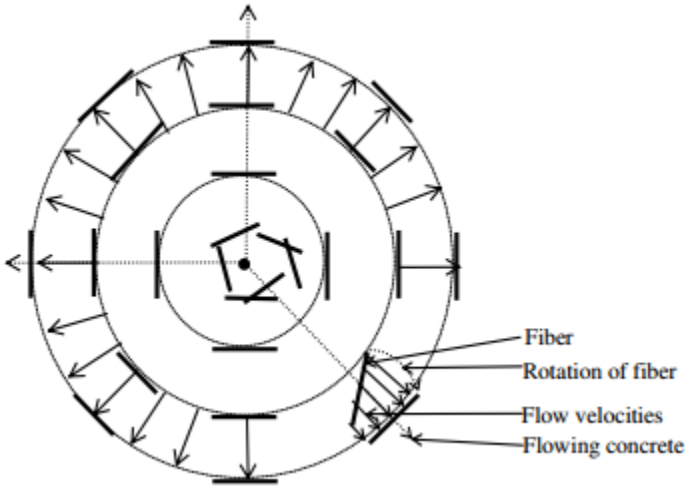

(b)

Figure 17.1 Explanation for fiber orientation due to flow velocity in: (a) canal channel flowing or confined flowing; (b) fountain or radial flowing (Boulekbache et al. 2010).

Meng and Khayat (2017) also performed an investigation on the effect of rheological parameters on fiber alignment using UHPC with 2% steel fibers of 13 mm (0.51 in.) in length and 0.2 mm (0.0078 in.) in diameter. They placed UHPC from one end of the beam mold (100 x 100 x 400 mm [4 x 4 x 16 in.]) using a chute with an inclined angle of 30-degree and let the UHPC flow to the other end of the mold. They reported that, adjusting the plastic viscosity of UHPC from 20-120 Pa·s (0.0029-0.0174 psi·s), which correspondingly increased the yield stress from 14-26 Pa (0.002-0.0037 psi), increased the fiber alignment along the flow direction by 19%. However, regarding the fiber dispersion (uniformity of fiber distribution), it was first improved with increasing viscosity and yield stress (up to a viscosity of 60 Pa·s [0.0087 psi] and yield stress of 19 Pa [0.0027 psi]) and then decreased with further increasing of plastic viscosity and yield stress.

Teng et al. (2021) also performed experiments to evaluate the effect of rheological parameters on fiber alignment using UHPC with 2% steel fibers of 13 mm (0.51 in.) in length and 0.2 mm (0.0078 in.) in

diameter. The study reported that, when UHPC was cast using a 30-degree chute, the fiber alignment along the flow direction increased by 20% with the increase of viscosity from 10 to 45 Pa·s (0.0014-0.0065 psi·s) and the corresponding increase of yield stress 36-43 Pa (0.0052-0.0062 psi) for self-consolidated UHPC; and fiber alignment along the flow direction increased by 5% with the increase of viscosity from 15 to 40 Pa·s (0.0021-0.0058 psi·s) and the corresponding increase of yield stress 14-17 Pa (0.002-0.0025 psi) for non-self-consolidated UHPC (flowable UHPC). The study also reported that, when UHPC casting was performed using L-shape device, the fiber alignment along the flow direction increased by 15% with the increase of viscosity from 10 to 45 Pa·s (0.0014-0.0065 psi·s) and the corresponding increase of yield stress 36-43 Pa (0.0052-0.0062 psi) for self-consolidated UHPC; however, fiber alignment along the flow direction reduced by 10% with the increase of viscosity from 10 to 65 Pa·s (0.0014-0.0094 psi·s) and the corresponding increase of yield stress 14-17 Pa (0.002-0.0025 psi) for non-self-consolidated UHPC (flowable UHPC).

In brief, it can be concluded that the fiber alignment in UHPC is greatly influenced by the mixture viscosity and yield stress, however, the relationship is complex and there exist several competing effects. In general, for consolidating UHPC, low yield stress and high viscosity is desirable for better fiber alignment. However, the yield stress and viscosity effect not only influence the fiber alignment but also may affect other aspects of workability, e.g., filling ability, segregation, and fiber dispersion, etc. For example, low yield stress improves the filling ability. However, a significant reduction in yield stress can make the mixture unstable leading to segregation and possible surface settlement and bleeding. Therefore, the optimum range to ensure the quality of UHPC needs to be considered based on all these factors.

All the above research on the effect of the rheological properties of UHPC on fiber orientation is performed in small-scale specimens in the laboratories. The optimal ranges of plastic viscosity are found from small-scale specimens and corresponding casting procedures, however, in large-scale specimens when the flow distance, formwork geometry, and casting methods are different, the optimum range of plastic viscosity might change.

18. Bond between UHPC and Steel Reinforcing Bars

All the discussions in previous sections focus on the effect of fiber orientation on the tensile or flexural properties of UHPC. Another important mechanical property that is also impacted by fiber orientation is the rebar pullout behavior. The pullout behavior is critical for the design of reinforced UHPC structures. In this section, studies on the rebar bond strength and pullout behavior in UHPC are reviewed. Unfortunately, research in this area is still very limited.

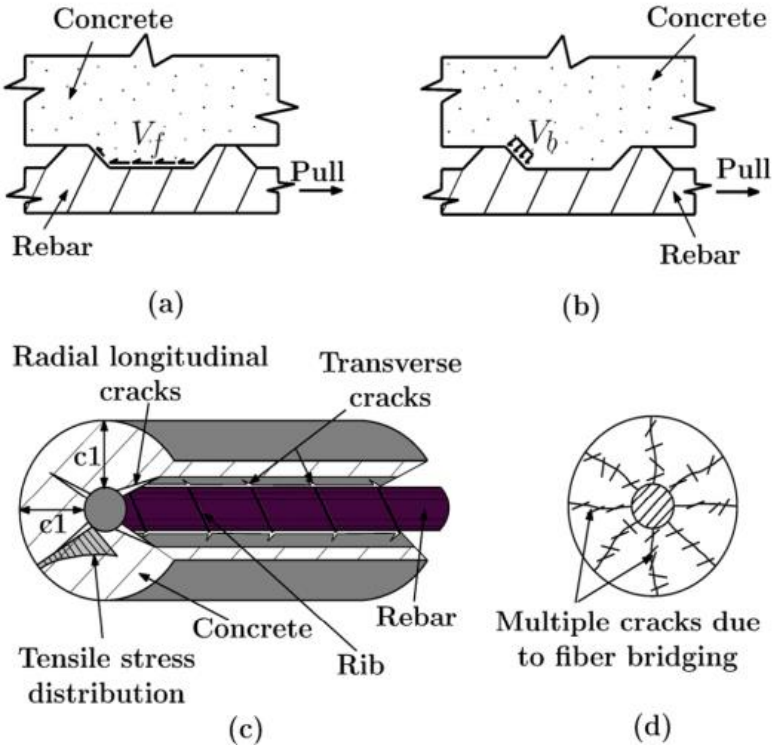

Figure 18.1 Bond mechanisms (idealized): (a) friction (Vf) (Joint ACI-ASCE Committee 408 2012); (b) bearing of the rib (Vb) (Joint ACI-ASCE Committee 408 2012); (c) radial longitudinal cracks in conventional concrete (Holschemacher and Weiße 2004); (d) crack bridging in fiber-reinforced concrete (FRC) (Chao et al. 2009, Roy et al. 2017).

In conventional reinforced concrete structures, the bond between the rebars and the concrete is a result of chemical adhesion, frictional resistance, and the bearing of the ribs on the concrete. Generally, friction and adhesion play a very small role in bond strength compared to the third mechanism, i.e., bearing of the ribs. After breaking free of chemical adhesion, the bar slips slightly and the ribs of the rebar bear against the concrete at an angle creating force components that act both parallel to and perpendicular outward from the length of the rebar (Figures 18.1a and 18.1b). The perpendicular component of the bearing force causes a tensile ring of radial stresses to develop along the perimeter of the bar leading to radial cracks, also known as, longitudinal cracks or splitting cracks (Figure 18.1c) (Joint ACI-ASCE Committee 408 2012; Roy et al. 2017). Bond failure occurs upon the formation of

excessive cracking. Therefore, the tensile strength of UHPC governs the bond strength and pullout behavior. Chao et al. (2009) performed an experimental investigation focusing on evaluating the bond stress versus slip response of deformed reinforcing bars in UHPC through direct pullout behavior. They reported that after initial cracking, the tensile ring was redistributed around the whole matrix due to the presence of fibers. Upon further progress of the slippage, following the fiber pullout, longitudinal cracks develop along the bar axis which corresponded with the approximate maximum bond strength. At this point, if the fibers are oriented in such a way that can effectively bridge the longitudinal cracks without excessive opening (Figure 18.1d), the failure will be a relatively ductile pullout failure. Otherwise, the longitudinal cracks will open, and the failure will be more of a sudden splitting failure.

Roy et al. (2017) investigated and characterized the pullout behavior of rebar (#3 and #4 bar, i.e., nominal diameter of 9.5 mm [0.37 in.] and 12.7 mm [0.5 in.] respectively) with embedment lengths of $8d_b$ and $12d_b$, where d_b is the diameter of the rebar, in UHPC. They prepared a customized channeled casting device (Figure 18.2a) to cast UHPC pullout specimen (Figure 18.2b) such that the fibers are aligned in different directions, i.e., (a) perpendicular fiber orientation, (b) parallel fiber orientation, (c) random fiber orientation (Figure 18.3). The UHPC mix used high-strength steel fibers of 0.2 mm [0.0078 in.] diameter and 13 mm [0.51 in.] length with 0, 1, 2, and 3% volume fractions. The study reported that, for a given rebar type with the same embedment length and fiber volume fraction, UHPC with fibers oriented perpendicular to the load direction developed the highest pullout load, and UHPC with fibers oriented parallel to the load direction recorded the lowest pullout load (Figure 18.4). The reason for that is the cracks due to pullout load propagating along the radial direction (Figure 18.1d) and the fibers aligned perpendicular to the rebar can bridge the cracks effectively.

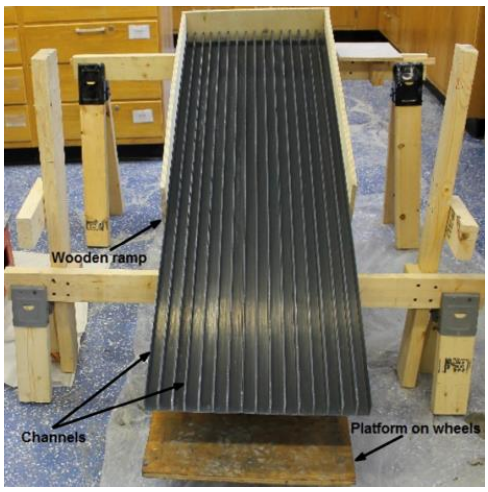

(a)

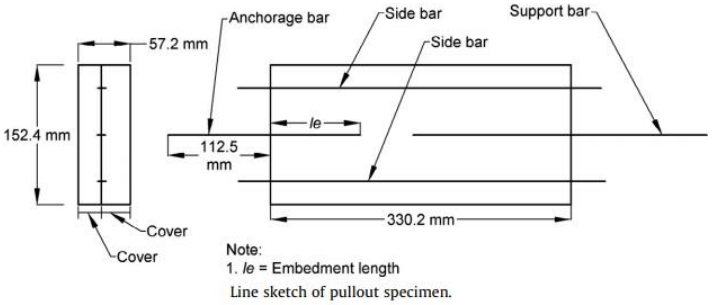

Line sketch of pullout specimen.

(b)

Figure 18.2 (a) Channeled casting device; (b) assembled pullout molds (Roy et al., 2017).

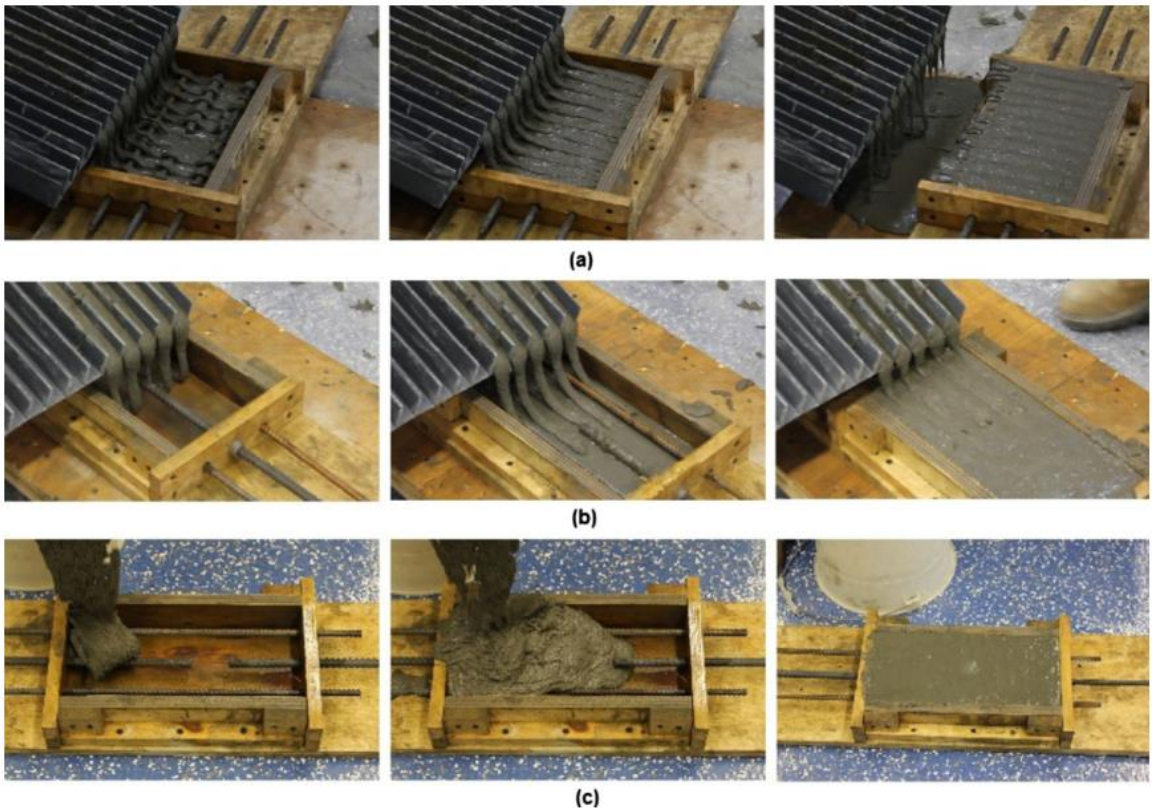

Figure 18.3 Casting methods: (a) perpendicular fiber orientation; (b) parallel fiber orientation; (c) random fiber orientation (Roy et al., 2017).

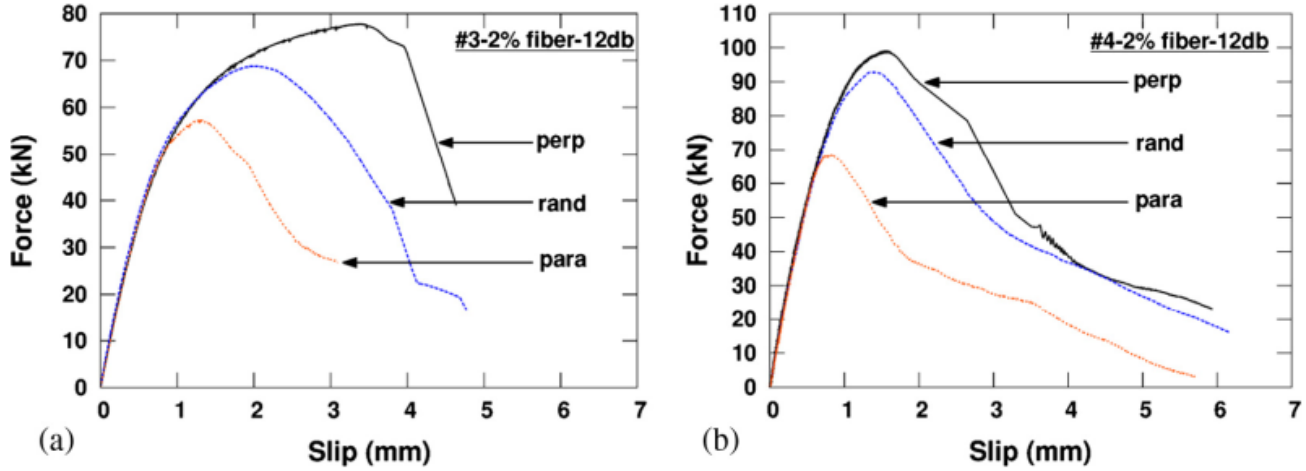

Figure 18.4 Effect of fiber orientation on the load-slip response: (a) #3 rebar with embedded length $12d_b$ (d_b =dia of rebar) and V_f (fiber volume fraction) = 2%; (b) #4 rebar with embedded length 12 d_b and V_f = 2% (Roy et al., 2017).

Alkaysi and El-Tawil (2017) investigated the bond between uncoated and epoxy-coated steel reinforcing bars and UHPC and the influence of fiber orientation by rebar pullout test. The UHPC mix used in the study was made of high-strength steel fibers of 0.2 mm (0.0078 in.) diameter and 13 mm

(0.51 in.) length with a 2% volume fraction. Two different bar sizes (diameter of 16 mm [#5 bar] and 19 mm [#6 bar]) were tested. Specimens were cast with fibers preferentially aligned parallelly with the bar and transversely to the bar using inclined pipes moving back and forth, or left and right as shown in Figure 18.5. They reported that the specimen with fiber alignment in the transverse direction showed slightly lower bond strength (Figure 18.6) compared to specimens with fibers oriented parallel to the rebar (Figure 18.5). However, the results are the opposite to the finding of Roy et al. (2017) and against intuition. It is suspected that they did not create a perfect alignment of the fibers.

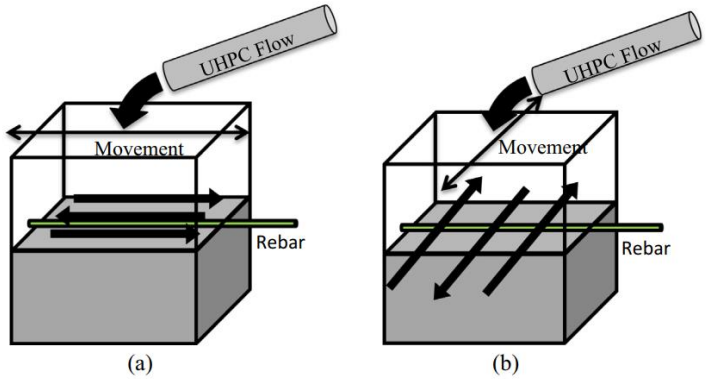

Figure 18.5 (a) Casting parallel to bar; (b) casting transverse to bar (Alkaysi and El-Tawil 2017).

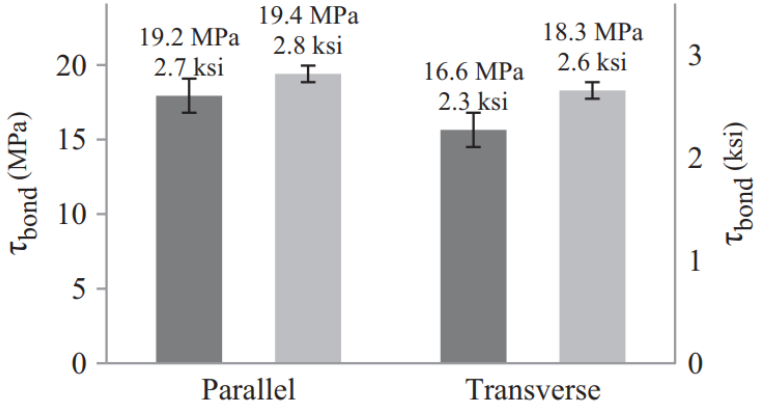

Figure 18.6 Peak bond strength (τbond) comparison (dark gray – 19 mm [0.75 in.] dia bars at 4.0 d_b, light gray – 16 mm [0.6 in.] dia bars at 6.4 d_b) (Alkaysi and El-Tawil 2017).

Shao and Billington (2021) also investigated the bond between steel reinforcement and UHPC (using steel fibers of 0.2 mm [0.0078 in.] in diameter and 13 mm [0.51 in.] in length) using beam-end specimens. UHPC materials with two fiber volumes are considered: 2% and 1%. Figure 18.7(a) presents the beam-end specimen design, which has an embedded length of $3d_b$. The side cover thickness was 24 mm (0.94 in.), which represents a typical value for UHPC applications. Figure 18.7(b) shows the casting flow direction. The UHPC was placed from one end of the specimen and allowed to freely flow to the other end (Figure 18.7b), which created a UHPC flow parallel to the test bar. A parallel UHPC flow is a representative flow condition in UHPC beam constructions. They reported that the calculated fiber orientation factor (measured by 2D-CT scan image analysis and

numerical calculation) is 0.78, indicating that fibers are primarily parallel to the test bar and the global flow direction. They reported that the splitting cracks were well restrained in UHPC with both fiber volumes. The bond strength of UHPC was over four times higher than that of conventional concrete. This indicates that even when fibers are aligned parallel to the bars, the bond strength between UHPC and rebars are still much higher than that of conventional concrete.

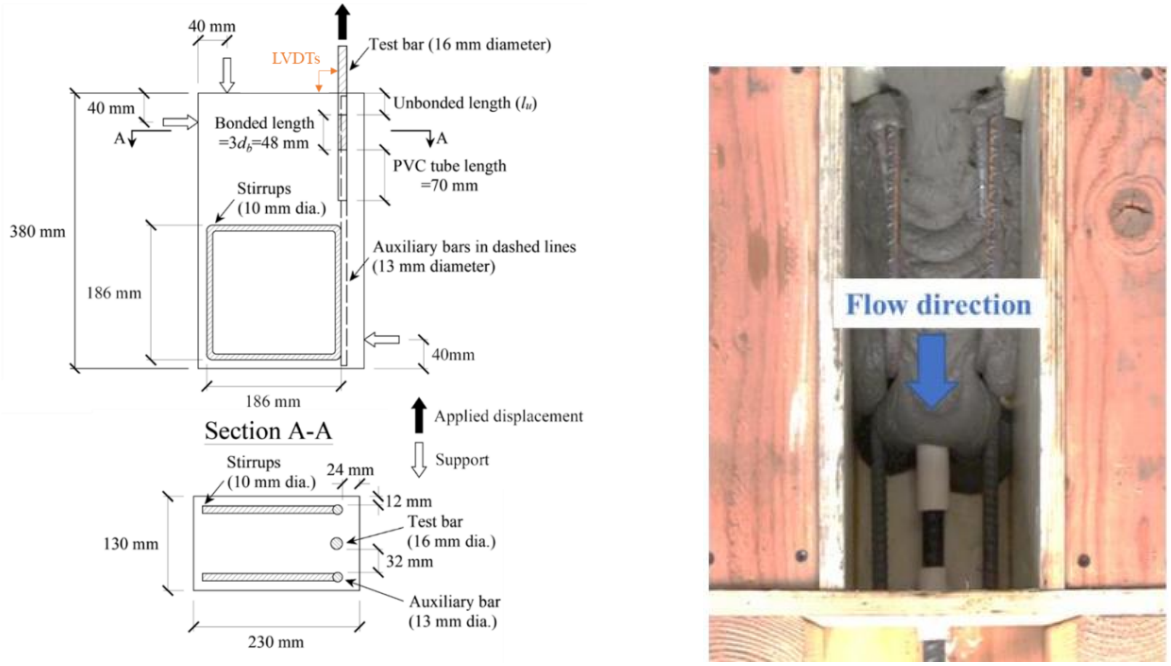

Figure 18.7 Schematic of the specimen design and casting flow direction (Shao and Billington 2021).

In many structural calculations and proposed equations for the development length of rebar bond strength, the random fiber orientation is assumed for the calculation of the tensile strength of UHPC. However, no quantification of the fiber alignment in the rebar region in large-scale structures has been conducted, therefore, the actual fiber orientation is unknown. Although the study indicates that even with fibers aligning parallel to the rebars, the UHPC-rebar bond strength is still much higher than that of conventional concrete, it is still necessary to fully understand the actual fiber orientation near the rebars in large scale structures and its influence on the rebar pullout behavior.

19. Conclusion

This document reviewed different UHPC recommendations and standards in Part 1 and the effect of the casting procedure on the fiber orientation and mechanical performance of small and large-scale UHPC structures in Part 2. The following conclusions can be drawn from the review:

1. Among all the recommendations and standard documents, the AFGC recommendations (2002, 2013) provide the most reliable method to directly measure the effect of fiber orientation. The AFGC recommendation is followed in many successful large-scale UHPC projects. Moreover, the fib Model Code (fib MC2010 and in progress fib MC2020) and the Canadian Highway Bridge Design Code (2019) (CSA S6:19) closely followed the AFGC recommendation in deriving the fiber orientation factor.
2. German (DAfStb 2012, 2019), Australian (AS 3600 2018), and Swiss (SIA 2052:2016) guidelines also take fiber orientation into account when modifying the design tensile properties. Many of these factors, however, deserve further examination.
3. Japanese (JSCE recommendations 2006 and 2008) and Korean (KICT Design Guideline for K-UHPC-2014 and KCl-M-19-006) codes did not consider fiber orientation explicitly, rather they used a lumped material factor and matched the overall safety factors to AFGC recommendations (2002, 2013). Additionally, Korean guidelines (2014, 2019) and JSCE recommendations (2006, 2008) recommend performing mock-up tests in accordance with the AFGC recommendation.
4. For the structural design of UHPC structural members, the AASHTO LRFD guide specification for structural design with UHPC (2021, proposed version) and CSA A23:19 do not take fiber orientation into account. To ensure uniformity of fiber dispersion, CSA A23:19 prescribes certain casting procedures to follow, while the proposed AASHTO guideline requires the designers to use proper construction methods to ensure proper fiber orientation and dispersion.
5. For relatively large-scale longitudinal specimens, literature shows that casting from one end and letting it flow to the other ends improves the fiber alignment along flow direction which is the principal stress direction. When casting from the middle, the fibers are less aligned due to a shorter flow distance. However, in the case of small-scale specimens, casting from the center increases the number of fibers at the middle of the specimen which increases crack bridging and flexural performance, while casting at the end in small-scale specimens showed a smaller number of fibers at the center and less aligned fiber along with the flow due to short flow distance and end wall effect.
6. For flat specimens, casting flow from the middle of a circular specimen tends to align the fibers tangentially or perpendicularly to the flow direction while casting from one end tends to align the fibers along the flow direction.
7. The longer flow distance allows the fibers to align the fibers along the flow direction which increases the fiber alignment as well as mechanical properties along the flow direction.
8. The rheology of the UHPC mix plays an important role in governing the fiber orientation and distribution, and mechanical performances. In general, higher viscosity and lower yield stress are

desirable for achieving better fiber alignment along the flow direction for self-consolidating UHPC.

9. The wall effect affects the orientation of fibers in UHPC, especially for relatively small specimens and longer fibers. These phenomena may be less noticeable in large-scale structures. As a result, the flexural strength obtained from small-scale specimens is generally higher than that of larger specimens.
10. Many casting devices have been proposed, the notable ones include 30-degree chute and L-shape devices which were efficient in fiber alignment along the flow direction. However, these studies are mostly at a small scale and their scalability and applicability for large-scale needs to be investigated.
11. The bond behavior of rebar in UHPC is also impacted by the fiber orientation. UHPC with fibers oriented perpendicular to the load direction developed the highest pullout load and oriented parallel to the load direction recorded the lowest pullout load. However, one contradicting study reported that the pullout strength of rebars in UHPC with parallelly aligned fibers was found slightly higher than that with transversely aligned fibers. Nevertheless, the bond strength between UHPC and rebars is much higher than that of conventional concrete.

There exists a knowledge gap on the fiber orientation of structural scale UHPC members cast from realistic casting procedures. Up to date, limited quantification of the fiber orientation in large-scale UHPC members has been conducted; the influence of casting procedures and rebar arrangement on the fiber orientation is not fully understood, and the effectiveness of special casting procedures at large-scale also requires further investigation.

20. Recommendations

After reviewing all relevant UHPC structure design codes and specifications, their relevant background work, and all other relevant research on the effect of the casting method of UHPC on the fiber orientation and mechanical properties, we found that there is a knowledge gap in the quantification of the fiber orientation in real scale structures based on casting procedure, understanding of the influence of different casting procedures in the final fiber orientation, as well as the effect of specimen geometry and rebar arrangement on the fiber orientation. However, the fiber orientation in small-scale lab cast specimens used to determine the mechanical properties of UHPC does not represent that in real structures. In addition, although several special casting procedures and casting devices were proposed by researchers to better align the fibers in the principal stress direction, there was no further investigation on their scalability or efficiency for casting large-scale structures.
To this end, the following future research directions are identified:

1. The concept of fiber orientation factors (K factors) from the AFGC recommendation is considered the most reliable method to determine and consider the effect of fiber orientation in the structural design of UHPC members. Therefore, it is recommended that the K factor concept be considered in the design of UHPC members for FDOT projects to enhance the reliability of the design.
2. Quantification of fiber orientation in large-scale structures is needed. Tests on mock-up sections following AFGC recommendations (2002, 2013) indicate that the fiber orientation in large scale structures is different from lab cast specimens, therefore, there is a need to understand the actual fiber orientation in the large structures for more effective design. Mock-up section testing on typical UHPC elements could be performed to understand the typical fiber orientation in these standard shapes, especially at critical locations or where the geometry is complex. This will increase the confidence of the UHPC structural design.
3. There is also a need for further investigation on the influence of rebar arrangement on the fiber orientation in large-scale structures, and the resultant effect on the rebar pullout behavior. Most casting procedures and casting devices are developed to align the fiber along the longitudinal direction, which may not be preferable for achieving high rebar bond strength. There has been no quantification of the fiber orientation conducted in the rebar region in large-scale structures. Therefore, it is necessary to evaluate the actual fiber orientation at the rebar location and its effect on rebar bond strength.
4. Studies regarding the influence of casting procedures on fiber orientation at large scales are needed. The proposed AASHTO guideline requires the designers to ensure uniform fiber orientation in the structural members. However, there is no guideline provided on how to achieve uniform fiber orientation. Therefore, there is an urgent need to understand the influence of casting procedures and identify the best practices for casting different UHPC elements to meet the requirement. Even if the AFGC method is selected for the design, optimization of the casting procedure is still desired to provide a more efficient and economical design.
5. Although many devices were developed to better align the fibers, their applicability for large-scale

casting requires further investigations. Possible upscaled devices could facilitate to align the fibers in preferential directions and improve the structural performance, which is worth further investigating.

6. Although several studies investigated the optimal range of rheology for fiber alignment in UHPC, these are conducted using small-scale specimens, and the optimal values are case-specific. In large-scale specimens, when the flow distance, formwork geometry, and casting procedure are different, the optimum range of rheological parameters may change, which may require further investigation.

References

AASHTO. 2020. AASHTO LRFD Bridge Design Specifications, Ninth Edition, LRFDBDS-9. American Association of State Highway and Transportation Officials, Washington, DC.

AASHTO. 2021. AASHTO LRFD guide specification for structural design with ultra-high performance concrete (proposed version), American Association of State Highway and Transportation Officials, Washington, DC.

AASHTO (TP 119). 2021. Standard Method of Test for Electrical Resistivity of a Concrete Cylinder Tested in a Uniaxial Resistance Test. American Association of State Highway and Transportation Officials, Washington, DC.

Abrishambaf, A., Barros, J.A. and Cunha, V.M., 2013. Relation between fibre distribution and post-cracking behaviour in steel fibre reinforced self-compacting concrete panels. Cement and Concrete Research, 51, pp.57-66.

American Concrete Institute Subcommittee 239C (ACI 239C). 2018. Emerging Technology Report (ETR): The Structural Design of Ultra-High Performance Concrete. American Concrete Institute, Farmington Hills, MI.

American Concrete Institute Subcommittee 239C (ACI 239C). 2019. Emerging Technology Report (ETR): An Overview of the Methods for the Structural Design of Ultra-High Performance Concrete. American Concrete Institute, Farmington Hills, MI.

American Concrete Institute Committee 318. 2008. Building Code Requirements for Structural Concrete. American Concrete Institute, Farmington Hills, MI, 473 pp.

American Concrete Institute Committee 544. 2009. Report on Fiber Reinforced Concrete (ACI 544.1R-96), American Concrete Institute, Farmington Hills, MI, 2009, 63 pp.

Association Francaise de Genie Civil – Service d'Etudes Techniques des Routes et Autoroutes (AFGC). 2002. Bétons Fibrés à Ultra-Hautes Performances—Recommandations Provisoires (*Ultra High Performance Fiber-Reinforced Concretes—Interim Recommendations*). AFGC, Paris, France.

Association Francaise de Genie Civil – Service d'Etudes Techniques des Routes et Autoroutes (AFGC). 2013. Bétons Fibrés à Ultra-Hautes Performances—Recommandations Provisoires (*Ultra High Performance Fiber-Reinforced Concretes—Interim Recommendations*). AFGC, Paris, France.

Alkaysi, M. and El-Tawil, S., 2017. Factors affecting bond development between Ultra High Performance Concrete (UHPC) and steel bar reinforcement. Construction and Building Materials, 144, pp.412-422.

Amin, A. and Foster, S.J., 2016. Shear strength of steel fibre reinforced concrete beams with stirrups. Engineering Structures, 111, pp.323-332.

ASTM A944-10, 2010. Standard test method for comparing bond strength of steel reinforcing bars to concrete using beam-end specimens. Annual Book of ASTM Standards.

ASTM C1609/C1609M-06, 2006. Standard Test Method for Flexural Performance of Fiber-Reinforced Concrete (Using Beam with Third-Point Loading). ASTM International, West Conshohocken, PA, pp.8.

Aveston, J. and Kelly, A., 1973. Theory of multiple fracture of fibrous composites. Journal of

Materials Science, 8(3), pp.352-362.
Barnett, S.J., Lataste, J.F., Parry, T., Millard, S.G. and Soutsos, M.N., 2010. Assessment of fibre orientation in ultra high performance fibre reinforced concrete and its effect on flexural strength. Materials and Structures, 43(7), pp.1009-1023.
Barragán, B.E., Gardner, D., Gettu, R. and Ferreira, L.E.T., 2000. Study of the distribution and orientation of fibers in cast cylinders. Structural Technology Laboratory, Universitat Politècnica de Catalunya.
Behloul, M. and Batoz, J.F., 2008, March. Ductal® applications over the last Olympiad. In Proc. 2nd Int. Symp. on Ultra High Performance Concrete, Kassel, Germany (pp. 855-862).
Behloul, M., Ricciotti, R., Ricciotti, R.F., Pallot, P. and Leboeuf, J., 2008. Ductal pont du diable footbridge, France. In Proceedings of the fib symposium ‘‘tailor made concrete structures (pp. 335-338).
Boulekbache, B., Hamrat, M., Chemrouk, M. and Amziane, S., 2010. Flowability of fibre-reinforced concrete and its effect on the mechanical properties of the material. Construction and Building Materials, 24(9), pp.1664-1671.
Casanova, P. and Rossi, P., 1997. Can steel fibers replace transverse reinforcements in reinforced concrete beams?. Materials Journal, 94(5), pp.341-354.
Chao, S.H., Naaman, A.E. and Parra-Montesinos, G.J., 2009. Bond behavior of reinforcing bars in tensile strain-hardening fiber-reinforced cement composites. ACI Structural Journal, 106(6), p.897.
Chen, S., Zhang, R., Jia, L.J. and Wang, J.Y., 2018. Flexural behaviour of rebar-reinforced ultra-high-performance concrete beams. Magazine of Concrete Research, 70(19), pp.997-1015.
CNR-DT 204, 2006. Guidelines for design, construction and production control of fiber reinforced concrete structures. National Research Council of Italy, Italy
Conforti, A., Cuenca, E., Zerbino, R. and Plizzari, G.A., 2021. Influence of fiber orientation on the behavior of fiber reinforced concrete slabs. Structural Concrete.
Canadian Standards Association (CSA A23). 2019. Concrete materials and methods of concrete construction/Test methods and standard practices for concrete, CSA group.
Canadian Standards Association (CSA- S6). 2019. Canadian Highway Bridge Design Code, CSA group.
Canadian Standards Association. 2019. Commentary on CSA S6:19, 2019. Canadian Highway Bridge Design Code, CSA group.
DAfStb (German Committee for Structural Concrete/Deutscher Ausschuss für Stahlbeton). 2012. DAfStb-Richtlinie Stahlfaserbeton (*DAfStb Guideline “Steel fibre reinforced concrete”*) (Draft copy).
DAfStb (German Committee for Structural Concrete/Deutscher Ausschuss für Stahlbeton) (DAfStb Heft 614). 2016. Commentary on the DAfStb Guideline "Steel Fibre Reinforced Concrete".
DAfStb (German Committee for Structural Concrete/Deutscher Ausschuss für Stahlbeton). 2019. DAfStb-Richtlinie Stahlfaserbeton (*DAfStb Guideline “Steel fibre reinforced concrete”*) (Draft copy).
de Andrade, R.G.M., Pfeil, M.S., Battista, R.C., Toledo Filho, R.D., de Araújo, O.M.O. and Lopes, R.T., 2021. Comparison between methods to determine the fibre orientation factor of an HPFRC

bridge box girder. Construction and Building Materials, 269, p.121291.
de Matteis, D., Novarin, M., Marchand, P., Fabry, N., Petel, A. and Chanut, S., 2008a. A fifth French bridge including UHPFRC components, the widening of the Pinel Bridge, in Rouen (France). In International Symposium on UHPC, Kassel.
de Matteis, D., Marchand, P., Petel, A., Thibaux, T., Novarin, M. and Chanut, S. 2008b. Un 5ÈME Pont Routier Français En BFUP: Le Triplement Du Pont Pinel À Rouen, IABSE Congress Chicago 2008.
Delplace, G., Hajar, Z. and Simon, A., 2012. Precast thin shells made of UHPFRC for a large roof in a wastewater treatment plant near Paris. Proc. of Hipermat, pp.1011-1018.
Deutscher Ausschuss fu¨r Stahlbeton (DAfStb), 2007. Guidelines for steel fiber reinforced concrete—23th Draft—richtlinie Stahlfaserbeton—DIN 1045 Annex parts 1–4, August 2007.
DIN 1045-2 Concrete, reinforced and prestressed concrete structures - Part 2: Concrete - Specification, properties, production and conformity - Application rules for DIN EN 206-1.
DIN 1045-3, Concrete, reinforced and prestressed concrete structures - Part 3: Execution of structures - Application rules for DIN EN 13670.
DIN, E. 206-1 Concrete - Part 1: Specification, performance, production and conformity; German version EN 206-1:2000.
Dupont, D. and Vandewalle, L., 2005. Distribution of steel fibres in rectangular sections. Cement and Concrete Composites, 27(3), pp.391-398.
Duque, L.F.M. and Graybeal, B., 2017. Fiber orientation distribution and tensile mechanical response in UHPFRC. Materials and Structures, 50(1), pp.1-17.
EN 14651, 2004. Test method for metallic fibre concrete-measuring the flexural tensile strength (limit of proportionality, residual). Varenna, Italy.
EN 14651, 2005. Precast concrete products-test method for metallic fibre concrete—Measuring the flexural tensile strength, European Standard: CEN, Brussels, Belgium.
EN 12390-1. 2000. Testing hardened concrete–Part 1: Shape, dimensions and other requirements for specimens and moulds. European Committee for Standardization, 2.
EN 1992. 2004. Eurocode 2: Design of concrete structures - Part 1-1: General rules and rules for buildings.
Fehling, E., Lorenz, P. and Leutbecher, T., 2012, March. Experimental investigations on anchorage of rebars in UHPC. In Proceedings of Hipermat 2012 3rd International Symposium on UHPC and Nanotechnology for High Performance Construction Materials (pp. 533-540).
Ferrara, L., Ozyurt, N. and Di Prisco, M., 2011. High mechanical performance of fibre reinforced cementitious composites: the role of "casting-flow induced" fibre orientation. Materials and Structures, 44(1), pp.109-128.
fib (*fédération internationale du béton*/International Federation for Structural Concrete) (fib MC2010). 2010. fib Model Code for Concrete Structures 2010. Berlin, Germany: Ernst & Sohn, 2013.
fib (*fédération internationale du béton*/International Federation for Structural Concrete) (fib MC2020). 2020. fib Model Code for Concrete Structures 2020 (in progress).
Korea Concrete Society. 2020. SUPER Concrete structural performance verification and Development of design guidelines. Final report on FRSC, 2020.

Foster, S., 2014. FRC design according to the draft Australian bridge code. In Proceedings of the FRC 2014 Joint ACI-fib International Workshop—Fibre Reinforced Concrete: from Design to Structural Applications (pp. 19-31).

Foster, S.J., Agarwal, A. and Amin, A., 2018. Design of steel fiber reinforced concrete beams for shear using inverse analysis for determination of residual tensile strength. Structural Concrete, 19(1), pp.129-140.

French Standards Institute (*Association Française de Normalisation [AFNOR]*) (NF P 18-451). 2018. Concrete - Execution of concrete structures - Specific rules for UHPFRC, Norme française (French standard).

French Standards Institute (*Association Française de Normalisation [AFNOR]*) (NF P 18-470). 2016. Concrete - Ultra-high performance fibre-reinforced concrete - Specifications, performance, production and conformity. Francis de Pressensé, France.

French Standards Institute (*Association Française de Normalisation [AFNOR]*) (NF P 18-710). 2016. National addition to Eurocode 2 - Design of concrete structures: specific rules for Ultra-high performance fibre-reinforced concrete (UHPFRC).

Graybeal, B.A., 2006. Structural behavior of ultra-high performance concrete prestressed I-girders (No. FHWA-HRT-06-115). United States. Federal Highway Administration. Office of Infrastructure Research and Development.

Groeneveld, A.B., Ahlborn, T.M., Crane, C.K., Burchfield, C.A. and Landis, E.N., 2017a. Dynamic strength and ductility of ultra-high performance concrete with flow-induced fiber alignment. International Journal of Impact Engineering, 111, pp.37-45.

Groeneveld, A.B., Ahlborn, T.M., Crane, C.K. and Long, W.R., 2017b. Effect of Fiber Orientation on Dynamic Compressive Properties of an Ultra-High Performance Concrete. US Army Engineer Research and Development Center Vicksburg United States.

Hasgul, U., Turker, K., Birol, T. and Yavas, A., 2018. Flexural behavior of ultra-high-performance fiber reinforced concrete beams with low and high reinforcement ratios. Structural Concrete, 19(6), pp.1577-1590.

Holschemacher, K. and Weiße, D., 2004. Bond of reinforcement in fibre reinforced concrete. In 6th International RILEM Symposium on Fibre Reinforced Concretes (pp. 349-358). RILEM Publications SARL.

Huang, H., Gao, X., Li, L. and Wang, H., 2018. Improvement effect of steel fiber orientation control on mechanical performance of UHPC. Construction and Building Materials, 188, pp.709-721.

Huang, H., Gao, X. and Zhang, A., 2019a. Numerical simulation and visualization of motion and orientation of steel fibers in UHPC under controlling flow condition. Construction and Building Materials, 199, pp.624-636.

Huang, H., Su, A., Gao, X. and Yang, Y., 2019b. Influence of formwork wall effect on fiber orientation of UHPC with two casting methods. Construction and Building Materials, 215, pp.310-320.

Huang, H., Gao, X., Li, Y. and Su, A., 2020. SPH simulation and experimental investigation of fiber orientation in UHPC beams with different placements. Construction and Building Materials, 233, p.117372.

Huang, H., Gao, X. and Khayat, K.H., 2021a. Contribution of fiber alignment on flexural properties

of UHPC and prediction using the Composite Theory. Cement and Concrete Composites, 118, p.103971.

Huang, H., Gao, X. and Teng, L., 2021b. Fiber alignment and its effect on mechanical properties of UHPC: An overview. Construction and Building Materials, 296, p.123741.

Huang, H., Gao, X., Khayat, K.H. and Su, A., 2021c. Influence of fiber alignment and length on flexural properties of UHPC. Construction and Building Materials, 290, p.122863.

Joint ACI-ASCE Committee 408 (ACI 408.2R). 2012. Report on Bond of Steel Reinforcing Bars Under Cyclic Loads, in: American Concrete Institute.

Japanese Society of Civil Engineers (JSCE Recommendations). 2006. Recommendations to the Japanese Provisional Recommendations for the Design and Construction of Ultra High Strength Fiber-Reinforced Concrete (UFC), JSCE guideline for concrete, No. 9.

Japanese Society of Civil Engineers (JSCE Guidelines). 2007. Standard Specifications for Concrete Structures 2007 "Design", JSCE Guidelines for Concrete No.15.

Japanese Society of Civil Engineers (JSCE Recommendations). 2008. Recommendations for Design and Construction of High Performance Fiber Reinforced Cement Composites with Multiple Fine Cracks (HPFRCC), Concrete Engineering Series 82.

Kahanji, C., Ali, F. and Nadjai, A., 2017. Structural performance of ultra-high-performance fiber-reinforced concrete beams. Structural Concrete, 18(2), pp.249-258.

Kang, S.T. and Kim, J.K., 2011. The relation between fiber orientation and tensile behavior in an Ultra High Performance Fiber Reinforced Cementitious Composites (UHPFRCC). Cement and Concrete Research, 41(10), pp.1001-1014.

Kang, S.T. and Kim, J.K., 2012. Investigation on the flexural behavior of UHPCC considering the effect of fiber orientation distribution. Construction and Building Materials, 28(1), pp.57-65.

Kang, S.T., Lee, B.Y., Kim, J.K. and Kim, Y.Y., 2011. The effect of fibre distribution characteristics on the flexural strength of steel fibre-reinforced ultra high strength concrete. Construction and Building Materials, 25(5), pp.2450-2457.

Kasper, T., Stang, H., Mjoernell, P, Thrane, L.N. and Reimer, L 2014. Design guideline for structural applications of steel fibre reinforced concrete. SFRC Consortium.

Khalil, W.I. and Tayfur, Y.R., 2013. Flexural strength of fibrous ultra high performance reinforced concrete beams. ARPN Journal of Engineering and Applied Sciences, 8(3), pp.200-214.

Kim, S.W., Kang, S.T., Park, J.J. and Ryu, G.S., 2008, March. Effect of filling method on fibre orientation and dispersion and mechanical properties of UHPC. In Proceedings of the 2nd International Symposium on Ultra High Performance Concrete, Kassel, Germany (pp. 185-192).

Korea Concrete Institute (KCI-M-12-003). 2012. Design Recommendations for Ultra-High Performance Concrete.

Korea Concrete Institute (KCl-M-19-006). 2019. The Structural Design Guidelines of Fiber Reinforced SUPER Concrete.

Korean Institute of Construction Technology. 2014. KICT Design Guideline for K-UHPC.

Laranjeira, F., Grünewald, S., Walraven, J., Blom, C., Molins, C. and Aguado, A., 2011. Characterization of the orientation profile of steel fiber reinforced concrete. Materials and structures, 44(6), pp.1093-1111.

Lee, S.C., Cho, J.Y. and Vecchio, F.J., 2011a. Diverse embedment model for steel fiber-reinforced concrete in tension: model development. ACI Materials Journal, 108(5), p.516.

Lee, S.C., Cho, J.Y. and Vecchio, F.J., 2011b. Diverse embedment model for steel fiber-reinforced concrete in tension: model verification. ACI Materials Journal, 108(5), p.526.

Loser, R., Justs, J. and Lura, P., 2018, Practical considerations on the application of the recent SIA 2052 guidelines on testing of Ultra-high-performance fiber reinforced concrete. In Proc. of RC2018: Fibre Reinforced Concrete: from Design to Structural Applications Joint ACI-fib-RILEM International Workshop (pp. 504-513).

Meng, W. and Khayat, K.H., 2017. Improving flexural performance of ultra-high-performance concrete by rheology control of suspending mortar. Composites Part B: Engineering, 117, pp.26-34.

Miletić, M., Guillard, F. and Marks, B., 2017. Effect of reinforcement on the fibre orientation within fibre reinforced concrete. Common Foundations, pp.165-170.

Ng, T.S., Htut, T.N.S. and Foster, S.J., 2012. Fracture of steel fibre reinforced concrete–The unified variable engagement model. UNICIV Rep. No. R-460, May 2012, The University of New South Wales Sydney, Australia.

Nguyen, T.N., Nguyen, T.T. and Pansuk, W., 2017. Experimental study of the punching shear behavior of high performance steel fiber reinforced concrete slabs considering casting directions. Engineering Structures, 131, pp.564-573.

Oesch, T.S., 2015. Investigation of fiber and cracking behavior for conventional and ultra-high performance concretes using x-ray computed tomography. University of Illinois at Urbana-Champaign.

Qiu, M., Shao, X., Wille, K., Yan, B. and Wu, J., 2020. Experimental investigation on flexural behavior of reinforced ultra high performance concrete low-profile T-beams. International Journal of Concrete Structures and Materials, 14(1), pp.1-20.

Qu, S., Zhang, Y., Zhu, Y., Huang, L., Qiu, M. and Shao, X., 2020. Prediction of tensile response of UHPC with aligned and ZnPh treated steel fibers based on a spatial stochastic process. Cement and Concrete Research, 136, p.106165.

Resplendino, J., 2008. Ultra-high performance concretes—Recent realizations and research programs on UHPFRC bridges in France. In Proc., 2nd Int. Symp. on Ultra High Performance Concrete (pp. 31-43). Kassel University Press, Kassel, Germany.

RILEM TC 162-TDF, 2002. Test and Design Methods for Steel Fibre Reinforced Concrete, Recommendations. Materials and Structures, V. 35, pp. 579-582.

Roy, M., Hollmann, C. and Wille, K., 2017. Influence of volume fraction and orientation of fibers on the pullout behavior of reinforcement bar embedded in ultra high performance concrete. Construction and Building Materials, 146, pp.582-593.

Schuler, F., Breit, W., Schnell, J. and Schladitz, K., 2017. *Computertomografie–den Fasern auf der Spur. Untersuchungen zum Faktor zur Beruecksichtigung der Faserorientierung kfF nach DAfStb-Richtlinie „Stahlfaserbeton "am Beispiel von Tunneltuebbings. Bautechnik, 94(10).*

Shao, Y. and Billington, S.L., 2019, June. Utilizing full UHPC compressive strength in steel reinforced UHPC beams. In International Interactive Symposium on Ultra-High Performance Concrete (Vol. 2, No. 1). Iowa State University Digital Press.

Shao, Y. and Billington, S.L., 2021. Bond Performance of Ultra-High-Performance Concrete (UHPC) Under Flexural States. In Proceedings of Fib Symposium 2021.

Swiss Society of Engineers and Architects (SIA 2052). 2016. *Béton fibré ultra-performant (BFUP); Matériaux, dimensionnement et execution*.

Simon, A., 2011. New AFGC Recommendations on UHPFRC: Chapter 1–Mechanical Characteristics and Behavior of UHPFRC. Designing and Building with UHPFRC, pp.723-742.

Simon, A., Corvez, D. and Marchand, P., 2013, October. Feedback of a ten years assessment of fibre distribution using K factor concept. In Int. Symposium on Ultra-High Performance Fibre-Reinforced Concrete, Designing and Building with UHPFRC: From Innovation to Large-Scale Realizations (pp. 669-678).

Singh, M., Sheikh, A.H., Ali, M.M., Visintin, P. and Griffith, M.C., 2017. Experimental and numerical study of the flexural behaviour of ultra-high performance fibre reinforced concrete beams. Construction and Building Materials, 138, pp.12-25.

Sritharan, S., Voort, T.V. and Suleiman, M., 2011. Effective use of UHPC for Deep Foundation Piles. Designing and Building with UHPFRC, pp.279-294.

Standards Australia Committee BD-002 (AS 3600). 2018. Australian Standard of Concrete structures.

Stähli, P., Custer, R. and van Mier, J.G., 2008. On flow properties, fibre distribution, fibre orientation and flexural behaviour of FRC. Materials and structures, 41(1), pp.189-196.

Teng, L., Meng, W. and Khayat, K.H., 2020. Rheology control of ultra-high-performance concrete made with different fiber contents. Cement and Concrete Research, 138, p.106222.

Teng, L., Huang, H., Du, J. and Khayat, K.H., 2021. Prediction of fiber orientation and flexural performance of UHPC based on suspending mortar rheology and casting method. Cement and Concrete Composites, 122, p.104142.

The MathWorks. 2014. Image Processing Toolbox (version 9.0). Computer program. Natick, MA.

Turker, K., Hasgul, U., Birol, T., Yavas, A. and Yazici, H., 2019. Hybrid fiber use on flexural behavior of ultra high performance fiber reinforced concrete beams. Composite structures, 229, p.111400.

Valente, R.M.G., 2017. Design of a pre-stressed bridge deck with ultra-high performance concrete. Universidade Do Porto.

Voort, T.V., Suleiman, M.T. and Sritharan, S., 2008. Design and performance verification of ultra-high performance concrete piles for deep foundations (No. IHRB Project TR-558). Iowa State University. Center for Transportation Research and Education.

Walsh, K.K., Hicks, N.J., Steinberg, E.P., Hussein, H.H. and Semendary, A.A., 2018. Fiber Orientation in Ultra-High-Performance Concrete Shear Keys of Adjacent-Box-Beam Bridges. ACI Materials Journal, 115(2).

Wille, K. and Parra-Montesinos, G.J., 2012. Effect of beam size, casting method, and support conditions on flexural behavior of ultra high-performance fiber-reinforced concrete. ACI Materials Journal, 109(3), p.379.

Yang, I.H., Joh, C. and Kim, B.S., 2010. Structural behavior of ultra high performance concrete beams subjected to bending. Engineering structures, 32(11), pp.3478-3487.

Yoo, D.Y. and Yoon, Y.S., 2015. Structural performance of ultra-high-performance concrete beams with different steel fibers. Engineering Structures, 102, pp.409-423.

Yoo, D.Y., Banthia, N. and Yoon, Y.S., 2017. Experimental and numerical study on flexural behavior of ultra-high-performance fiber-reinforced concrete beams with low reinforcement ratios. Canadian Journal of Civil Engineering, 44(1), pp.18-28.

Yoo, D.Y., Banthia, N., Kang, S.T. and Yoon, Y.S., 2016a. Size effect in ultra-high-performance concrete beams. Engineering Fracture Mechanics, 157, pp.86-106.

Yoo, D.Y., Kang, S.T. and Yoon, Y.S., 2014. Effect of fiber length and placement method on flexural behavior, tension-softening curve, and fiber distribution characteristics of UHPFRC. Construction and Building materials, 64, pp.67-81.

Yoo, D.Y., Kang, S.T. and Yoon, Y.S., 2016b. Enhancing the flexural performance of ultra-high-performance concrete using long steel fibers. Composite Structures, 147, pp.220-230.

Zhang, Y., Zhu, Y., Qu, S., Kumar, A. and Shao, X., 2020. Improvement of flexural and tensile strength of layered-casting UHPC with aligned steel fibers. Construction and Building Materials, 251, p.118893.

Zhou, B. and Uchida, Y., 2017. Relationship between fiber orientation/distribution and post-cracking behaviour in ultra-high-performance fiber-reinforced concrete (UHPFRC). Cement and Concrete Composites, 83, pp.66-75.
